ABSTRACT

Title of Document:	ANALYSIS OF HEAT PUMP CLOTHES DRYER
	Zhilu Zhang, Master of Science, 2015
Directed By:	Yunho Hwang, Research Professor, Department of Mechanical Engineering

Clothes dryers (CD) offer a rapid means to dry laundry in households, but consume a large portion (4%) of residential electricity. Heat pump clothes dryers (HPCD) can be much more energy-efficient than conventional electric CDs, but have not emerged in the U.S. market yet. In this study, experiments were conducted for a state-of-the-art commercial hybrid HPCD from the European market with two different operational modes followed by Department of Energy's test procedure. The HPCD's system performances were analyzed through measurements on humidity ratio (HR), temperature and power consumption for both Eco and Speed Modes. About 70% energy consumption reduction potential was observed as compared with a typical electric CD in the United

States. The heating and cooling capacities during the Eco Mode were 1.48 kW and 1.18 kW, respectively, and the dehumidification rate was 0.372 g/s. The heat exchangers were modeled with CoilDesigner and their performances were simulated. The UA of the evaporator was mainly affected by the air flow rate (AFR), inlet air HR and refrigerant MFR while that of the condenser was mainly affected by the condensing temperature, AFR, and refrigerant MFR. The air leakage was estimated to be 24% to 45% in which the water vapor leakage was 26% and the energy loss was 5%. The mass transfer process through the drum was discussed and the mass transfer coefficient k between the cloth surface and air was calculated to be 0.237 $g/m^2 \cdot s$. This study provides the performances of HPCDs and their design analysis, which can be used for developing improved HPCDs.

ANALYSIS OF HEAT PUMP CLOTHES DRYER

By

Zhilu Zhang

Thesis submitted to the Faculty of the Graduate School of the

University of Maryland, College Park, in partial fulfillment

Of the requirements for the degree of

Master of Science

2015

Advisory Committee:

Research Professor Yunho Hwang, Chair

Professor Jelena Srebric

Professor Jungho Kim

Dedication

This thesis is dedicated to my parents who always support me without a reason and to my boyfriend who always has words of encouragement.

Acknowledgements

To begin with, I would like to thank Dr. Reinhard Radermacher and Dr. Yunho Hwang for offering me the opportunity to be a part of CEEE (Center for Environmental Energy Engineering) in the last two years where I made friends and gained a lot of engineering knowledge and experiences. I would like to acknowledge with my deepest gratitude to Dr. Hwang who serves as my academic advisor and patiently provided me with valuable guidance and advices throughout my study, and helps me completing my master's degree. I would especially like to thank Jan Muehlbauer who trained me with the skills necessary to work in the lab. I would also like to extend my appreciation to Dr. Jiazhen Ling and Dr. Hoseong Lee for their help; and Mary Baugher for her encouragement and care. Besides, I would like to thank UMD Dryer team and Tao Cao with the assistance of this project at the beginning. In addition, since graduate research is hardly an individual adventure, I am very grateful to have met and worked together with my colleagues whose passion and spirit about their work influenced me, and learning from them was of great value to me. Furthermore, my thankfulness goes to my parents who support me, cheer me every step of my way and made my scholastic journey in the United States possible, which accelerated my growth and will be an important chapter of my life. Finally, I would like to thank myself to have made such a decision to take the challenge of working towards a master's degree in mechanical engineering in my twenties. The completion of this thesis is a fresh start, not a destination.

Table of Contents

List of Tables

List of Figures

Nomenclature

Abbreviations:

A	Area	[m²]
a	Activity Coefficient	[-]
AFR	Air Flow Rate	[m³/s]
AHAM	Association of Home Appliance Manufacturers	
BDW	Bone Dry Weight	[pound]
C_P	Specific Heat	[J/kg·K]
CD	Clothes Dryer	
CEF	Combined Energy Factor	[-]
CFR	Code of Federal Regulations	
COP	Coefficient of Performance	[-]
DAQ	Data Acquisition System	
DOE	Department of Energy	
E	Energy Consumption	[kWh]
EF	Energy Factor	[-]
EES	Engineering Equation Solver	
EEV	Electric Expansion Valve	
EIA	Energy Information Administration	
EPA	Environmental Protection Agency	
FPM	Feet per Minute	[ft/min]
h	Enthalpy	[kJ/kg]

h	Heat Transfer Coefficient	[W/m²·K]
h_{latent}	Enthalpy of Vaporization	[kJ/kg]
HP	Heat Pump	
HR	Humidity Ratio	$[kg_{water}/kg_{air}]$
k	Mass Transfer Coefficient between the Clothes Surface and the Air	[kg/m²·s]
L	Characteristic Linear Dimension	[m]
M_c	Moisture Content of Clothes	[kg/kg]
$\dot{m}$	Mass Flow Rate	[kg/s]
MCHX	Micro-channel Heat Exchanger	
MFR	Mass Flow Rate	[kg/s]
Nu	Nusselt Number	[-]
ORNL	Oak Ridge National Laboratory	
OSI	Ohio Semitronics, Inc.	
Pr	Prandtl Number	[-]
SLHX	Suction Line Heat Exchanger	
PDM	Post Dry Mass	[lb]
Re	Reynolds Number	[-]
RH	Relative Humidity	[%]
RMC	Remaining Moisture Content	[%]
RPM	Revolution per Minute	[rev/min]
SEC	Specific Energy Consumption	[kWh/kg]
SHF	Sensible Heat Factor	[-]

SMER	Specific Moisture Extraction Rate	[kg/kWh]
T	Temperature	[ºC]
TC	Thermocouple	
U	Overall Heat Transfer Coefficient	[W/m²·K]
$\dot{V}$	Volume Flow Rate	[m^3/s]
v	Velocity	[m/s]
VIC	Vapor Injection Cycle	
VCC	Vapor Compression Cycle	
W	Power Consumption	[kW]
x	Vapor Quality	[-]

Greek Symbols:

β	Desorption-isotherm Constant	[-]
γ	Desorption-isotherm Constant	[-]
δ	Desorption-isotherm Constant	[-]
η	Efficiency	[-]
ρ	Density	[kg/m³]
k	Thermal Conductivity	[W/m·K]
μ	Dynamic Viscosity	[kg/m·s]
u	Uncertainty	[-]
ω	Humidity Ratio	[kg_{water}/kg_{air}]

Subscripts:

a	Air
comp	Compressor
cond	Condensor
dis	Discharge
displace	Displacement
evap	Evaporator
in	Tube Inside
isen	Isentropic
o	Tube Outside
rand	Random
ref	Refrigerant
suc	Suction
sys	Systematic
v	Water Vapor
vol	Volumetric

1 Introduction

1.1 Background of Energy Consumption

One of current most important research topics is to develop innovative ways to decrease the usage of the conventional energy resources. Since the industrial revolution in the 18th century, there has been a huge increase in the energy demand, so that the fossil fuel consumption has also rapidly grown. Fossil fuels are formed via a natural process over millions of years and are usually defined as non-renewable resources. The U.S. Energy Information Administration (EIA) estimated that by November 2014, the major energy usage consisted of 81.58% fossil fuels, which were 18.47% of coal, 27.60% of natural gas and 35.52% of petroleum for the year 2014. In addition, renewable energy includes 2.51% hydroelectric power, 0.22% geothermal, 0.44% solar, 1.78% wind and 4.82% bio energy, amounting to 9.78%, and 8.48% nuclear electric power. The primary energy consumption by source from 1949 to 2013 in the U.S. is shown in Figure 1. The average energy consumption increase was about 0.93% since 1950 in the U.S. [1]. According to EIA's report, International Energy Outlook, released in September 2014, the world energy consumption is estimated to increase by 56% between 2010 and 2040 [2].

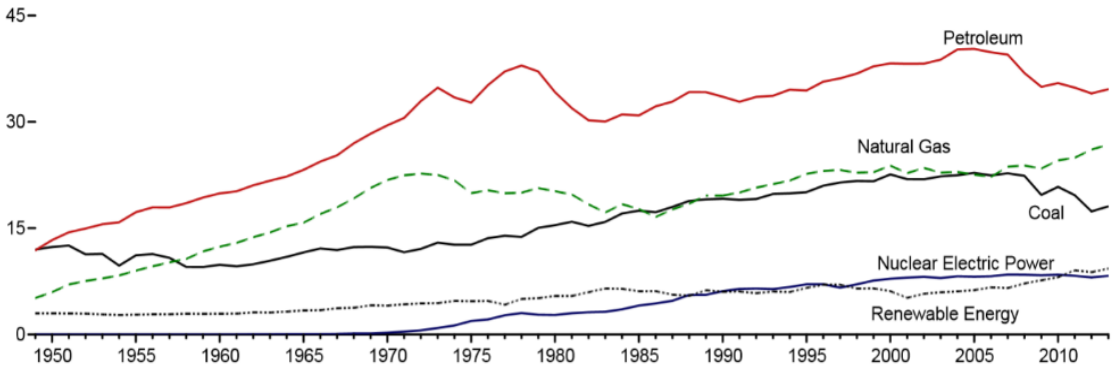

Figure 1: Primary energy consumption by source in Quadrillion Btu, 1949-2013 [1]

The excessive use of fossil fuels raised concerns on the environment. The burning of fossil fuels produces about 5 billion metric tons of carbon dioxide per year in the U.S. [3], among which only half of the quantity could be absorbed naturally. Furthermore, carbon dioxide causes the greenhouse effect, which raises the average surface temperature and leads to global warming.

The summary for the primary energy consumption by sectors demonstrates that the energy consumption could be divided into transportation, industrial, residential and commercial sectors as shown in Figure 2, which reflects the end-use sector shares in the U.S. Residential takes 22% of the total energy consumption in 2011. Figure 3 shows the total energy consumption by sector from 1949 to 2013 in the U.S.

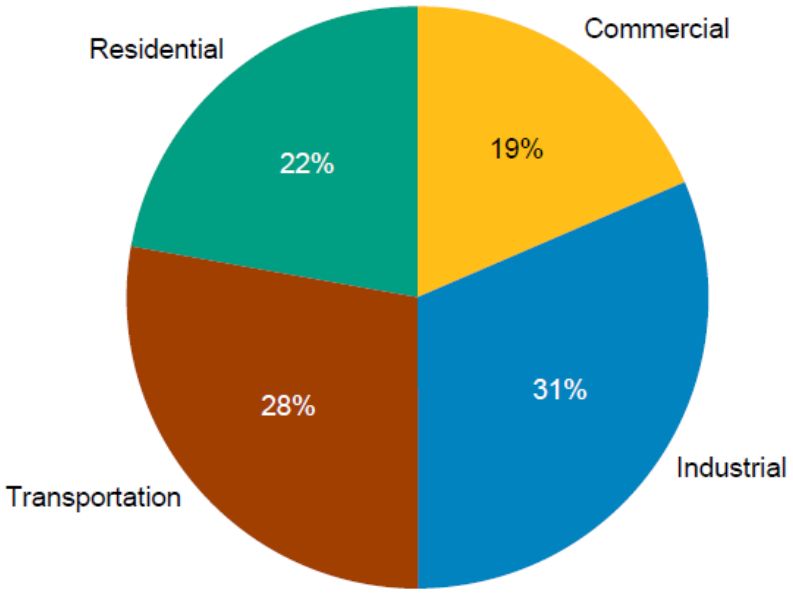

Figure 2: Sector share of energy consumption, 2011

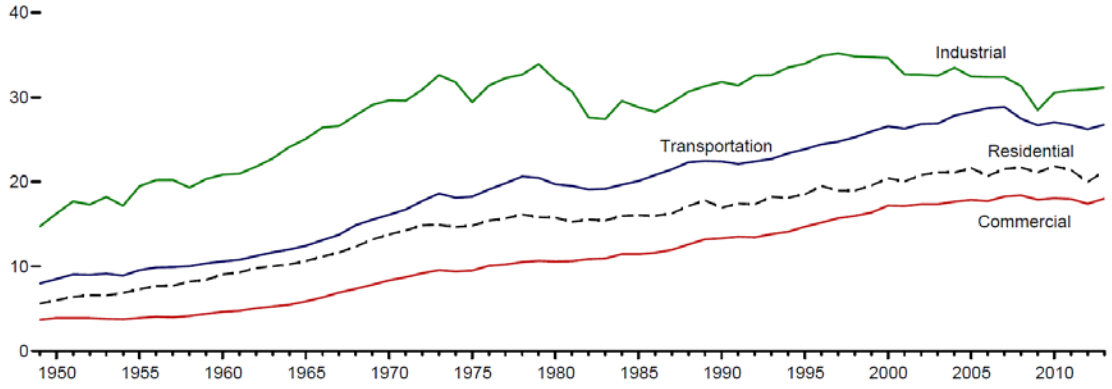

Figure 3: Total energy consumption by sector in quadrillion Btu, 1949-2013 [1]

1.2 Background of Clothes Dryers and Heat Pump Clothes Dryers

Figure 4 shows the estimated residential electricity consumption by end use in the U.S. in 2012.

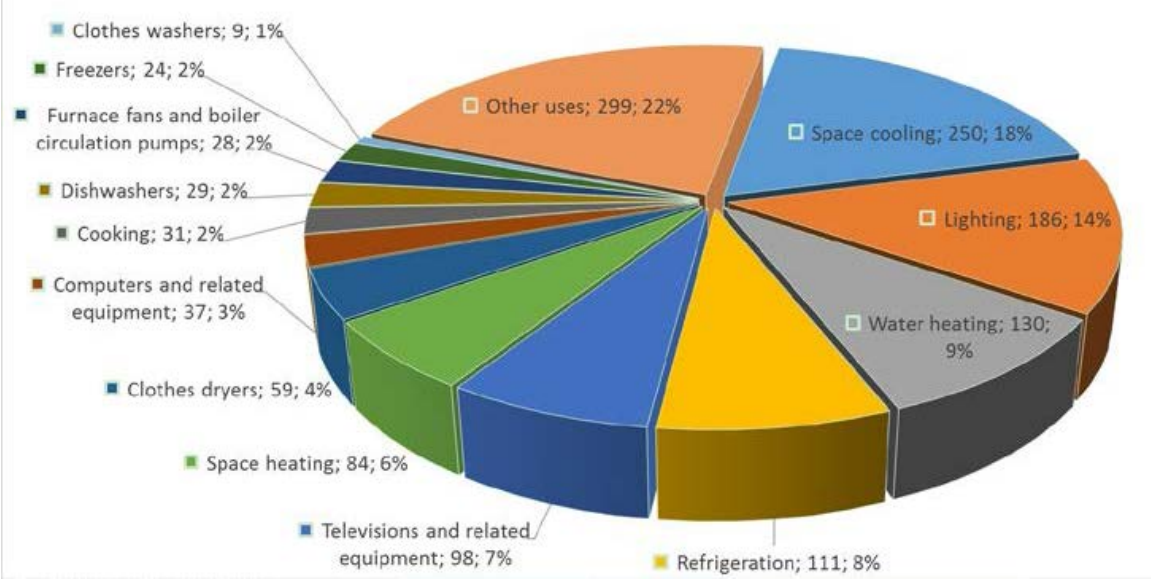

Figure 4: U.S. residential electricity consumption by end use in billion kilowatt hours, 2012 [4]

Among the domestic electric appliances, clothes dryers (CD) consumed 59 billion kilowatt hours in 2012, which takes a share of 4% of the total residential electricity use. Clothes drying is considered to be one of the most energy-intensive processes among the household appliances. A clothes dryer offers a rapid and convenient way to dry laundry that serves as a commonly used device in ordinary households in many countries, especially in the U.S.; some European countries also have a large market share.

According to a survey conducted by the Association of Home Appliance Manufacturers (AHAM), 5.6 million residential CDs were sold in the U.S. in 2008 [5], 6.5 million in 2010; 90.2 million U.S. households (around 80% of the total households) have a CD at home in 2010, among which, electric CDs take 71.8 million (80% of the total CDs) [6].

Electrical CDs and gas-fired CDs dominated the U.S. residential market: about 80% are electric CDs, while the remaining are gas CDs. However, only less than 1% are ventless while most of the CDs are vented [7].

Venting out hot air through the exhaust vents of dryers wastes a great deal of heat. Referring the DOE 2009 survey, in about 82% of the households, CDs were used every time after the clothes were washed [5], and the cycle number was assumed to be 283 cycles per year according to the test procedure published by DOE in 2011 [8]. Most of the electric CD models in the U.S. consume similar amounts of electricity energy. The energy consumption per household is more than 900 kWh for a conventional CD in the U.S. market [9]. The general average lifetime of a CD is estimated to have a range from 12 to 16 years [10] [11]. There would be a potential for good energy savings if the overall state-of-art electric clothes dryer efficiency could be increased in addition to introducing alternative resources.

However, heat pump clothes dryers (HPCD) consume much less electricity than conventional condensing dryers, and HPCDs have already emerged in European, Japanese and Australian markets, and have the potential of growing. HPCDs were first introduced in Europe by Electrolux in 1997. There were several European HPCD manufacturers in the year of 2007: Schulthess, Arcelik, and Electrolux, and one Japanese manufacturer, Panasonic. However, more companies expanded to the HPCD market later such as Miele, Metall Zug AG, Bosch and Siemens. The market share of HPCD was about 4% in 2009 (200,000 shipments per year). About 90 different HPCD models were available in European markets provided by 18 different manufacturers in 2012, as reported in the Topten Survey [12]. In Switzerland, an energy regulation was established

in 2012 that allowed only HPCDs on the Swiss market, so that the HPCD market share increased from 1.7% (in 2004) to 100% (in 2012). In Germany, Austria and Italy, about 40% is dominated by HPCD [13]. The clothes-drying industry expects that in Europe the HPCDs will continue to gain in market share. However, there are no HPCD models available in the U.S. market yet. The European consumers are more used to and patient with longer drying time and the ventless feature, while the U.S. customers prefer larger volume capacity and faster drying.

1.3 Working Principle of Clothes Dryers

1.3.1 Electric Clothes Dryer Working Principle

The operation principle of a conventional electric clothes dryer is demonstrated in Figure 5. Figure 6 shows a picture of commercial electric CD. The ambient air is drawn into the cabinet of the electric CD, heated up by the electric heater and then passes through the drum. After picking up the moisture from the wet clothes in the drum, the humid air is vented to the ambient air in most of the U.S. electric CD models. The electric heater consumes most of the energy as it is the functioning component of the dryer system. The discharged air carries out the moisture as well as some heat that has not been completely utilized, which is a waste of energy.

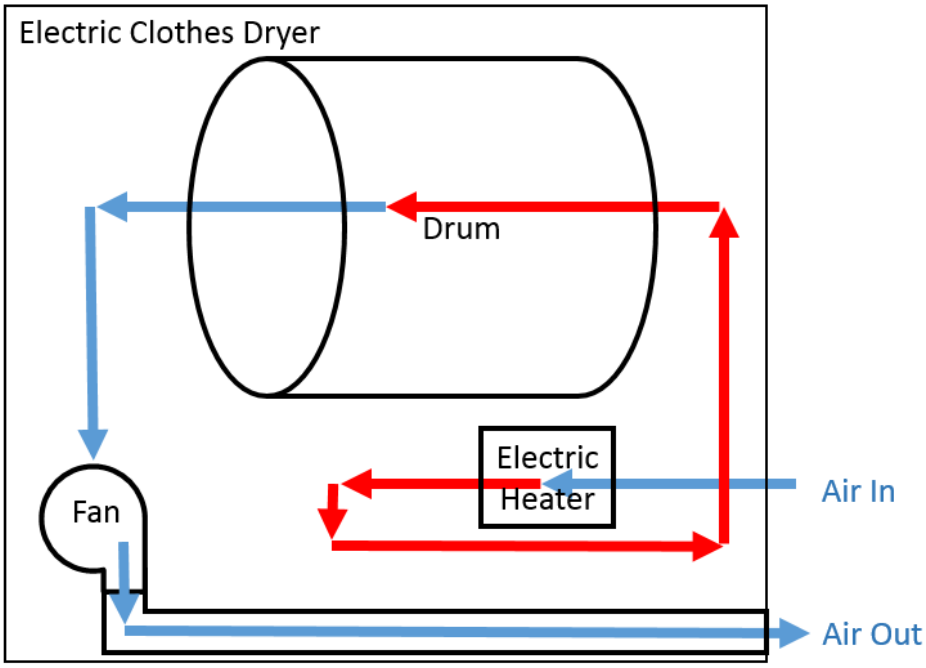

Figure 5: Drying process schematic diagram of an electric clothes dryer

Figure 6: GE electric clothes dryer (Model number: GHDN520EDWS)

1.3.2 Heat Pump Clothes Dryer Working Principle

A HPCD works as explained below. It integrates a vapor compression cycle (VCC) into the CD system that is usually located underneath the drum in the cabinet. A VCC is used widely in residential air conditioners and refrigerators. A typical VCC consists of four major components: compressor, evaporator, condenser and expansion valve as shown in Figure 7.

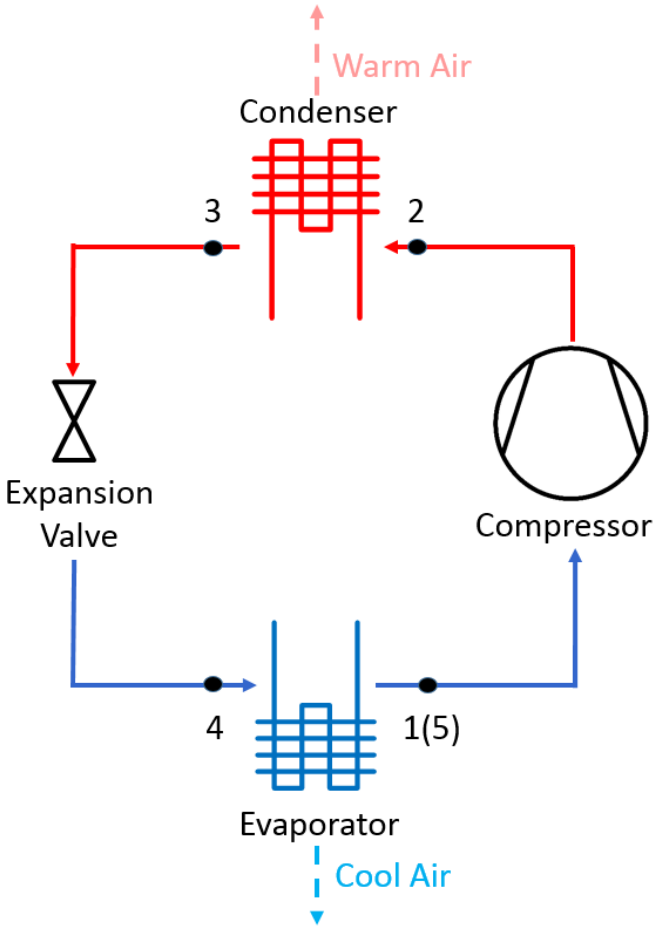

Figure 7: Schematic diagram of a typical vapor compression cycle

The refrigerant evaporates in the evaporator where it absorbs the heat so that it can provide cooling to the surroundings; at the same time, it converts two-phase refrigerant to a single phase vapor. Then, the low temperature low pressure vapor is

compressed by the compressor to a higher temperature and higher pressure vapor state. The refrigerant is then supplied to the condenser where it is cooled down to the saturation temperature corresponding to the high-side pressure and then condensed, during which the heat is rejected out. The condensed liquid passes through the expansion valve, where a portion of the refrigerant evaporates and then becomes vapor-liquid mixture. The temperature and pressure both decrease. Then, the refrigerant is supplied back to the evaporator. This refrigerant circulation is repeated to make use of the energy from the compressor to offer cooling and heating through evaporator and condenser.

To have a mass balance throughout the process, all these four components have the same mass flow rate under the steady state. Also, the process obeys the energy balance law, so that the heat rejected at the condenser should be the sum of cooling provided by the evaporator and the work input to the compressor.

According to the second law of thermodynamics, it is impossible to construct a device that operates without any work to transfer heat from a cooler body to a hotter one, so that the system requires energy input to the compressor to transfer heats from the low temperature level to the high temperature level, which is the main energy consumption part in a VCC system.

Figure 8 shows the pressure versus enthalpy (P-h) relationship for a typical ideal VCC. There is no heat exchange for the throttling process through the expansion valve, where the process undergoes isenthalpic process. For an ideal VCC, it is assumed that there is no pressure drop through the heat exchangers or pipes, the expansion process is isenthalpic while the compression process is isentropic, the vapor leaving the evaporator is in a saturated state, and so is the liquid leaving the condenser. The realistic VCC in a

HPCD is very similar to the ideal VCC, except that, in a real case, there would be superheating and subcooling, as well as a pressure drop through heat exchangers as shown in Figure 9 and Figure 10. Besides, the compression process is non-isentropic, and the isentropic efficiency of the compression should be considered. Point 0 and point 2 in Figure 10 show the isentropic and non-isentropic compression in a P-h diagram, respectively.

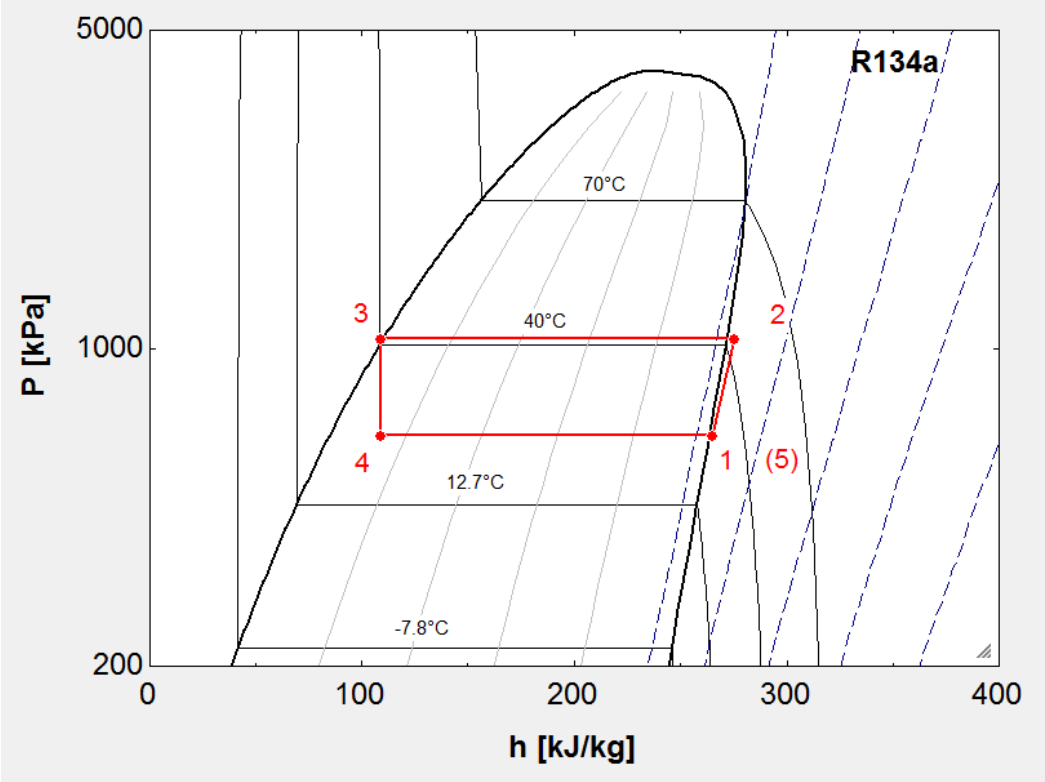

Figure 8: P-h diagram for an ideal vapor compression cycle

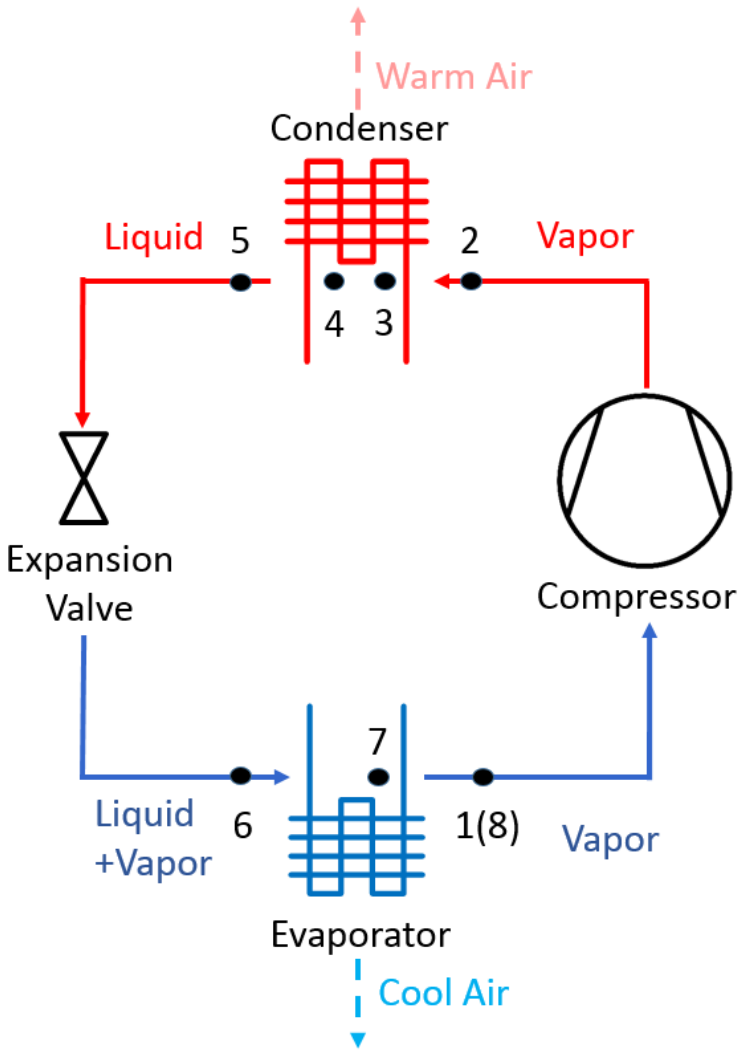

Figure 9: Schematic diagram for a realistic vapor compression cycle

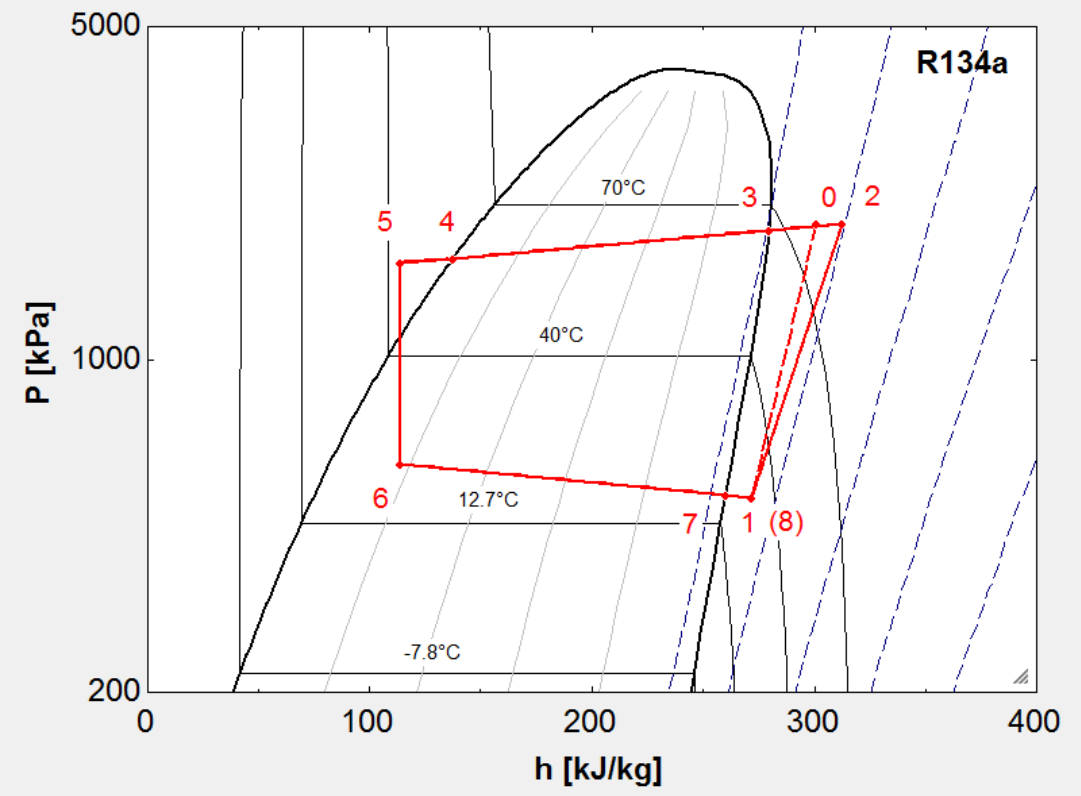

Figure 10: P-h diagram for a realistic vapor compression cycle

Figure 11 is a picture of commercial hybrid HPCD tested in this thesis. For the air-side, the air is circulated via the drum and the heat exchangers by a fan as described in Figure 12. The hot and dry air passes through the drum to absorb the moisture in the clothes (from point a3 to a1), and leaves in a warm and wet state. Then, the air passes through the evaporator where the moisture is condensed and removed from the humid air (from point a1 to a2). The cooler and dryer air is heated up by passing through the condenser (from point a2 to a3), and then flows back to the drum to capture the moisture again. The air cycle is formed in a closed-loop manner and repeated throughout the drying process until the laundry reaches the drying target.

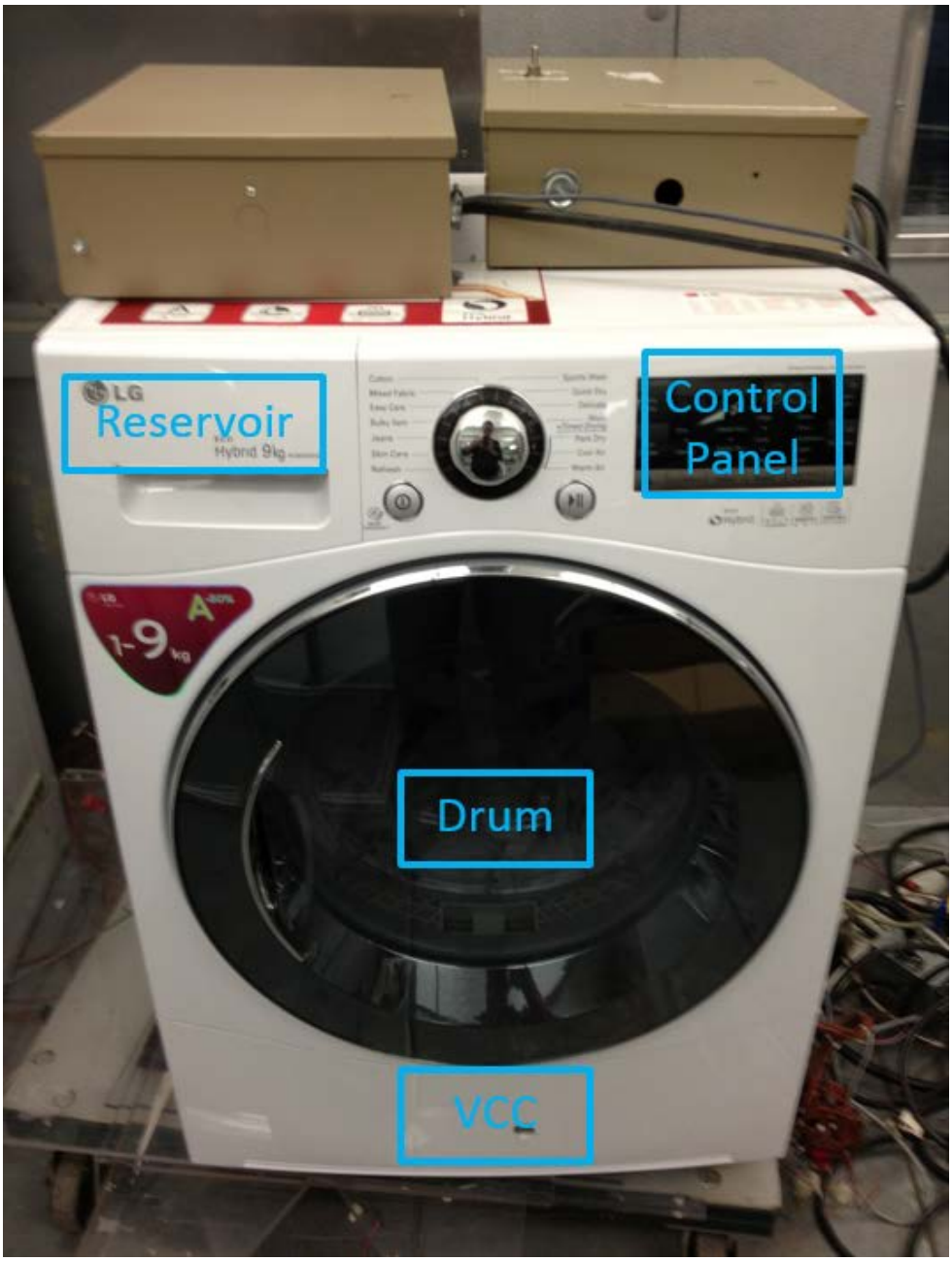

Figure 11: LG hybrid Heat Pump Clothes Dryer (Model number: RC9042AQ3Z)

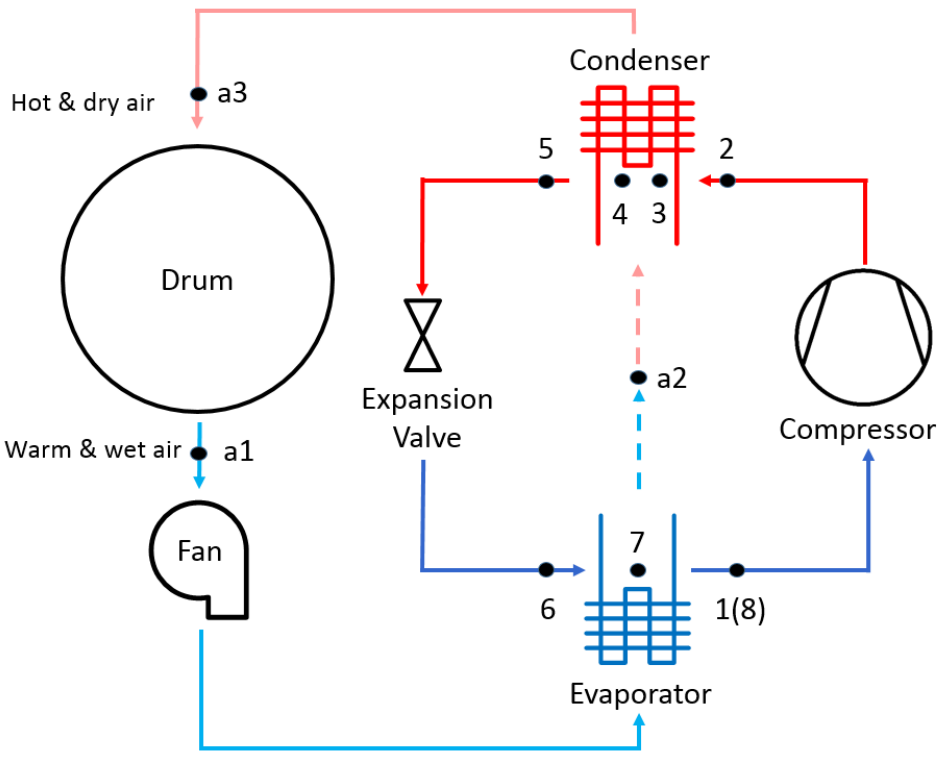

Figure 12: Schematic diagram of a heat pump clothes dryer

As shown in Figure 13, the VCC is located at the bottom of the CD system. The condenser is utilized as the heat source in a HPCD instead of the electric heater used in an electric CD. The evaporator and condenser installed adjacent to each other, form a counter flow with the air path. The humid air from the drum flows through the evaporator first where the heat is absorbed by the refrigerant and the water vapor is condensed and drained down, and then the dried air passes across the condenser where the refrigerant rejects heat into the air-side so that the air is heated up again before returning back to the drum. The refrigerant also circulates until the drying process terminates. The condensed water is pumped up into the reservoir located at the top left of the HPCD (shown in Figure 11) through the pipes (shown in Figure 14). In an HPCD, most of the energy is consumed by the compressor, which drives the vapor compression cycle.

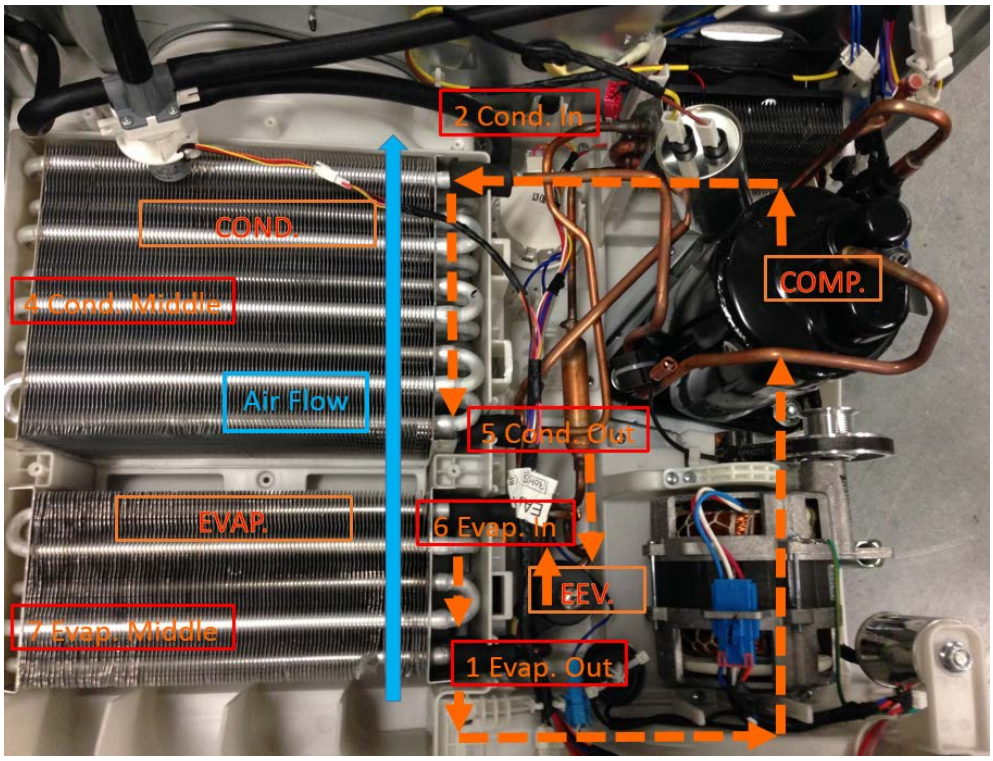

Figure 13: Vapor compression cycle in LG heat pump clothes dryer

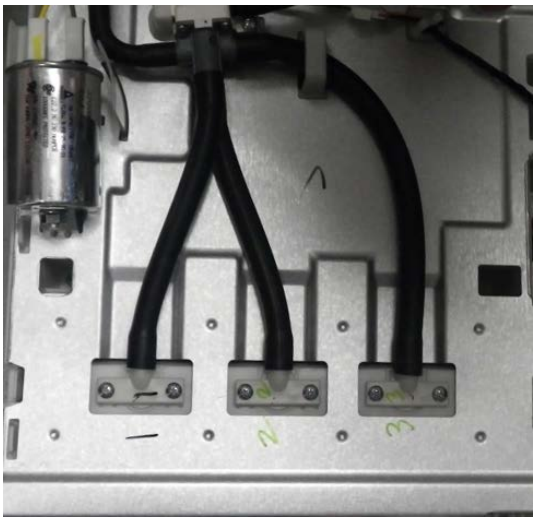

Figure 14: Pipes collecting condensed water

1.4 Objectives

As pointed out in the literature review, although HPCDs are much more energy-efficient than conventional residential electric CDs and have been popularized in Europe and some other countries, they are currently unavailable in the U.S.

The objectives of this study have been established as follows:

- Conduct experiments with a commercial hybrid HPCD from the European market, following the U.S. Department of Energy's (DOE) CD test standards
- Analyze and compare the performance under two different operational modes of the hybrid HPCD
- Explore HPCDs' potential for energy saving
- Analyze HPCD designs in detail
- Discuss the future improvements

2 Experiment

2.1 Test Standards

2.1.1 DOE Test Procedure

The rating and testing for residential CDs in the U.S. follow the Department of Energy's (DOE) test procedure. It is codified in Appendix D, Appendix D1 and Appendix D2 to subpart B of Part 430 of Title 10 of the Code of Federal Regulations (CFR) referred as DOE test standard 2005, 2011 and 2013 in this thesis [14].

DOE released the revisions for the CD test procedure in January 2011, January 2013, and August 2013. DOE is adopting proposals from organizations (such as AHAM, IEC and ORNL) to clarify some corresponding provisions in the test procedure [15], and therefore is presenting the latest version of the rule served as the basis for testing [16]. This revised CD test procedure, Appendix D1 introduced in January 2011 [17], demanded the manufacturers to comply with CD testing starting January 1, 2015. It updates a manual termination test procedure to offer a clearer rule, explains more regarding the cycle settings for different types of CD models, and also introduces the observation for standby mode and off mode for energy use. The drum capacity measurement methods as well as the test cloth measurements were clarified. A new energy efficiency metric, combined energy factor (CEF) which is defined as the bone-dry weight (BDW) per kWh of electricity consumed, is presented. Another major change is the larger test load with less moisture content and wet in a cooler water temperature.

Appendix D2 aims to include the testing methods used for a better observation for the automatic termination cycle. It is a remarkable feature for CD energy savings. By

effectively sensing the time when the laundry is dry, the system could terminate the drying process automatically right on time to avoid unnecessary energy consumption from over-drying. It is permitted that manufacturers comply with Appendix D2 early, but combining test standards is forbidden when rating the commercial CDs' energy-saving performance.

The major comparison among the DOE procedures is summarized and listed in Table 1 [15].

2.1.2 Energy Efficiency Evaluation Index

In the DOE 2005 standard, Energy Factor (EF) is a commonly used index utilized to assess the CDs' performance. It is described as the bone-dry weight (BDW) in pounds divided by the dehumidification energy consumption. Based on the same standard test procedure, a larger energy factor implies better CD performance, whereas in some academic literature entire energy consumption divided by BDW is utilized, which offers a more obvious way to show energy savings over EF based on BDW.

However, there are some other popular criterions in the academic or industrial fields. EF based on the weight of wet clothes (pre-dry weight) is a commonly used term, which is apparently defined as wet pre-dry mass divided by the total energy consumed. A specific moisture extraction rate (SMER) number provides evaluation of the tumble dryer's dehumidification performance. It calculates the evaporated water amount in kilogram per energy unit, which is a more straightforward index showing the dehumidification capacity. A high SMER infers a low energy loss [18]. Specific energy consumption (SEC) is another popular criteria. It is the ratio of the energy consumed in kWh to the moisture removed in kg, which is the inverse of SMER [19].

Table 1: Comparison of test procedures in Appendix D, D1, and D2

Appendix		**Appendix D**	**Appendix D1**	**Appendix D2**
Release Date			Jan. 6, 2011	Jan. 2013
Effective Date		Feb. 10, 2014	Feb. 10, 2014	A later date
Mandatory Date		Before Jan. 1, 2015	Jan. 1, 2015	A later date
Standby/off Mode Test Methods		None	Incorporates by reference IEC Standard 62301 with additional clarifications	
Ventless Test Methods		No	Yes	
Number of Cycles Per Year		416	283	
Referenced AHAM Standard		HLD-1-1974	HLD-1-2009	
Cycle Settings		Maximum temperature		Timer Dryers: Maximum temp.
				ATD: "Normal" Automatic Dry Cycle; Maximum Temp.; "Normal" or "Medium" Dryness
Cycle Termination		Timed dry		Timer Dryers: Timed dry
				ATD: Automatic Termination
Test Clothes		50 % cotton & 50 % polyester		
Test Load BDW	**Compact Size Dryers**	3.00 lbs. ± .03 lbs.		
	Standard Size Dryers	7.00 lbs. ± .07 lbs.	8.45 lbs. ± .085 lbs.	
Wetting Water Temperature		100 ± 5 °F	60 ± 5 °F	
Initial Remaining Moisture Content		70 % ± 3.5 %	57.5 % ± 3.5 %	57.5 % ± 0.33 %
Final Remaining Moisture Content		2.5 % ~ 5.0 %		Timer Dryers: 1 % ~ 2.5 %
				ATD: Run until completion of automatic cycle; < 2 %

*ATD: Automatic Termination Dryers

However, these generally utilized indexes based on the same standard are with the same BDW, weight of water contained in and the post dry mass (PDM), therefore, it is effortless to convert among these indexes.

The freshly introduced index CEF in Appendix D1, combines both the energy used in the active drying period (which is reflected by EF) and the standby/off mode, which is not mandatory to use before January 2015.

The U.S. Environmental Protection Agency (EPA) began to include the CDs in the ENERGY STAR program on May 19, 2014, and is effective on January 1, 2015 [20]. CEF is a key criteria for labeling an ENERGY STAR certified CD [21].

2.1.3 Energy Efficiency Requirements

Both DOE and ENERGY STAR list minimum efficiency requirements for residential CDs as shown in Table 2 [21] [22] [23]. The DOE minimum standard was revised in 2011, and will be effective in and after January 2015. Its efficiency level is relatively higher than that from the previous standards, which reflects the current market's progress in efficiency [13].

Table 2: Minimum efficiency requirements for residential clothes dryers

CD Product Classification	DOE		ENERGY STAR
	EF (products manufactured between May 14, 1994 ~ Dec. 31, 2014) (lbs./kWh)	CEF (products manufactured on or after Jan. 1, 2015) (lbs./kWh)	CEF (lbs./kWh)
i. Electric, Standard (4.4 ft^3 or greater capacity)	3.01	3.73 (Vented)	3.93 (Ventless or Vented)
ii. Electric, Compact (120V) (less than 4.4 ft^3 capacity)	3.13	3.61 (Vented)	3.8 (Ventless or Vented)
iii. Electric, Compact (240V) (less than 4.4 ft^3 capacity)	2.90	3.27 (Vented)	3.45 (Vented)
iv. Gas	2.67	3.30 (Vented)	3.48 (Vented)
v. Ventless Electric, Compact (240V) (less than 4.4 ft^3 capacity)	N/A	2.55	2.68
vi. Ventless Electric, Combination Washer-Dryer	N/A	2.08	N/A

2.1.4 Testing Load Material

DOE has been adjusting the test procedure from time to time. However, it does not reflect all issues identified in lab testing. For instance, the drying load material and shape varies substantially in the real world, while in DOE test procedure, only 50% cotton and 50% polyester in two dimensions is included [24]. It is desired to include diversity in clothing material as well as its shape to resemble the real households' laundry better than what is defined in the current test procedure. AHAM 1992 standard presents cotton fabric loads with significant diversity in the thickness, which resembles the actual clothing in some degree. In contrary, IEC standard suggests a mixture of cotton and synthetic clothing while it varies in its shape. However, partial cotton-content clothing with both diversity in thickness and shape is not included in any official standards [24]. Table 3 summarizes the fabric from different standards.

Table 3: Test load comparison [25]

Test Load Standard	**DOE 2005**	**AHAM 1992**	**IEC**
Fabric Composition	50% cotton 50% polyester	100% cotton	35% cotton 65% polyester
Fabric Type	2D sheets	Variety of clothing and linens	Shirts & pillow cases,
Characteristic	Basic material & shape	Diversity in thickness; Simulating realistic performance	Little diversity in thickness; Real clothing

Figure 15 shows the test loads used by Denkenberger et al., 2013 [25] for different standards. It clearly presents the information for each of these standard test loads in terms of the clothing fabric and thickness, where the bubble size reflecting the weight of a single piece in each load. Particularly, the bubbles for AHAM 1992 standard demonstrate the fabric's diversity in thickness and weight.

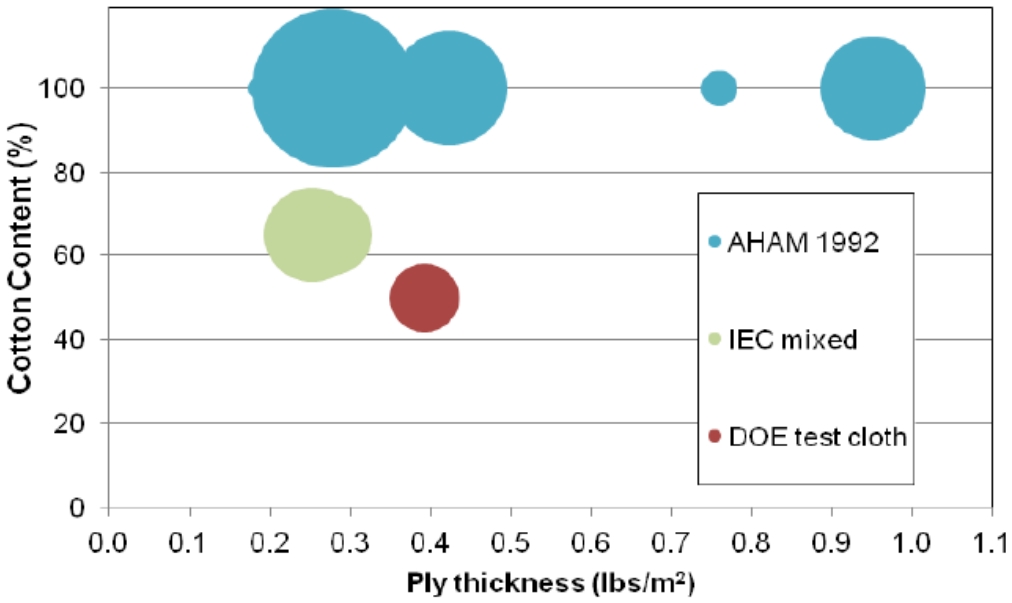

Figure 15: Test load comparison from three standards [25]

2.2 *Instrumentation and Measurement*

A hybrid LG HPCD from the European market was selected for testing in this thesis work. More product information is provided in Chapter 2.3.

In order to evaluate the hybrid HPCD performance, various kinds of measurements were performed by setting up instrumentations. The details of all sensors utilized, as well as their corresponding accuracy were listed in Table 4.

Table 4: Specifications of instruments

Instrument	Manufacturer	Model No.	Range	Systematic Uncertainty
Thermocouple	Omega	T type	-185 ~ 300 °C	± 0.5 °C
Relative Humidity Sensor	Omega	HX94C	3 ~ 95%	± 2 %
Anemometer	Omega	FMA-904-V	10 ~ 2000 FPM	± 1.5 % F.S.; Add ± 0.5 % of reading
Watt Meter	Ohio Semitronics	PC5-002X5	0 ~ 1 kW	± 0.5 % F.S.
		PC5-024D	0 ~ 12 kW	
Current Transformer	Ohio Semitronics	10424	0 ~100 A 100 : 5 (Current ratio)	1.5 % at 60 Hz.
Current Transducer	Kele	SC200-1	0 ~ 50 A	± 0.5 %

2.2.1 Temperature Measurement

A total of nineteen thermocouples were utilized. To keep the experiment consistent with the manufacturer's specification, the experiment was conducted as shipped. With this reason, T-type thermocouples were installed on refrigerant tube surface for refrigerant-side temperature measurement instead of using in-stream

thermocouples. Moreover, insulations were added to have better reading results. Air stream temperature measurements were taken with 12 thermocouples along with one thermocouple for the ambient air. Four thermocouples were installed at the inlet of the drum, another four between the evaporator and condenser, and also the remaining four at the outlet of the drum. Each set of readings was consolidated in the LabVIEW program with an accuracy of ± 0.25 °C for each region.

The thermocouple arrangement for the air stream is graphed in Figure 16, and in which the locations between evaporator and condenser is further illustrated in Figure 17.

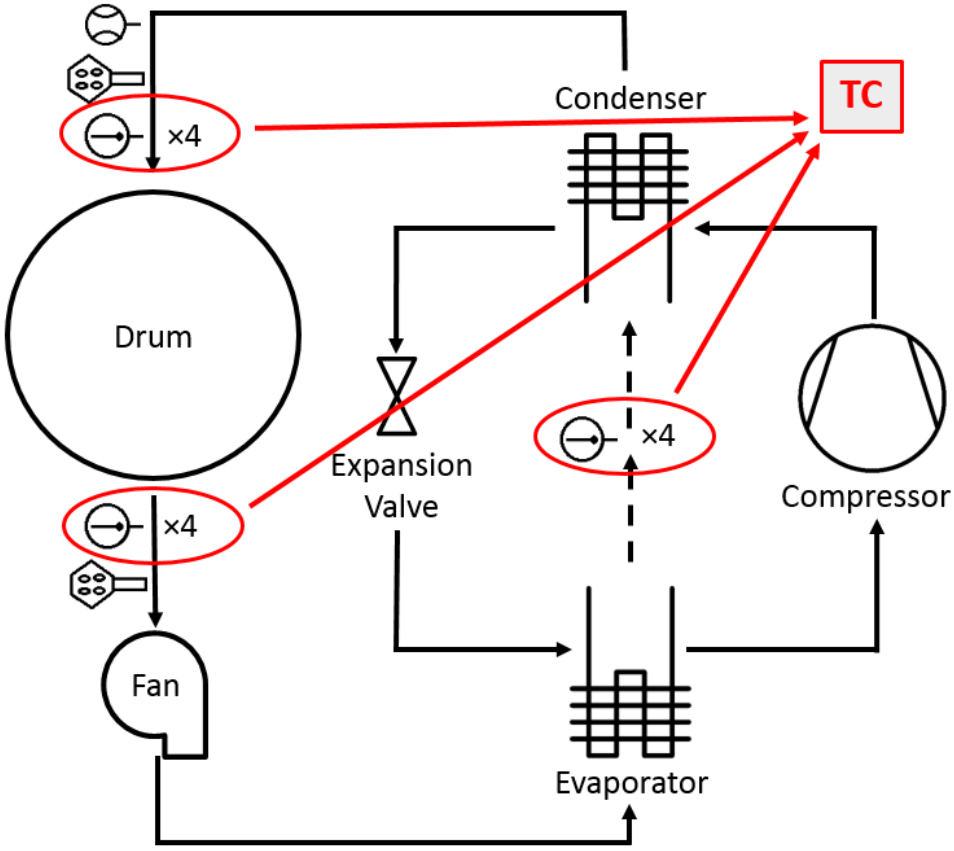

Figure 16: Locations of the thermocouples for air stream

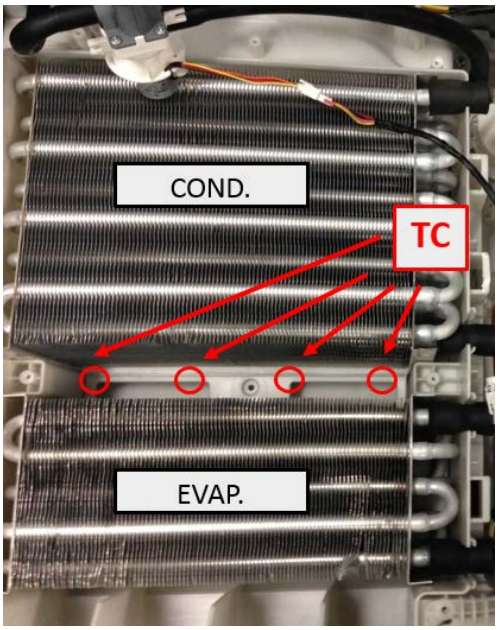

Figure 17: Air-side thermocouple locations between evaporator and condenser

At the same time, six thermocouples were distributed over the heat exchangers for refrigerant temperature readings. Similarly, they were divided into two parts: evaporator and condenser. The layout is shown in Figure 18: inlet, middle and outlet of evaporator, and condenser.

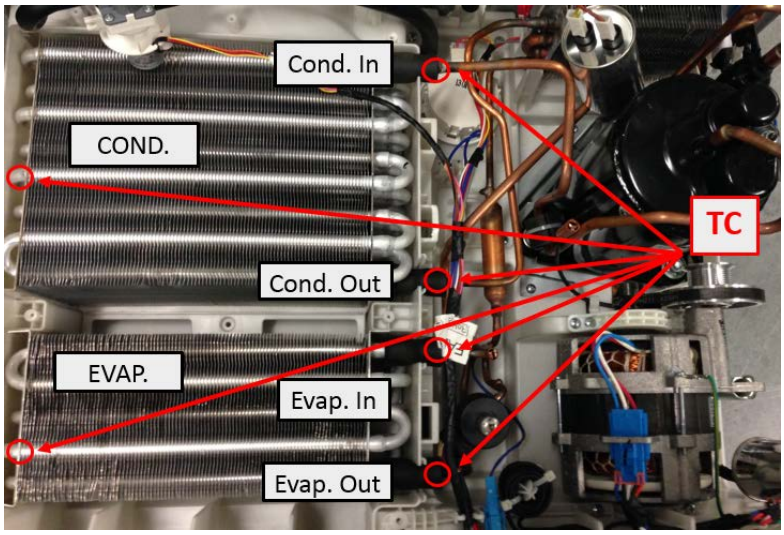

Figure 18: Referigerant-side thermocouples profile

2.2.2 Relative Humidity Measurement

Relative humidity was one of the most important properties in the analysis of a CD's performance. Two relative humidity (RH) sensors were installed to evaluate the relative humidity at both the inlet and outlet of the drum. One was placed after the lint trap of the drum before the fan, while the other was located at the back of the cabinet, in the air duct connected to the drum. They were both placed in the center of the air duct. The RH range was 3 to 95% with a systematic error of ± 2%, and with a temperature sensor ranging from -20 to 85°C. The moisture removed by VCC can be computed later from the RH measurements. Figure 19 is the picture of RH sensor utilized in the experiment.

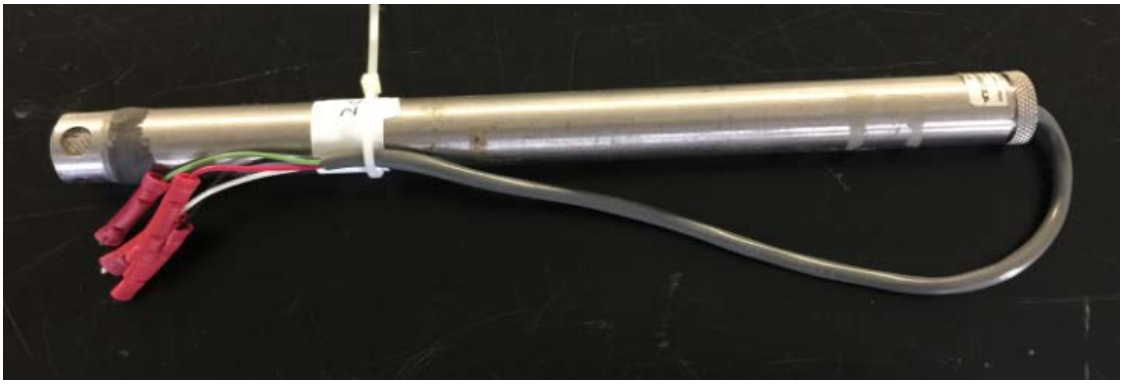

Figure 19: Relative humidity sensor

2.2.3 Air Flow Measurement

A hot wire anemometer was installed at the center of the drum inlet duct to measure the air flow velocity, which was then used to estimate the air flow rate. FMA-904-V shown in Figure 20 was selected with a 0 to 2,000 FPM air velocity range and a ±1.5% full scale accuracy at room temperature. Factory calibration data was taken.

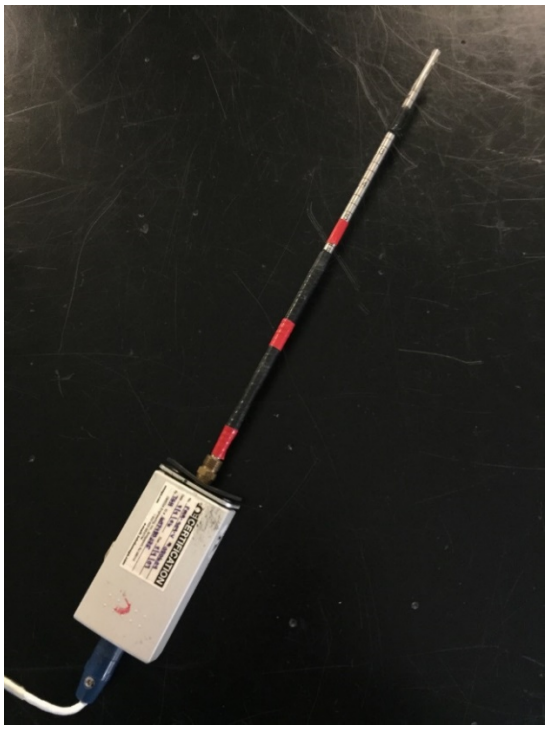

Figure 20: Anemometer

2.2.4 Power Consumption Measurement

Two different sensors were introduced to measure the power of the hybrid HPCD: watt meter and current transducer. Since the total power was informative in comparing among various drying operations, the total power consumption was measured with two watt meters: one for the electric heater, and the other for the remaining components, which turned on in Eco Mode. A watt meter selected for the electric heater power measurement was from Ohio Semitronics, Inc. (OSI) whose model number was PC5-024D. In order to increase measurement accuracy, a current transformer (shown in Figure 22) was also used. Another watt meter, PC5-002X5, was chosen to measure the power consumption of components other than the electric heater, which was also from OSI. It has a 0 ~1 kW power range with a ± 0.5% full scale accuracy. However, the model PC5-

002X5 measured the combined power including the compressor, drum motor, electric expansion valve and the control system. In order to see the power consumption of the compressor, a current transducer from Kele (model number, SC200-1) was added (as shown in Figure 23). It has a 0 to 50 A current range, along with a ± 0.5% full scale accuracy. The watt meter was connected externally to the HPCD's main power cable in a custom assembled electric box. The wire was also grounded for safety purposes (as shown in Figure 21). Since the LG HPCD targets the European market, it was designed with a voltage of 230 V and a frequency of 50 Hz. Therefore, the unit power was connected after the frequency converter.

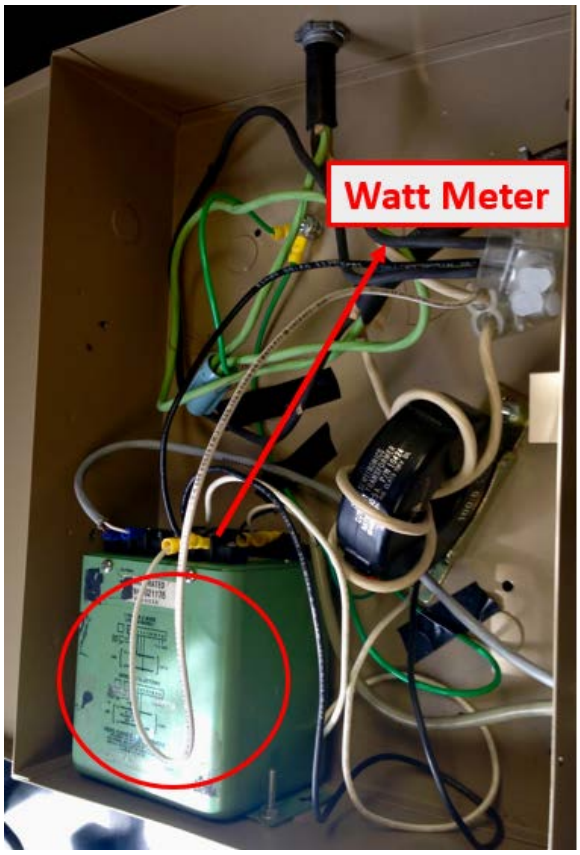

Figure 21: Watt meter for power consumption measurements in an electric box

Figure 22: Current transformer

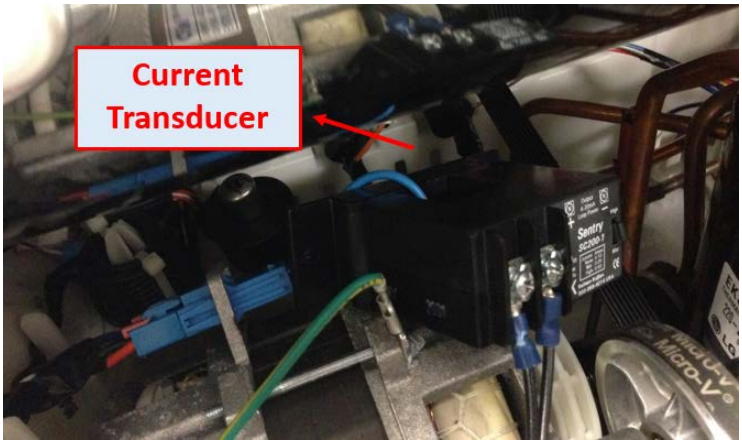

Figure 23: Current transducer for power consumption measurements

2.2.5 Data Acquisition System

All sensors were wired to a National Instrument's data acquisition system and connected with a computer for data recording, monitoring and processing by using a National Instrument's LabVIEW program. This program was integrated with a refrigerant

property module, XProps, to evaluate thermophysical properties of refrigerant [26]. Basic calculations were programmed and the results together with the collected data were displayed in LabVIEW for real-time data monitoring. For ease of data observation during testing, the graphical user interface (GUI) of LabVIEW was developed to show up to three graphs throughout the test. Moreover, all data were recorded at one second interval. The data was exported to an Excel file for further data analysis after each experimental test. Figure 24 shows the LabVIEW's GUI for the experimental tests.

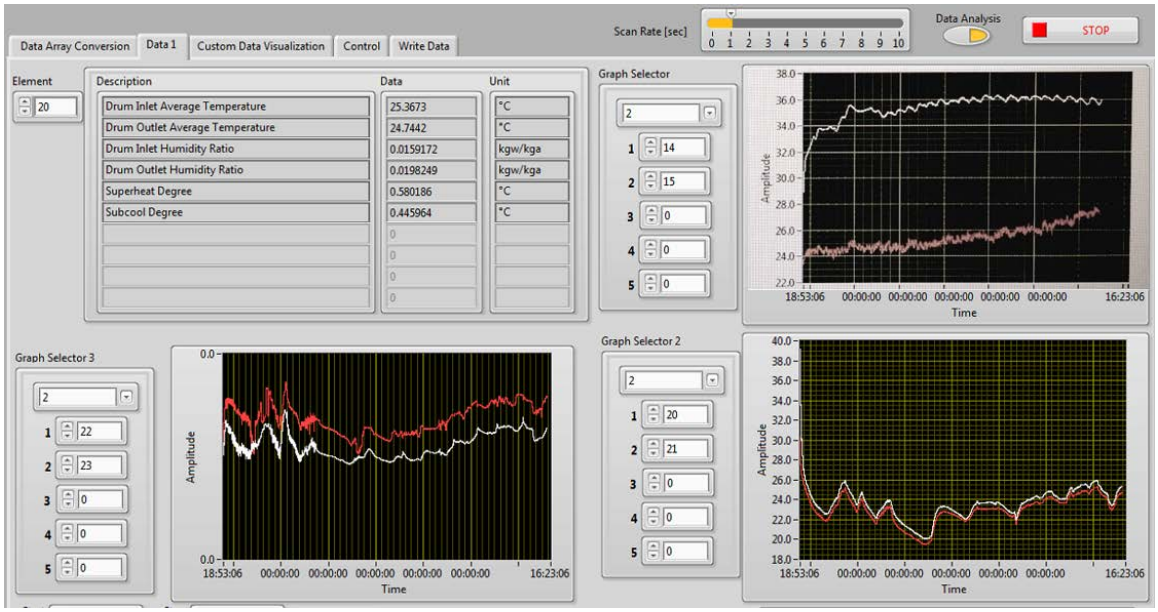

Figure 24: Graphical user interface of LabVIEW

2.3 Testing of the Heat Pump Clothes Dryer

After all instruments were installed, the hybrid HPCD was ready for testing. Before starting up with the actual testing, a few more preparation steps should be done first as described next.

2.3.1 Selection of Test Standard

In order to evaluate and compare the CD performance and efficiency, all the tests should be conducted according to the same test standard. The DOE 2005 test procedure was used for the experimental tests in this thesis work, which is used for specifying CD performance for almost all of the commercial CD products as well as experimental research work for CDs conducted prior to 2015.

2.3.2 Clothes Dryer Testing Mode Selection

A Hybrid HPCD was selected for testing in this thesis work as was mentioned in Chapter 2.2. It was a product from the European market and provided by LG Electronics, Inc., (Model number: RC9042AQ3Z), with a rated drying capacity of 9 kg and a drum capacity measured to be 130.3 liters (4.6 ft^3). It provides many clothes drying programs to satisfy different drying requirements. In terms of energy-saving feature, there are two types of programs: Eco Mode and Speed Mode. Eco mode is designed to save energy in which only VCC works, while speed mode is used to save drying time where both VCC and the electric heater work to speed up the drying process.

In order to have a better comparison for both drying processes, the dryer was tested in both modes. Moreover, the test was performed while using the dryer's sensor-dry feature without applying the manual termination specified in the DOE 2005 standard, so that the energy consumption could be calculated until its automatic termination period. However, the actual dehumidification completion state could be reevaluated from the measured data in each test. Therefore, the EF index defined in the DOE 2005 standard could be calculated accordingly. In addition, the energy consumption during the entire

programmed process including the standby period (which is in similar calculation manner to CEF in DOE 2011 standard) was also calculated for comparison.

2.3.3 Testing Cloth Preparation

Since the drum size of LG HPCD is 4.6 ft^3, which falls into the category of a standard size dryer (a CD with a drum capacity of 4.4 ft^3 or greater), so the testing load mass was selected to be 7 lbs (3.2 kg). Two different kinds of test cloths were purchased as preparation for the experiment: pure finished bleached sheets and T-shirts both with a combined material of 50% cotton and 50% polyester. The sheets were tailored to smaller pieces of 24 inches by 36 inches in accordance with the standard. During the shake down tests, a substantial amount of lint was collected after each test, which severely affected the behavior of the CD. As a result, the test cloth was switched to T-shirts in tests. Since the weight of each T-shirt was fixed, it was difficult to exactly match 7 ± 0.07 lbs, test weight was in a 5% deviation from the standard by using all possible combinations of different sizes and quantities.

2.3.4 Chamber Setup

The hybrid HPCD was located in a testing chamber, which could control environmental conditions from 5 to 45 ºC. Chamber was controlled to provide the ambient conditions at 25°C, and 50% RH to comply with the standard.

2.3.5 Testing Steps

Each of the tests was conducted in the same manner, and the main steps are described as follows:

1) Clean the lint trap completely before each of the tests to ensure a smooth circulation of the air.
2) Gather 7 lbs dry clothes and measure its BDW.
3) Wet the clothes to contain 70% moisture of the BDW with 100 °F water.

The DOE test procedure requires a standard clothes washer for the cloth load's treatment. Since the clothes washer exceeded the project funding, the preconditioning of the clothes was done by imitating the rinsing process.

4) Place the load into the drum of the LG HPCD.
5) Set the mode to be on "Eco" with only VCC working;

   Or set the mode to be on "Speed" with both VCC and electric heater working for comparison.
6) Record the data with DAQ while the dryer is in operation for further analysis.
7) Weigh the post dry mass (PDM) of the load after the drying cycle to see if it is within the acceptable range, or the test would be considered to be invalid and the test needed to be repeated.

The test conditions were summarized in Table 5.

Table 5: Test conditions summary

Mode	Test No.	BDW	Wet Water Temp	Wet Mass (PreDry)	Dry Mass (PostDry)	Total Water Removed	Total Operation Time
		g	°F	g	g	g	Minutes
Eco	**1**	3,336	99.6	5,678	3,347	2,331	119
	2	3,337	99.6	5,708	3,341	2,367	126
Speed	**1**	3,360	100.1	5,711	3,336	2,375	112
	2	3,347	100.3	5,680	3,337	2,343	112

3 Test Results

After a series of experimental tests were conducted with LG Hybrid HPCD, four valid test results were obtained: two for Eco-mode and other two for Speed-mode.

3.1 Data Analysis

Since the one of objectives is to investigate the performance of a HPCD, the first test conducted in Eco Mode was analyzed and presented in detail in this chapter. A comparison between Eco Mode and Speed Mode is provided in Chapter 3.2, and the total energy consumption is compared in 3.2.3.

All raw data collected in LabVIEW were exported to Excel for data analysis. Software packages including EES and CoilDesigner were utilized for further data analysis. EES is the abbreviation for Engineering Equation Solver. It is a useful tool to solve a set of complex equations, generates high-quality plots, and does uncertainty analysis. It especially calculates the thermophysical properties with its internal property databases [27]. CoilDesigner is a sophisticated heat exchanger design tool, which is widely used in designing, analyzing, and optimizing an air-to-refrigerant heat exchanger in a steady-state [28].

3.1.1 Humidity Ratio

Humidity ratio (HR) is an important factor for tracking the drying process, and can be used to determine the termination time point. It is taken into major account by the CD manufacturers not only for saving the energy, but also for protecting the clothes from the damage by exposure to high temperature air during the over-drying period. The

humidity ratio was not directly measured, but calculated from the temperature and RH measurement from the tests. Figure 25 shows the inlet and outlet HRs of the drum. As indicated in the figure, the inlet and outlet HRs achieved a balance after 85 minutes from the start. The default drying time programmed in CD product was 200 minutes for Eco Mode, while the actual drying time was only 119 minutes, which was determined by its sensor-dry feature. Moreover, the compressor also shut down at the end of the automatic cycle according to the power measurement. The HRs continued to decrease after 85 minutes, which could be resulted from air leaks as is discussed in Chapter 4.2.2.

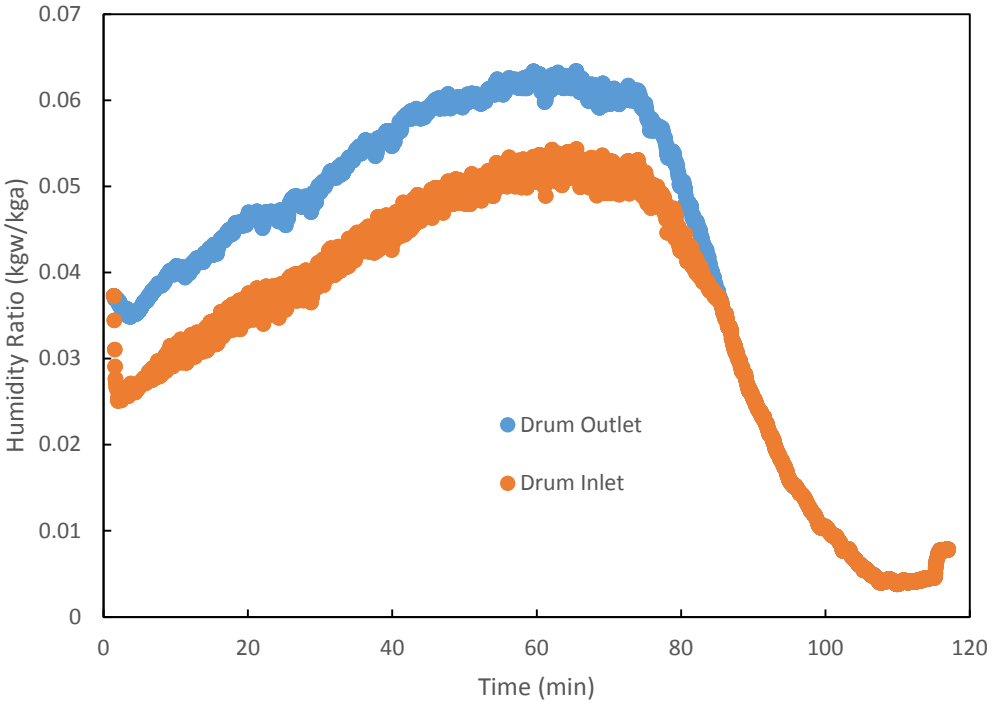

Figure 25: Drum inlet and outlet humidity ratios

One possible reason for the 34-minute gap between the completion of dehumidification and the termination of the dryer is that the RH sensor installed at the bottom front provided inaccurate humidity information to the controller of the HPCD.

Since the RH is affected by the temperature even at the same HR, it is better to use the HR, which is the property providing the information on the amount of water vapor in the air, for determining the actual status of the drying process. Another reason could be that due to the distance between the center of the drum and the front door, the sensor fails to sense the correct RH value inside the drum properly. A third reason might be that the CD manufacturer needs to consider all circumstances for ensuring a complete drying for any type of clothing. Because of this, the default drying time is also relatively long. A fourth reason could be the HPCD takes into account the cooling-down period before taking the clothes out of the drum so that the users could take the clothes at temperatures similar to sunbathing condition instead of a relatively high temperature. While the current experimental study concerns more on the energy saving, the cooling-down phase is included for the CDs' evaluation in the updated DOE procedure [29] so that the corresponding CEF was calculated for comparison in Chapter 3.2.3. Figure 26 shows the moisture sensor installed by the manufacturer.

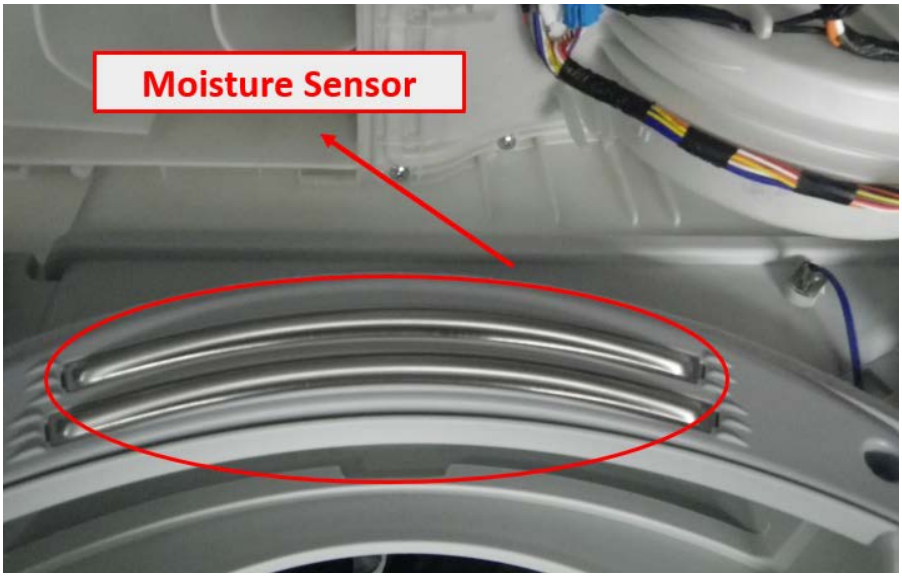

Figure 26: Moisture sensor of LG heat pump clothes dryer

Figure 27 clearly demonstrates the dehumidification inside the drum by taking the HR difference between the inlet and outlet. The HR difference fluctuated around about 0.01 kgw/kga up to 80 minutes, and then fell down dramatically in the following five minutes. After that all the moisture was removed from the load. And the peak moisture removal rate occurred at 45 minutes.

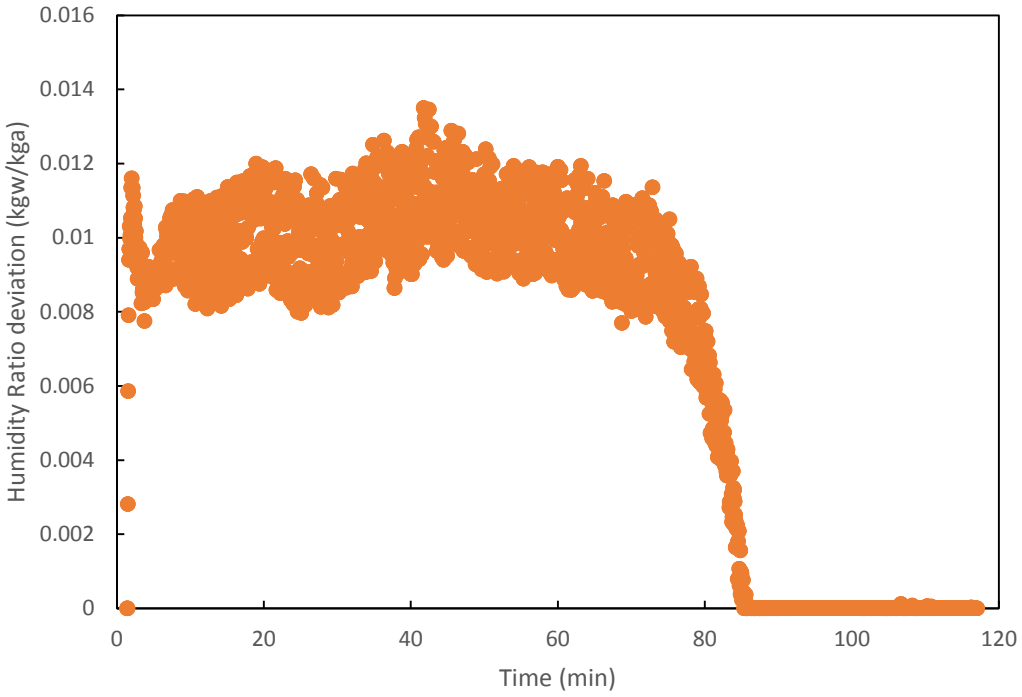

Figure 27: Humidity ratio deviation inside the drum

By reviewing the measured RH data in Figure 28, it was found that both the inlet and outlet RH levels dropped and reached to the same level towards the end of the test. The RH deviation keeps at about 74% between 5 and 70 minutes, and then sharply decreased to zero during the last 35 minutes.

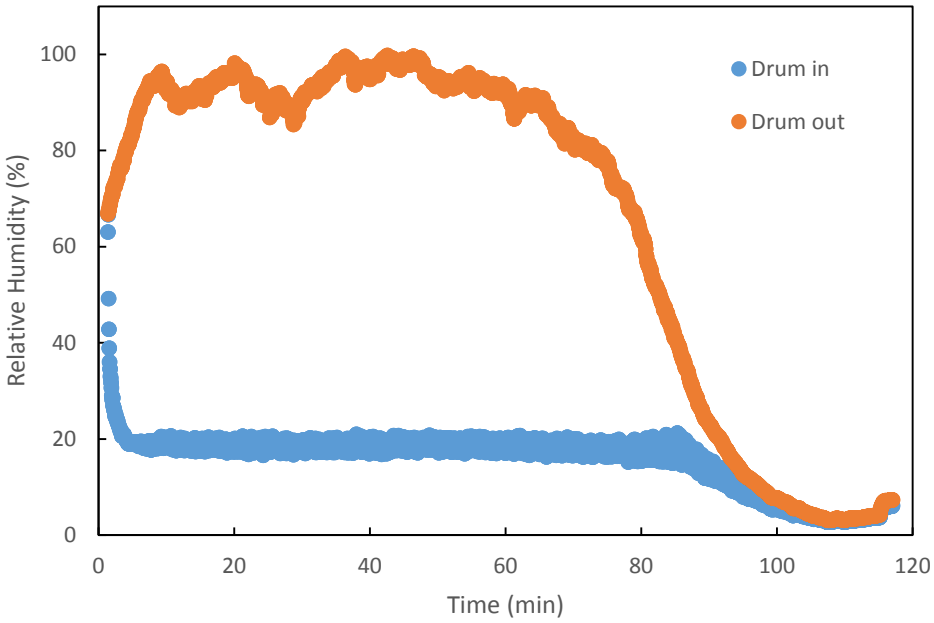

Figure 28: Drum inlet and outlet relative humidity

3.1.2 Temperature

Temperature data was directly measured from thermocouples.

3.1.2.1 Refrigerant-side Temperature

3.1.2.1.1 Evaporator Refrigerant Temperature

Figure 29 shows the refrigerant temperatures collected at the inlet, middle and outlet of the evaporator. In overall, three temperature profiles had similar trend. As the dehumidification proceeded, the refrigerant temperature increased due to the increased drum outlet temperature (Figure 32). However, as the moisture contained in the clothes was reduced, the drum outlet dew point temperature started to decrease and deviated from its dry-bulb temperature as shown in Figure 30. Therefore, the sensible heat factor of the evaporator increased, which resulted in a reduced cooling capacity and reduced evaporator temperature in the second part of the test.

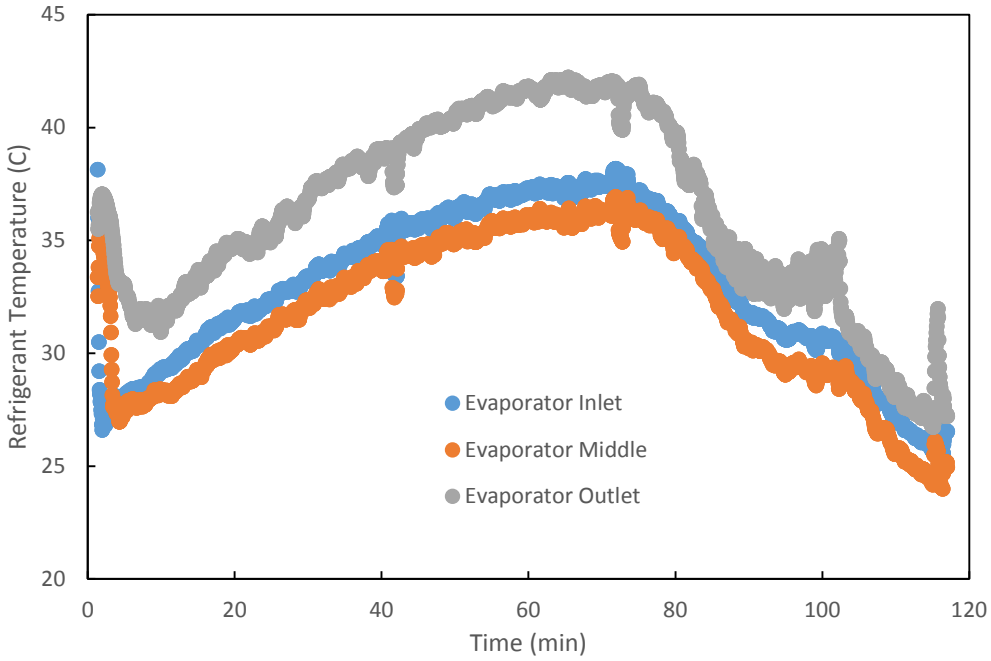

Figure 29: Evaporator-side refrigerant temperatures in Eco Mode

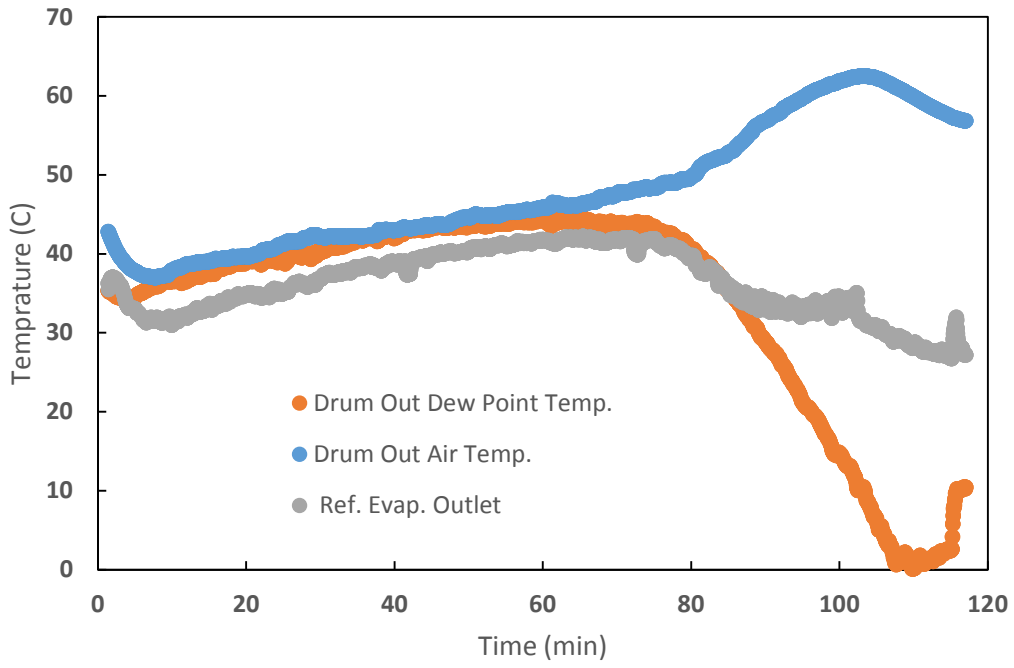

Figure 30: Air-side and ref-side temperature at evaporator outlet

3.1.2.1.2 Condenser Refrigerant Temperature

Similarly, the refrigerant temperature profiles of the condenser are presented for the inlet, middle and outlet in Figure 31.

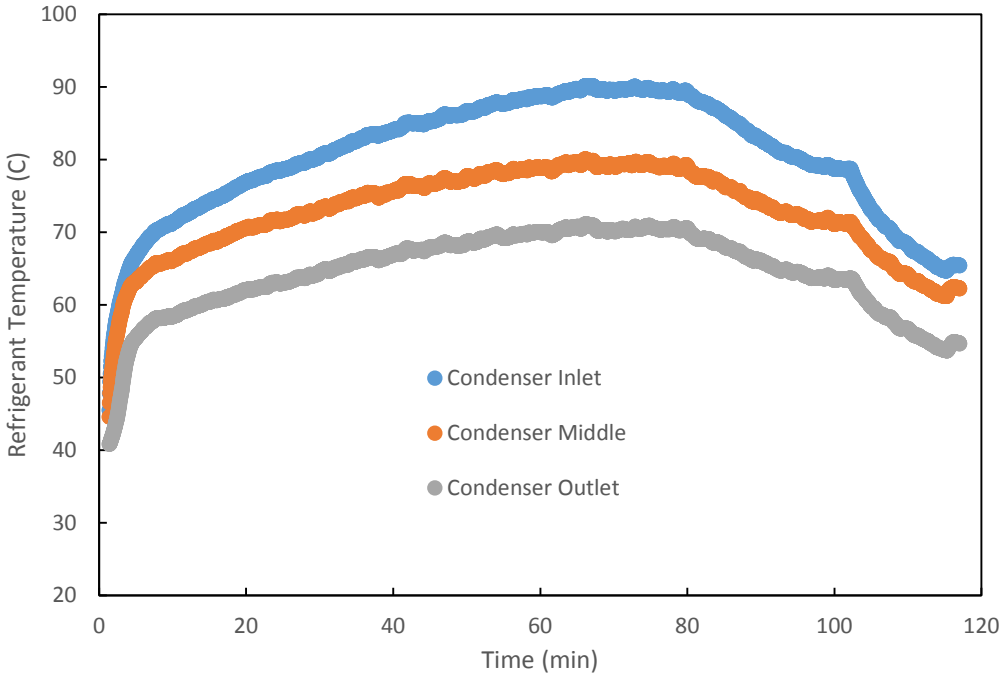

Figure 31: Condenser-side refrigerant temperatures in Eco Mode

3.1.2.2 Air Side Temperature

The air-side temperature of Eco Mode profile is illustrated in Figure 32.

3.1.2.2.1 Drum Inlet Air Temperature

Drum inlet air is the air that discharged from the condenser after gaining heat from the refrigerant so that its temperature shows a similar trend with the condenser refrigerant-side temperature with an average approach temperature of 9.3K.

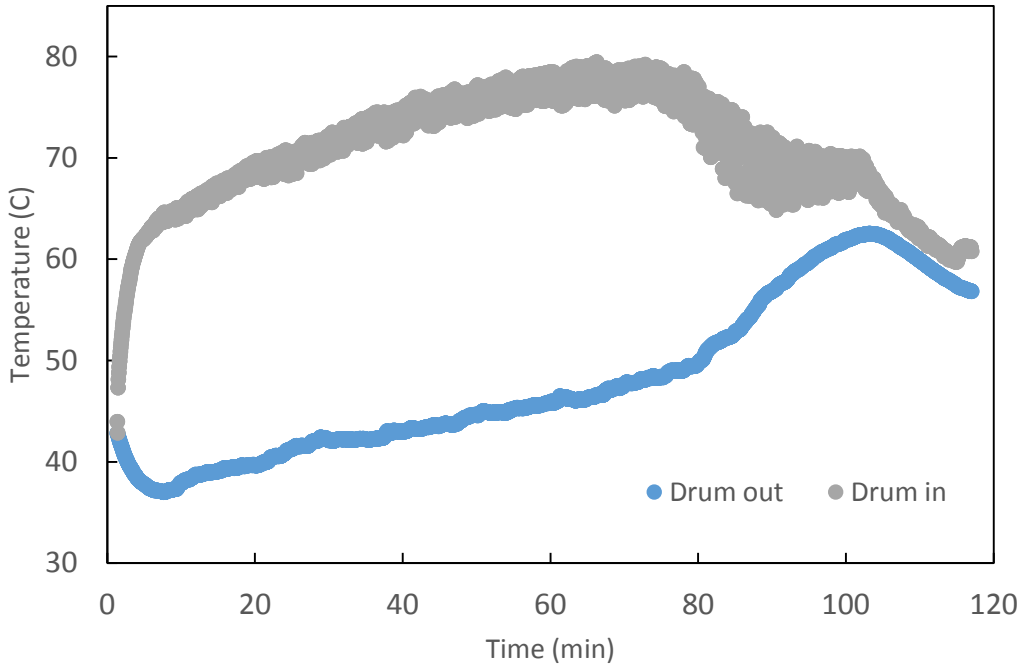

Figure 32: Air-side temperature profiles in Eco Mode

3.1.2.2.2 Drum Outlet Air Temperature

Figure 32 shows that the drum outlet temperature steadily increased at a relatively smaller rate, 0.16 ºC/minute, until 85 minutes. During this period, the evaporator's approach temperature between the refrigerant- and air-side was calculated to be 2.2K. The drum outlet temperature increased rapidly after 85 minutes, which is the drum dehumidification termination time point according to the HR analysis.

3.1.2.2.3 Drum Dehumidification Process

During the first 85 minutes, most of the condenser heat transferred to the drum inlet air was used to increase clothes and drum metal temperature, which helped the

vaporization of the water contained in the clothes. When the drum metal temperature became high enough, the drum lost heat to the ambient by convective and radiative heat transfer although it was relatively smaller than one used for clothes drying. As a result, there was a drop in air temperature from the inlet to the outlet. And the temperature difference remained at about 30 K as shown in Figure 33.

3.1.2.2.4 After Dehumidification Process

After the dehumidification was completed at 85 minutes, the heat supplied by the condenser gradually shifted for sensible heating of the drum and clothes from the vaporization of water contents in clothes. This heating speed was an average of 0.4ºC/ minute from 85 minutes to 103 minutes. Therefore, the drum and clothes temperature was getting closer to the drum inlet temperature. However, the drum inlet temperature was decreased during this process because of the decrease in the dehumidification in the evaporator, which resulted in condensation temperature decrease. Moreover, the drum inlet and outlet reached an average temperature at 66ºC before starting the cooling down period. This process is also reflected by the temperature deviation in Figure 33.

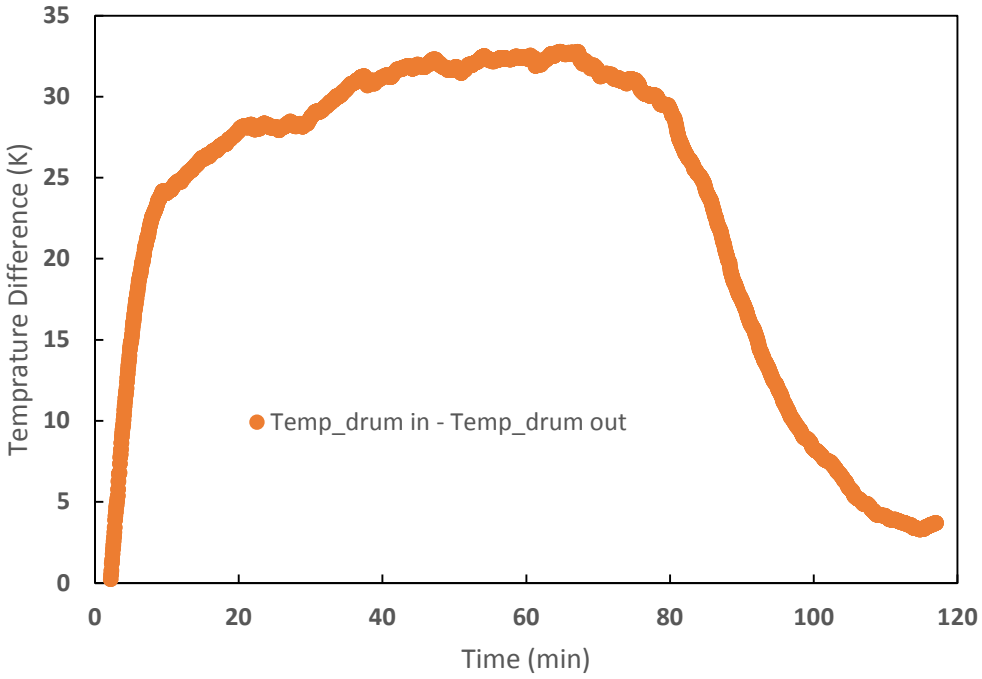

Figure 33: Air temperature difference between drum inlet and outlet

3.1.3 Pressure

Since the experiment test was conducted with the HPCD as shipped, only temperature information was collected. Therefore, the saturation pressures were calculated from the evaporator inlet (point 6) and condenser middle temperatures (point 4) as shown in Figure 9 as they were considered to be in two-phase. Figure 34 shows the condensing and evaporating pressures during the drying process, which were approximately 2,546 kPa and 929 kPa, respectively, from 40 minutes to 80 minutes.

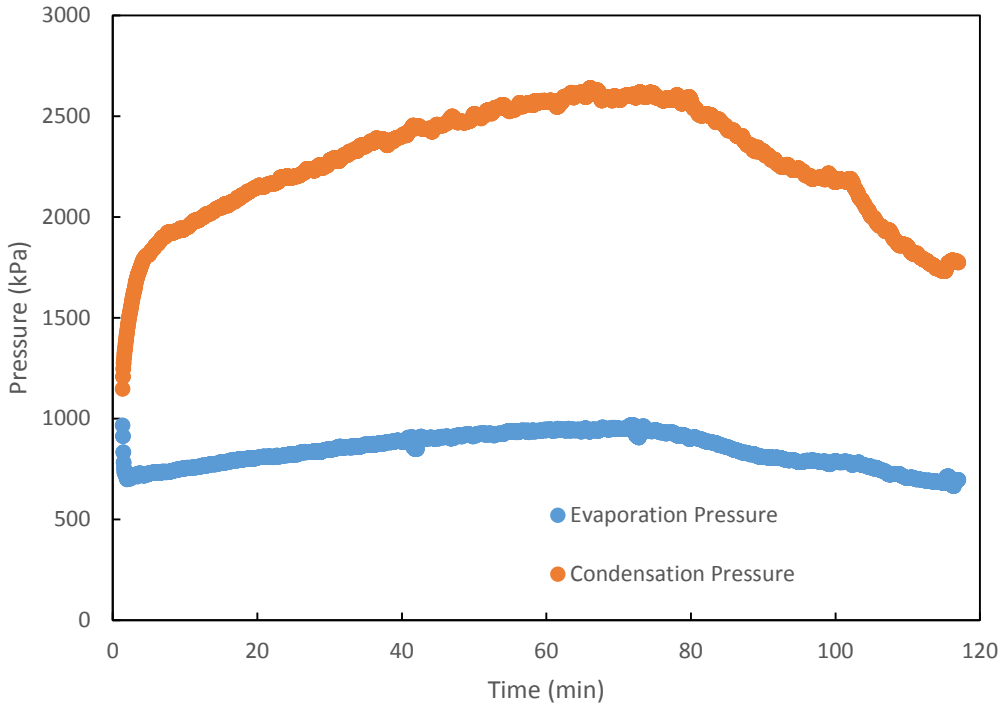

Figure 34: Refrigerant pressure profiles

3.1.4 Refrigerant Mass Flow Rate

LG HPCD utilized a rotary compressor from its own company. The model number of the compressor installed was EKS080PAA. According to manufacturer's compressor catalog [30], the compressor's displacement volume was 80 cc/rev, and its rotational speed was 3,000 RPM (50 Hz times 60 seconds), while in simulation, the rotational speed was assumed to be 2,950 RPM, considering the motor slip in the compressor. The detailed compressor specifications are listed in Table 6.

Table 6: Specifications of Compressor (EKS080PAA)

Model Name	Representation	Information
E	Refrigerant	R134a
K	Compressor Size	Φ112
S	Generation Code	Super EER
080	Capacity	Displacement Volume: 080 = 8.0cc / rev × 10
P	Phase / Power Source / Frequency	Single / 220 ~ 240 V / 50 Hz
A	Motor Specification	A type
A	Exterior Specification	A type

The isentropic efficiency is the ratio of the work for the isentropic compression to the work input to the compressor shaft as shown in Equation 1.

$$\eta_{isen} = \frac{h_{dis,isen} - h_{suc}}{h_{dis} - h_{suc}} \qquad \text{Equation 1}$$

The compressor efficiency is the product of the isentropic and the compressor motor efficiency. The motor efficiency was assumed to be 85% in this study. Then the calculated isentropic and compressor efficiencies were to be 65% and 55%, respectively.

Then, from the definition of the compressor efficiency as show in Equation 2, the refrigerant mass flow rate (MFR) could be calculated. The average MFR was estimated to be 9 g/s.

$$\dot{m}_{ref} = \frac{P_{comp} \cdot \eta_{comp}}{h_{dis,isen} - h_{suc}} \qquad \text{Equation 2}$$

When taking the compressor suction pressure and temperature from the experimental data, the suction density could be determined. Volumetric efficiency is the ratio of the actual MFR of the gas entering the compressor to the theoretical MFR of the compressor as shown in Equation 3. Then the calculated volumetric efficiency was 60% for this compressor.

$$\dot{m}_{ref} = \eta_{vol} \times \rho_{suc} \times \dot{V}_{displace}(RPM/60) \qquad \text{Equation 3}$$

Both the isentropic and volumetric efficiencies are influenced by the pressure ratio through the compressor [31].

Figure 35 shows the calculated results of the MFR throughout the whole drying process. The profile shows a relatively steady condition during the drying process.

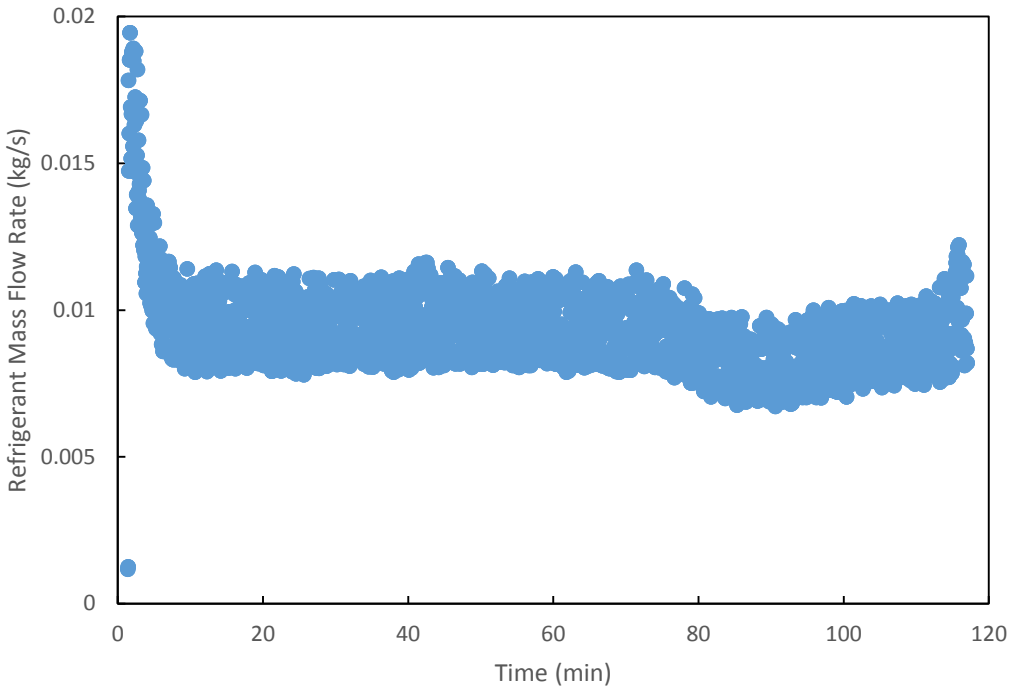

Figure 35: Refrigerant mass flow rate profile

3.1.5 Air Flow Rate

The average air velocity was 8.46 m/s (1,667 fpm) from the data taken from the anemometer. It should be noted that the velocity was measured at the duct center. According to the turbulent velocity profile shown in Equation 4, the average velocity could be calculated.

$$\frac{\langle u \rangle}{v_c} = \left(1 - \frac{r}{R}\right)^{1/n} \qquad \text{Equation 4}$$

where: R is the radius of the circular pipe;

r is the distance from the center in the circular pipe;

$\langle u \rangle$ is the average velocity at r;

v_c is the center velocity;

and the number n is normally between 6 to 10 for turbulent flow as shown in Figure 36 [32].

The average velocity of the air flow is,

$$\bar{u} = \frac{\int_0^R \langle u \rangle dr}{R} \qquad \text{Equation 5}$$

And it is calculated to be:

$$\bar{u} = \frac{n}{n+1} v_c \qquad \text{Equation 6}$$

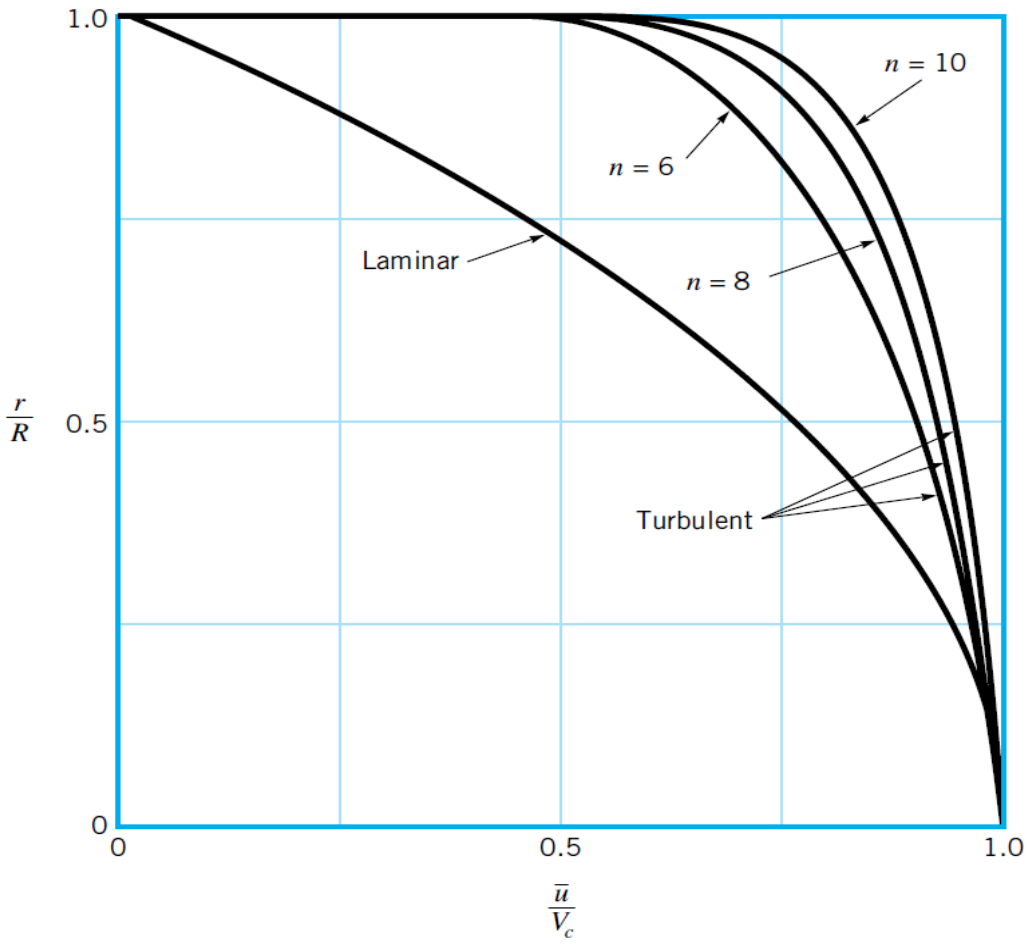

Figure 36: Turbulent velocity profile [32]

Since the air flow was highly turbulent according to the velocity measurement, a higher value for n was more appropriate. Moreover, the deviation between 9 and 10 for n was only 1%. Therefore, 9 was chosen for calculation, and the overall average velocity should be 90% of the center average velocity.

The air-flow rate (AFR) was then calculated by considering the velocity profile as well as the cross-sectional area where it was located, and was calculated to be 0.0378 m^3/s.

3.1.6 Uncertainty Analysis

Uncertainty analysis was considered for all measured and calculated variables. Systematic uncertainty and random uncertainty were both considered. The systematic uncertainty, u_{sys}, is affected by the accuracy of the measurement instruments and Equation 7 is utilized for computation [33].

$$u_{sys} = \sqrt{\left(\frac{\partial f}{\partial x_1} * u_1\right)^2 + \left(\frac{\partial f}{\partial x_2} * u_2\right)^2 + \cdots + \left(\frac{\partial f}{\partial x_i} * u_i\right)^2} \quad \text{Equation 7}$$

where, u_n means the systematic uncertainty for each measured component;

$\frac{\partial \mathrm{f}}{\partial \mathrm{x}_n}$ represents the partial derivative for each calculated component with respect to each measured component x_n.

Table 7 summarizes the systematic uncertainties of the instruments.

Table 7: Systematic uncertainties of measured parameters

Parameter	**Range**	**Systematic Uncertainty**
Thermocouple	-185 ~ 300 °C	± 0.5 °C
Relative Humidity Sensor	3 ~ 95%	± 2 %
Anemometer	10 ~ 2000 FPM	± 1.5 % F.S.; Add ± 0.5 % of reading
Watt Meter	0 ~ 1 kW	± 0.5 % F.S.
Current Transformer	100 : 5	1.5 % at 60 Hz.
Current Transducer	0 ~ 50 A	± 0.5 %

The random uncertainty, u_{rand}, is the outcome from the unpredictable fluctuations of the readings, which is influenced by the measurement precision and it could be expressed by standard deviation for each measurement as shown in Equation 8.

$$u_{rand} = \sqrt{\frac{1}{n-1}\sum_{i=1}^{n}(x_i - \bar{x})^2} \quad \text{Equation 8}$$

where n means the number of the data points in a data set,

x_i indicates the measured parameter data point,

and $\bar{x}$ illustrates the average for the measured parameters of the data set.

The total uncertainty is the summation of systematic uncertainty and random uncertainty.

$$u_{total} = u_{sys} + u_{rand} \quad \text{Equation 9}$$

3.2 Comparison of Operational Modes

Test results were compared for two different operational modes in this section.

3.2.1 Humidity Ratio Comparison

By calculating the HR for all four tests in the same manner as in 3.1.1, the dehumidification termination time point was observed by comparing the HR difference between the drum inlet and outlet. A summary is listed in Table 8.

Table 8: Dehumidification time summary

Operational Mode	**Dehumidification Time**	
	Minutes	
Eco Mode 1	85	89
Eco Mode 2	92	
Speed Mode 1	73	72
Speed Mode 2	70	

Speed Mode took about 20% less time to finish the drying process, which makes sense because the electric heater promotes the heating capacity and therefore accelerates the dehumidification process. Since test results under the same operational mode were similar to each other, only Eco Mode 1 and Speed Mode 1 results were compared from hereafter.

Figure 37 shows the HR comparison between Speed Mode test 1 and Eco Mode test 1.

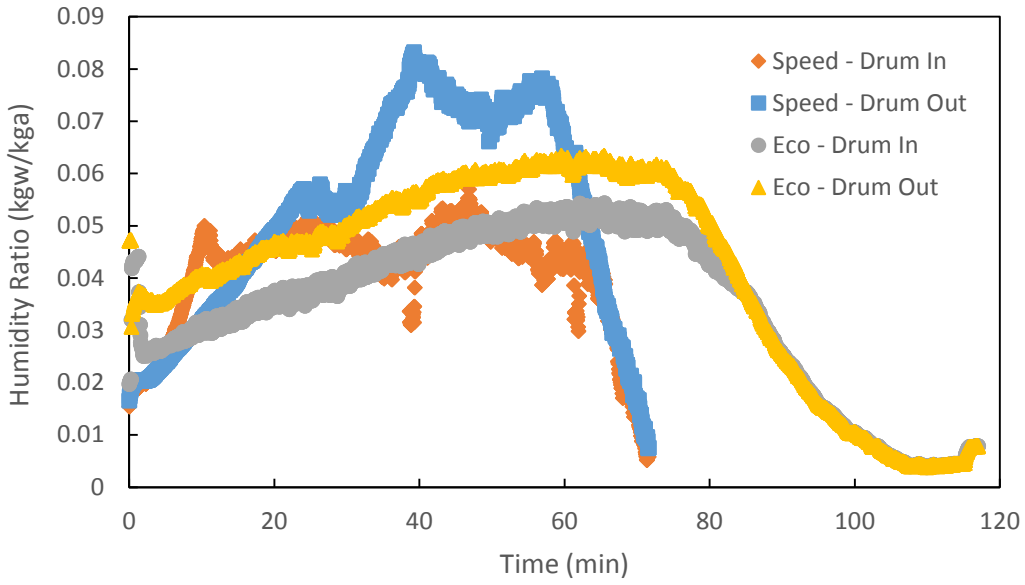

Figure 37: Humidity ratio comparison between Eco Mode 1 and Speed Mode 1

The average HR difference between drum inlet and outlet in speed mode 1 (0.012 kgw/kga) was larger than that in eco mode 1 (0.008 kgw/kga), and the highest moisture removal rate typically occurred at the 40 to 60 minutes in Speed Mode 1. However, it was varied gently in Eco Mode 1.

3.2.2 Temperature Comparison

An air-side temperature comparison between Eco Mode test 1 and Speed Mode test 1 is shown in Figure 38.

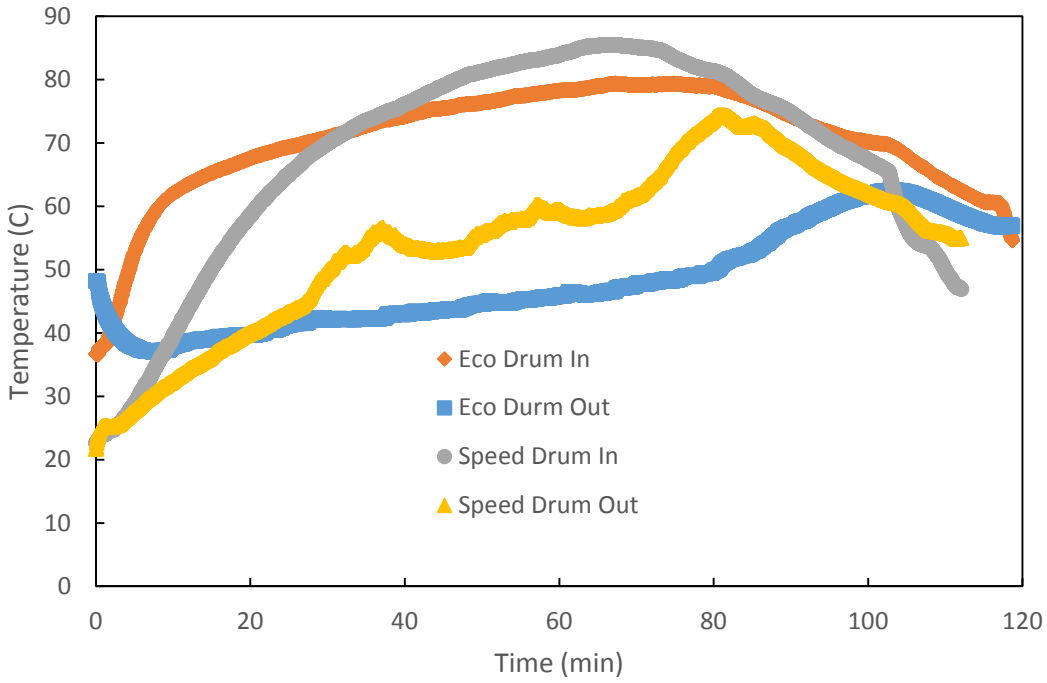

Figure 38: Air-side temperature comparison between Eco Mode and Speed Mode

This graph includes the cooling down process, in which air was cooled down towards 55ºC in both tests. The electric heater increased the drum inlet temperature by 7 ºC compared with that from the Eco Mode. However, the average temperature difference between the drum inlet and outlet narrowed down from 22 K to 14 K, which could have resulted from the higher heating capacity. More heat was used not only to vaporize the water contained in the clothes but also increase the temperature of the drum and the clothes resulting in higher outlet temperature.

3.2.3 Energy saving analysis

The measured power consumption is studied first. Followed by the energy consumption, and then the energy factor was evaluated.

3.2.3.1 Power Consumption Comparison

Figure 39 shows the compressor, motor and total power consumption profiles in the first Eco Mode test. The compressor power was calculated from the current measurement by assuming 230 V, and the motor power in the figure represents the power consumed by the system except for the compressor.

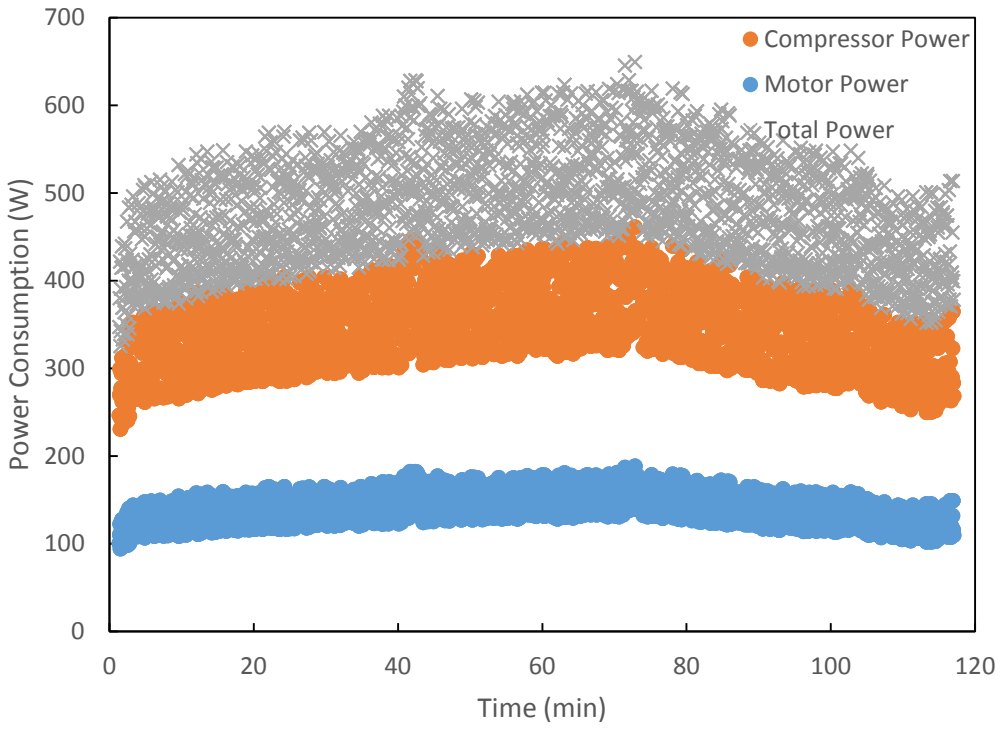

Figure 39: Power consumption profiles in Eco Mode 1

In contrast, the corresponding power consumption profile in the Speed Mode test 1 is presented in Figure 40.

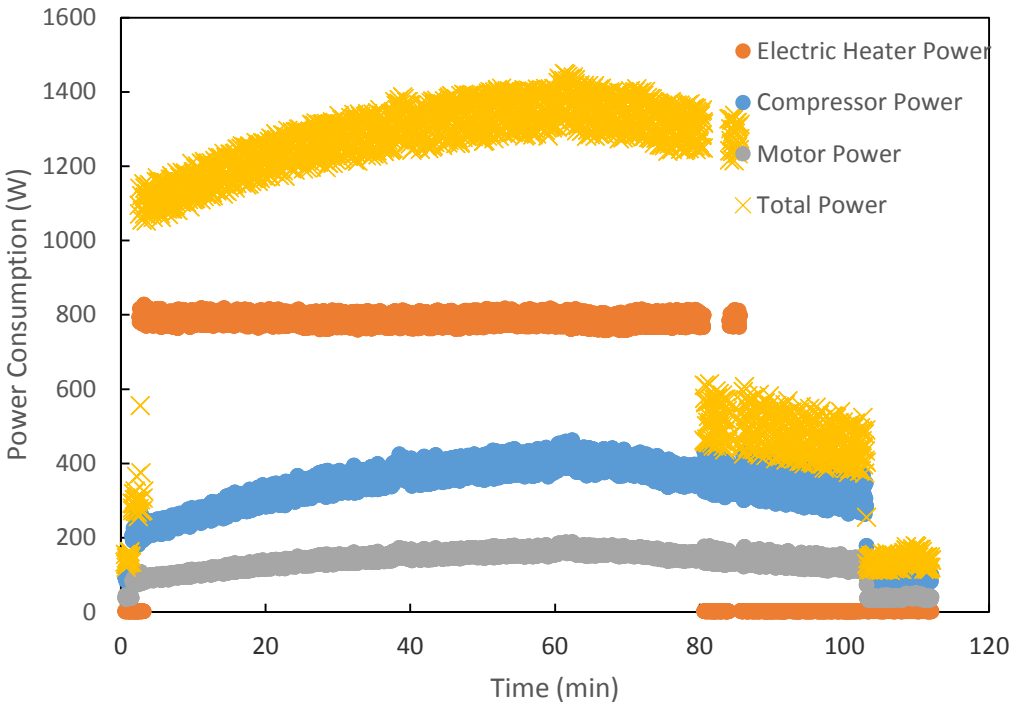

Figure 40: Power consumption profiles in Speed Mode 1

As clearly shown in the above figures, the peak total power in Speed Mode 1 (with both the heater and VCC on) was more than twice higher than that in the Eco Mode 1, while the compressor power and the motor power showed similar consumption levels. In Speed Mode 1, the electric heater shut off after 85 minutes, long before the automatic termination, where the drum outlet temperature started to decrease as shown in Figure 38. The compressor was also turned off after 103 minutes. The active running time (dehumidification process) was 20% less than that of the Eco Mode 1, since the Speed Mode is designed to offer a fast-drying function.

Table 9 summarizes the key time points regarding the termination and the main heat source on-offs.

Table 9: Time points for four tests in minutes

Test	Automatic Termination	Dehumidification Termination	Comp. On	Comp. Off	Heater On	Heater Off
Eco 1	118.7	85.2	1.0	116.8	N/A	N/A
Eco 2	126.1	91.7	0.9	124.1	N/A	N/A
Speed 1	112.1	72.6	1.0	102.5	2.3	85.0
Speed 2	111.6	70.2	1.0	102.6	2.0	77.5

3.2.3.2 Energy Consumption Analysis

Taking one step further into the energy consumption, the total energy consumption of the Speed Mode was about twice that of the Eco Mode, due to the introduction of the heater. Table 10 is the energy consumption summary for four tests.

Table 10: Energy consumption summary

Operational Mode		Eco 1	Eco 2	Speed 1	Speed 2
Total Average Power	**W**	472	455	1,018	967
Total Energy Consumption	**kWh**	0.93	0.96	1.90	1.80
Annual Energy Consumption	**kWh/year**	263.19	271.68	537.70	509.40
Dehum. Energy Consumption	**kWh**	0.69	0.71	1.51	1.46
Comp. Average Power	**W**	341	328	349	346
Comp. Energy Consumption	**kWh**	0.66	0.67	0.59	0.59
Heater Average Power	**W**	N/A	N/A	784	779
Heater Energy	**kWh**	N/A	N/A	1.04	0.95

When the CDs usage number is assumed to be 283 cycles per year by DOE standard 2011 [15], the total energy consumption is 267 kWh/year and 524 kWh/year for Eco Mode and Speed Mode, respectively. A total of 256 kWh/year (or 49%) can be saved if the Eco Mode is chosen instead of the Speed Mode for a LG hybrid HPCD. Moreover, the Eco Mode in LG hybrid HPCD could save about 70% of energy than a typical electric CD in the U.S. (which normally consumes about 900 kWh/year [9]). According to the survey conducted by EIA, the residential CD's energy consumption was 60 billion kilowatt hours in 2012 [4], so the estimated nationwide energy savings can be 35.9 billion kWh/year if all conventional CDs could be replaced by HPCDs. Therefore, HPCDs offer a great opportunity to save energy for clothes drying.

EF, defined as BDW divided by the dehumidification energy consumption, is an index used to evaluate the energy consumption performance of CDs according to DOE standard 2005. CEF, defined as the BDW divided by the total energy consumption, is an updated index for DOE standard 2011. Both are calculated for comparison as shown in Table 11. For both indexes, larger values imply higher efficiency.

Table 11: Energy Factor summary

Operational Mode	**EF (lbs./kWh)**		**CEF (lbs./kWh)**	
Eco 1	10.62±0.05	10.51±0.05	7.87±0.04	7.78±0.04
Eco 2	10.38±0.05		7.69±0.04	
Speed 1	4.91±0.02	4.99±0.03	3.90±0.02	4.00±0.02
Speed 2	5.06±0.03		4.10±0.02	

The EF of the Eco Mode shows a 111% increase over that of the Speed Mode in average, and the CEF shows a 95% increase in average. They are both far beyond the energy index requirements as referred in Table 2.

4 Discussions

4.1 Heat Exchanger Performance

4.1.1 CoilDesigner Simulation

Heat exchangers utilized as evaporator and condenser in LG hybrid HPCD were both modeled in CoilDesigner to analyze their performance [28]. The heat exchangers used in the HPCD were tube-and-fin, and the fin type was flat. Their geometric specifications were measured as shown in Table 12.

Table 12: Heat Exchangers' Geometric Specifications

Geometric Parameters	**Condenser**	**Evaporator**
Length (cm)	23.50	23.50
Tube Horizontal Spacing (cm)	2.25	2.25
Tube Vertical Spacing (cm)	2.25	2.25
Tube OD (cm)	0.95	0.95
Tubes per bank	8	5
Number of bank	5	4
FPI	10.81	10.81

The refrigerant circuitries simulated in CoilDesigner are presented in Figure 41 and Figure 42 for evaporator and condenser, respectively. Figure 43 shows the 3-D view of the coils. The red and blue dots represent refrigerant inlets and outlets, respectively.

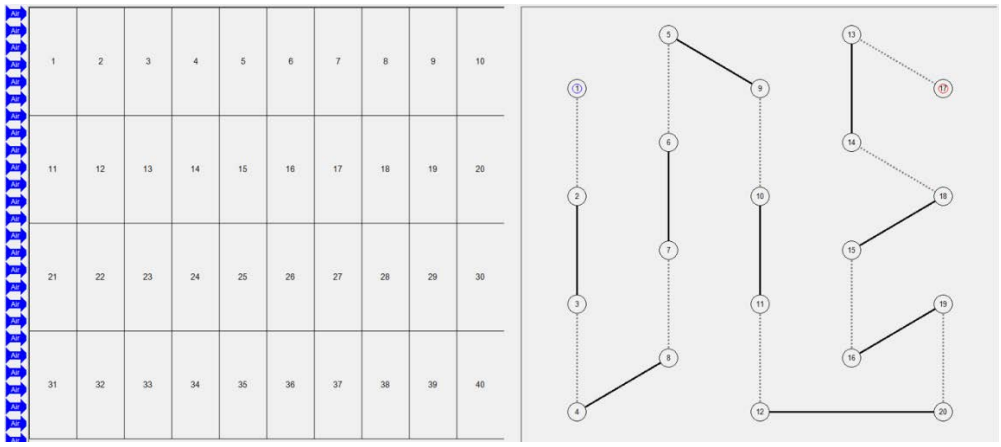

Figure 41: Evaporator's coil circuitry in CoilDesigner

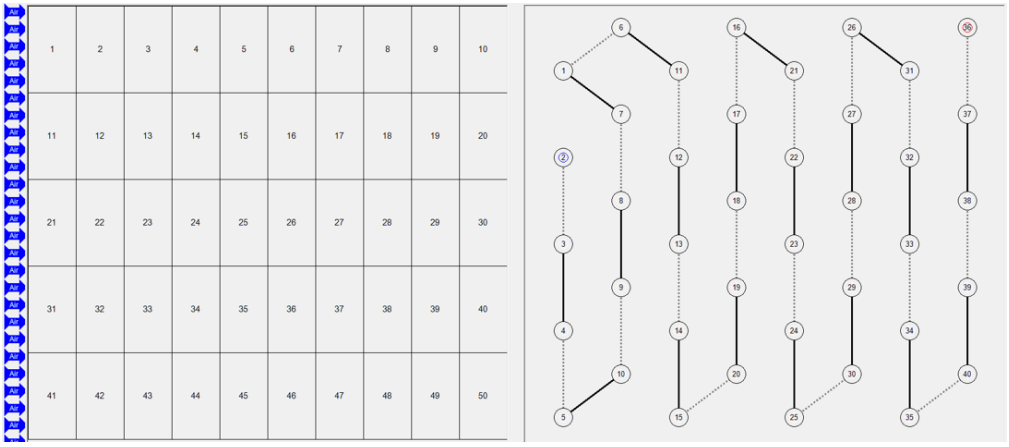

Figure 42: Condenser's coil circuitry in CoilDesigner

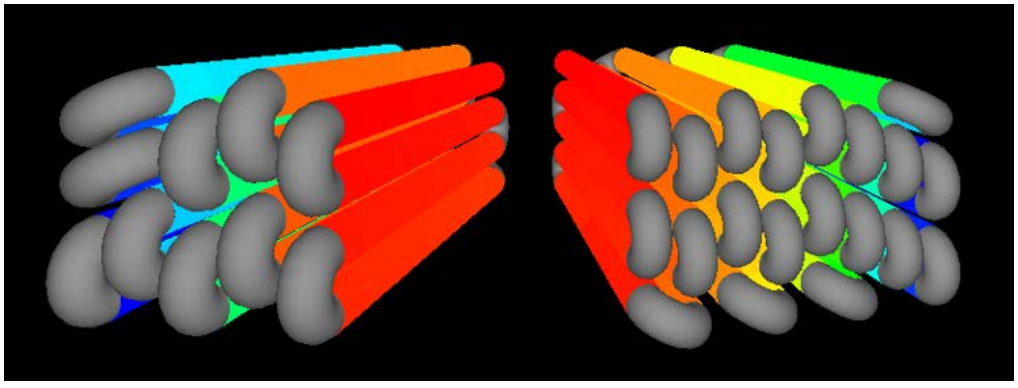

(a) Evaporator **(b) Condenser**

Figure 43: Evaporator and condenser's geometry in 3-D view

For the evaporator, the inlet air temperature, RH and air flow rate were used as input for the air-side, and the saturation temperature, inlet vapor quality and mass flow rate were for the refrigerant-side. All of these data were taken from Eco Mode test 1 results, in which the drum outlet temperature implies the evaporator inlet air temperature, and the vapor quality was determined based upon the isenthalpic expansion process through the expansion valve.

Similarly, for the condenser, the air inlet temperature, RH and air flow rate, as well as the refrigerant condensation temperature, saturation delta (which is the difference between the condenser inlet and the saturation temperature), and MFR were taken from the experimental data as the input operating conditions. Since the condenser inlet RH was not directly measured in the test, a calculated evaporator outlet RH from CoilDesigner program was utilized instead.

4.1.2 Heating and Cooling Capacity

A parametric study was conducted in CoilDesigner for overall observation of the entire process of the Eco Mode test 1. The heating capacity from the condenser was utilized to warm up the cool air from the evaporator. The directly calculated heating capacity from the experimental data had an average of 1.42 kW while the simulated heating capacity from CoilDesigner remained at around 1.48 kW, and the average deviation was 4.23% due to the vibration of refrigerant MFR in the real test. Figure 44 shows the heating capacity profiles.

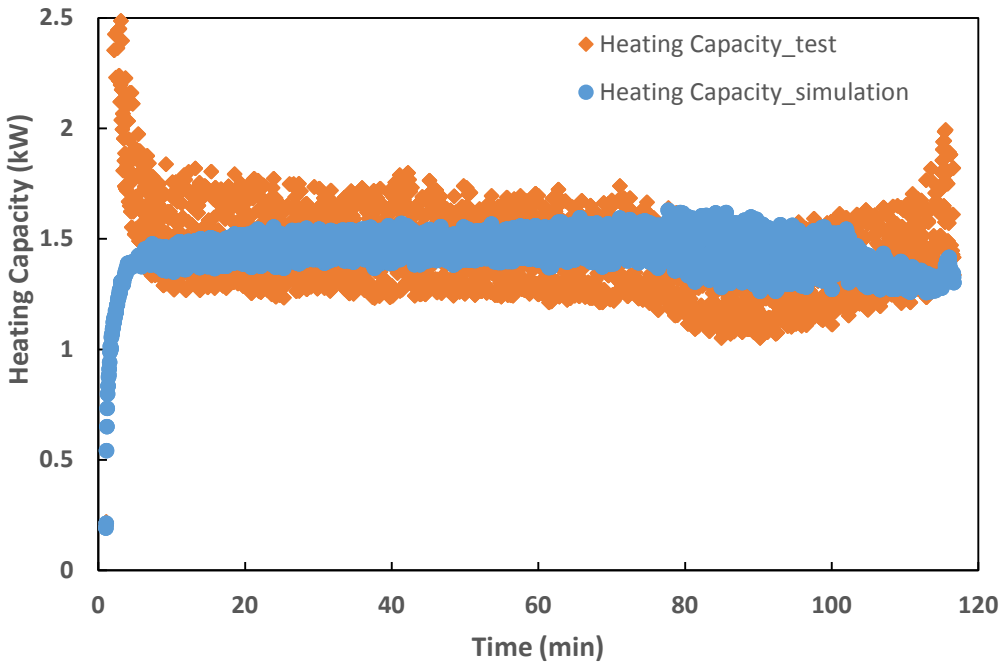

Figure 44: Heating capacity of Eco Mode test 1

The electric expansion valve was controlled to maintain the degree of superheating at a relatively constant level (an average of 6.8 K during dehumidification), to guarantee the refrigerant state provided to the compressor to be in the vapor phase, and to provide a stable heating capacity. Similarly, the degree of subcooling was controlled to ensure that the refrigerant leaving the condenser stayed in the liquid phase, therefore, maintaining the mass flow rate through the expansion valve in stable condition. Figure 45 illustrates the degree of superheating and subcooling as simulated by the CoilDesigner. As shown, the degree of subcooling had higher value and wider variations than the degree of superheating. It was due to the relatively high condensing temperature and random clothes mixing in the drum.

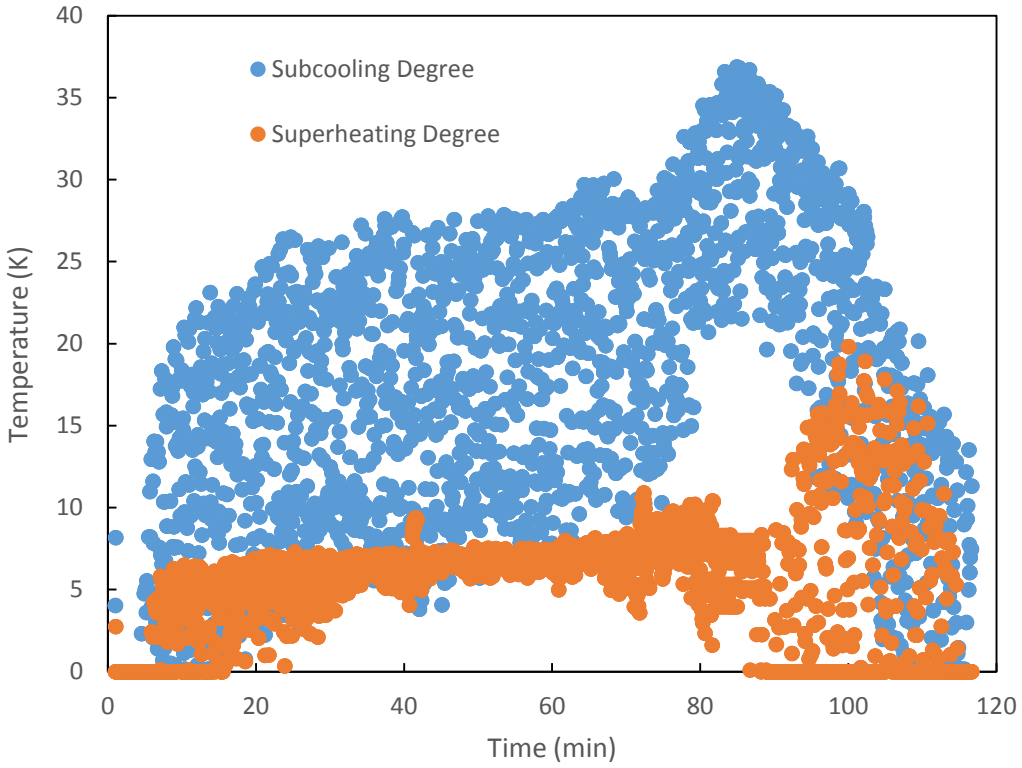

Figure 45: Superheating and subcooling degree of Eco Mode test 1

Cooling capacity is mainly utilized to dehumidify the moisture from the drum. The evaporator cooling capacity is classified into two parts: sensible capacity and latent capacity. The sensible capacity is used for changing in temperature without phase change, while the latent capacity is used for changing water vapor to liquid through phase transition. The sensible heat factor (SHF) is defined as the ratio of the sensible capacity to the total capacity (or the summation of the sensible and latent capacities) as shown in Equation 10.

$$SHF = \frac{Q_{sensible}}{Q_{sensible}+Q_{latent}} \qquad \text{Equation 10}$$

The latent capacity of the evaporator can be correlated with the SHF. Figure 46 and Figure 47 show the sensible and latent capacities of the evaporator and the SHF,

respectively. As shown, the latent capacity dominated the total cooling capacity (with an average of 0.92 kW out of 1.18 kW) until 80 minutes, and the remaining 0.25 kW was the sensible capacity, or with a SHF of 0.22 (Figure 47). After 80 minutes, the latent capacity decreased as clothes became drier. However, on the contrary, the sensible capacity was increased, which matches with the temperature trend shown in Figure 32. The calculated cooling capacity from the experimental test is also included in Figure 46 for comparison, which has an average of 1.13 kW, and the average simulation deviation was 4.42%.

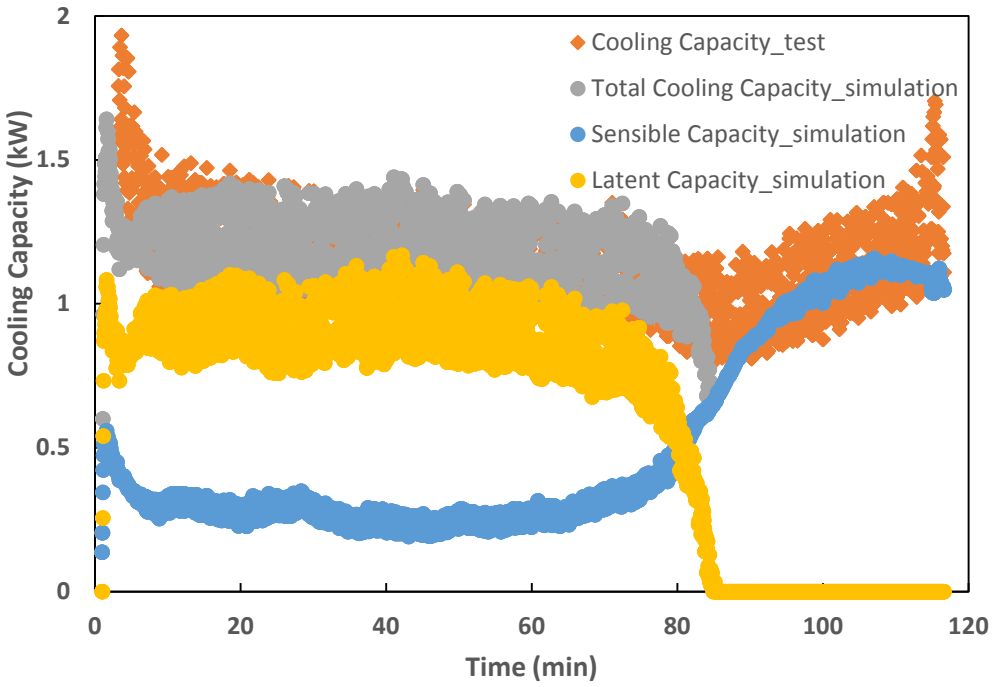

Figure 46: Cooling capacity of Eco Mode test 1

The dehumidification rate through the evaporator was calculated from the temperature and RH before and after the evaporator by the following correlations:

$$\omega_{evap,in} = \left(T_{air,evap,in}, RH_{evap,in}\right) \quad \text{Equation 11}$$

$$\omega_{evap,out} = \left(T_{air,evap,out}, RH_{evap,out}\right) \quad \text{Equation 12}$$

$$\dot{m}_{dehumidification} = \left(\omega_{evap,in} - \omega_{evap,out}\right) * MFR_{air}$$ Equation 13

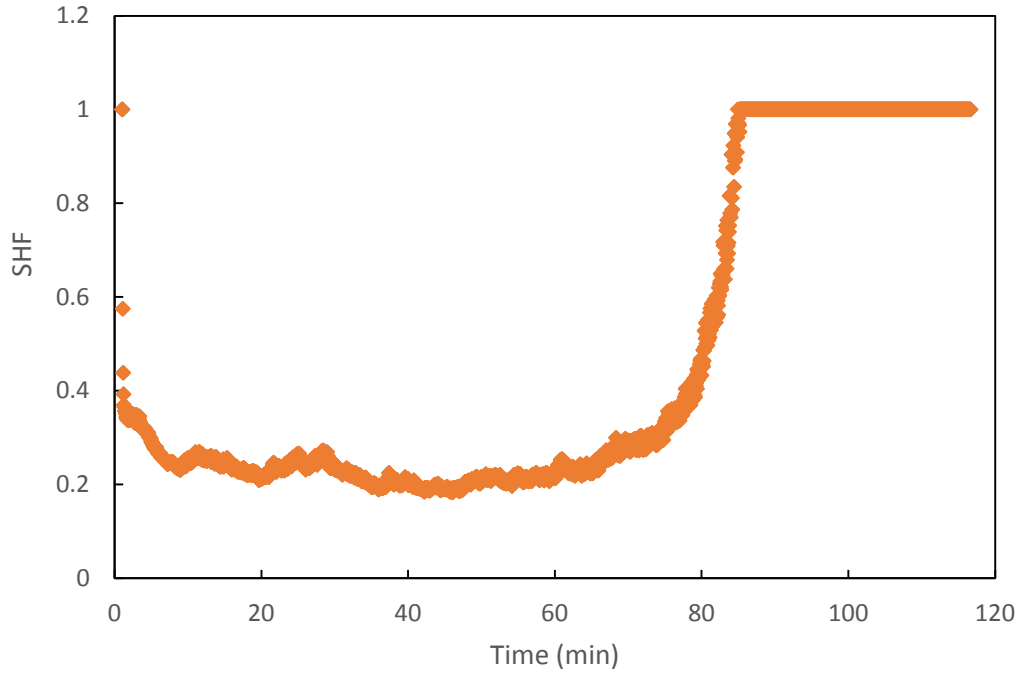

Figure 47: Evaporator sensible heat factor of Eco Mode test 1

Here, the evaporator inlet air temperature and RH are considered to be the same with those of the drum outlet, and the evaporator outlet air temperature is the temperature measured between the evaporator and condenser. Since no RH sensor was installed between the evaporator and condenser due to not enough space available, the evaporator outlet HR and RH were calculated from CoilDesigner, and plotted in Figure 48 and Figure 49, respectively.

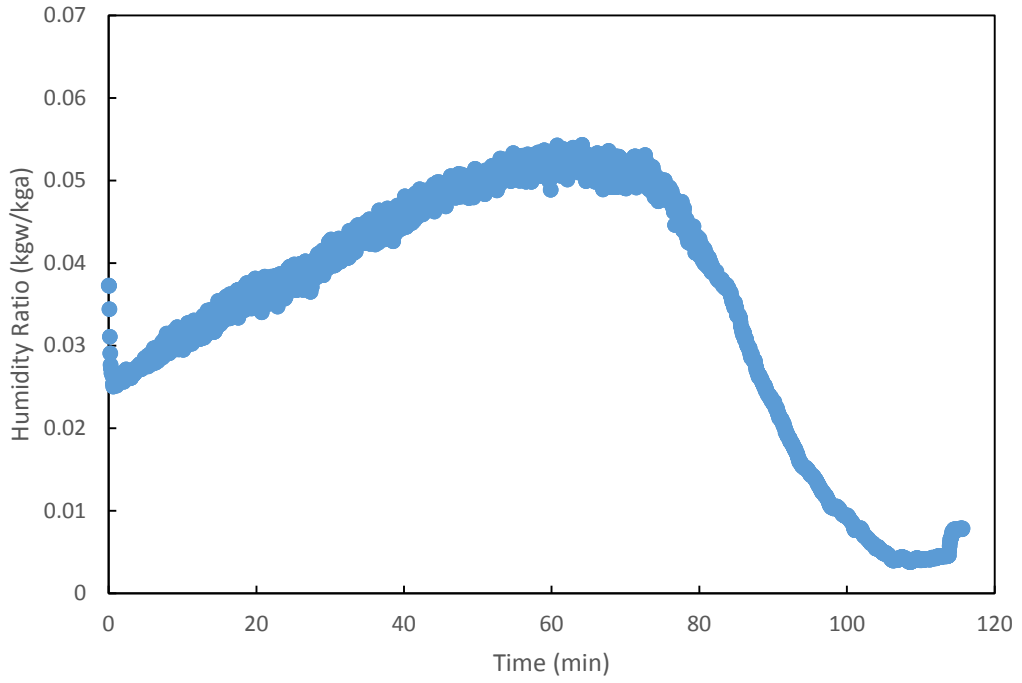

Figure 48: Humidity ratio at the evaporator outlet of Eco Mode test 1

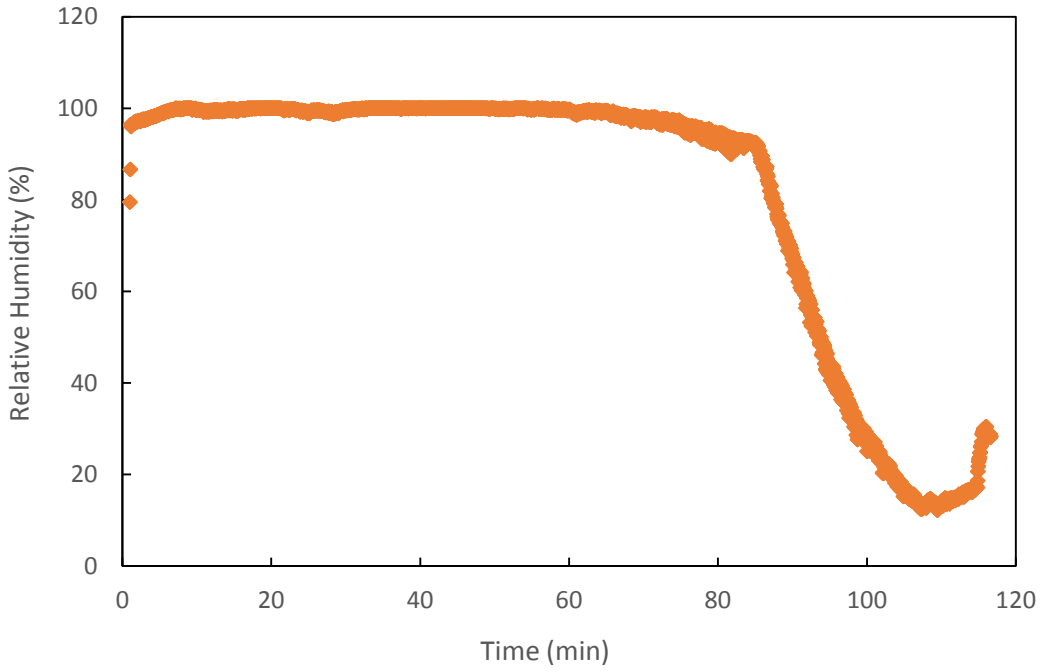

Figure 49: Relative humidity at the evaporator outlet of Eco Mode test 1

The HR at the condenser inlet is the same with that of the condenser outlet (refer Figure 25), since there is no dehumidification through the condenser. In Figure 49, it is clearly demonstrated that the evaporator outlet air was at a saturated condition during the dehumidification period, and then decreased significantly according to the evaporator inlet RH (as shown in Figure 28).

The calculated dehumidification rate through the evaporator is shown in Figure 50. The average dehumidification rate was 0.372 g/s. By integrating the dehumidification rate with time, the total water removed by the evaporator was calculated to be 1.731 kg, while the actual water removal weight measured from the test was 2.331 kg. Therefore, the calculation error was 25.72%, which indicated the possibility of the air leakage.

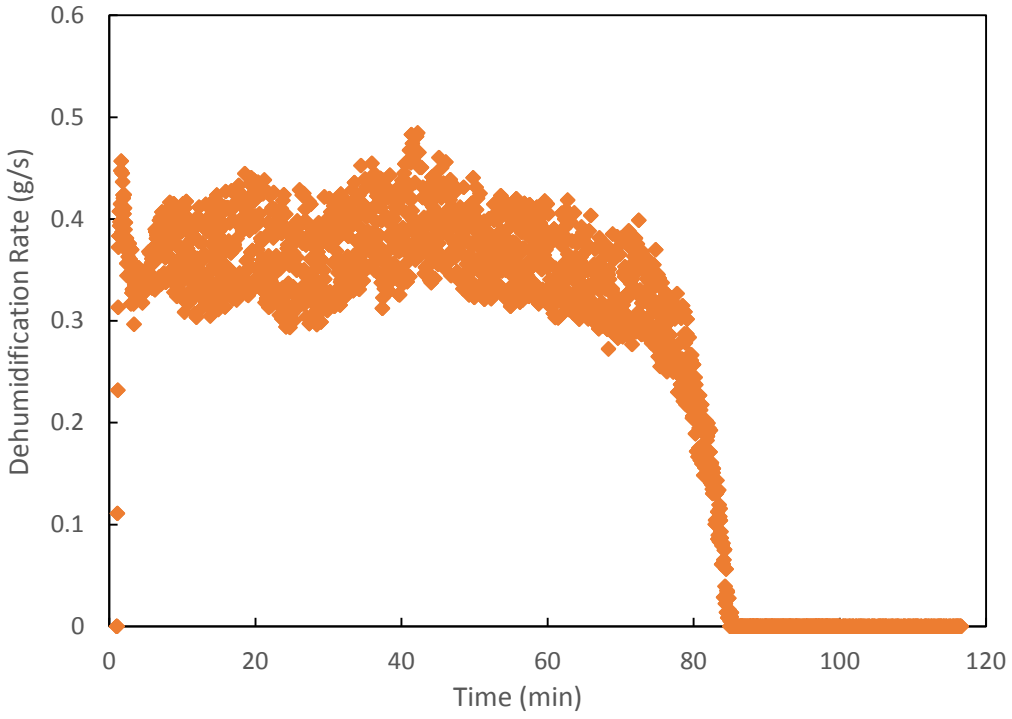

Figure 50: Dehumidification rate through the evaporator

4.1.3 Heat Exchanger Overall Conductance

The overall heat transfer coefficient (U) is the proportion factor between the heat flux and the heat transfer driving force (temperature difference).

$$Q = UA\Delta T \qquad \text{Equation 14}$$

where,

Q is the heat transfer rate,

U is the overall heat transfer coefficient,

A is the contact area,

ΔT is the temperature difference between the hot and cold working fluids, generally analyzed using either the logarithmic mean temperature difference (LMTD) or the effectiveness-number of transfer units (ε-NTU) [34].

The overall heat transfer coefficient (U) is determined by Equation 15 [35].

$$\frac{1}{UA_{out}} = \frac{1}{h_{in}A_{in}} + \frac{1}{\eta_{fin}h_{out}A_{out}} \qquad \text{Equation 15}$$

where,

U is the overall heat transfer coefficient (W/m²·K);

A_{in} is the refrigerant-side heat transfer area, which is the primary heat transfer area (m²);

A_{out} is the air-side heat transfer area, which is the secondary heat transfer area (m²);

h_{in} is the average refrigerant-side heat transfer coefficient (W/m²K);

h_{out} is the average air-side heat transfer coefficient (W/m²K);

η_{fin} is the average fin efficiency.

Since A is a constant value for each heat exchanger, the overall conductance (UA) was evaluated instead of U alone.

A sensitivity study was conducted by using the parametric analysis feature in CoilDesigner to see how each factor would affect the outputs.

For the evaporator, the model in CoilDesigner requires six input parameters: the inlet air temperature, inlet RH, AFR, inlet refrigerant vapor quality, evaporating temperature, and refrigerant MFR. The first three have influence on the heat exchanger air-side performance, while the latter three affect the behavior of the refrigerant-side. However, there are cross effects, too.

In the sensitivity analysis, the set point for each parameter was chosen from the test at the 30 minutes. For each study, one of the parameters was set to vary linearly starting at the set point (as the middle value), assuming up to 60% increase as well as decrease and at the same time to ensure that the range had a physical meaning, except for RH, which was varied from 1% to 100%. At the same time, the remaining parameters stay the same at the set point. The UA value calculated at the set point was 75.5 W/K, and its variation range corresponding to each parameter variation is listed in Table 13, along with its deviation percentage from the set point (75.5 W/K). The sensitivity study results for the evaporator are also shown in Figure 51. From the results, it was found that the most influential parameters are the AFR, air inlet temperature and MFR, which affect both the air-side and refrigerant-side heat transfer coefficient, therefore, affect the UA value.

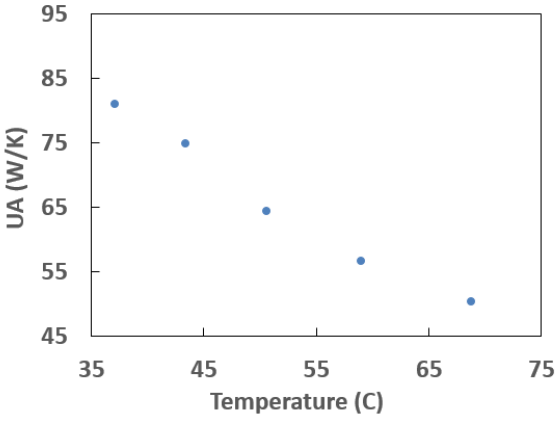

(a) UA versus air inlet temperature

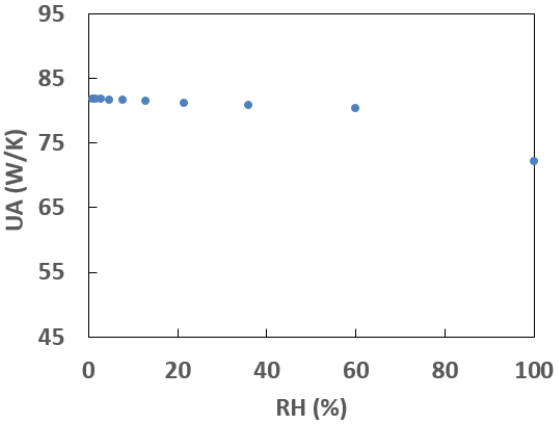

(b) UA versus air inlet RH

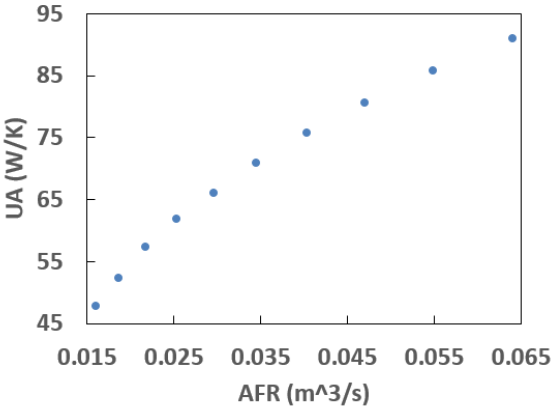

(c) UA versus AFR

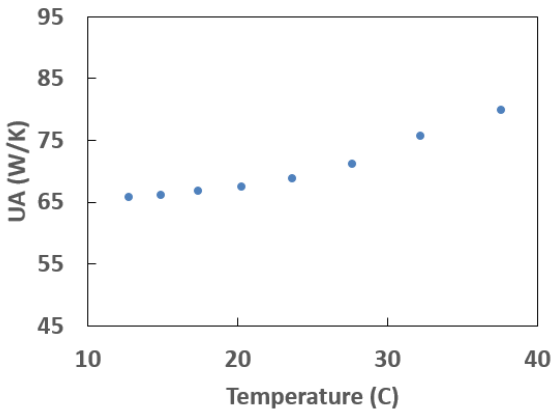

(d) UA versus evaporating temperature

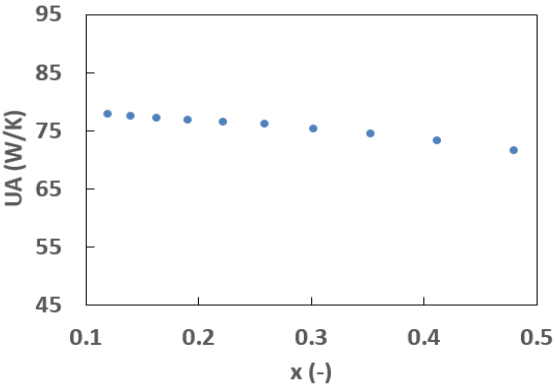

(e) UA versus inlet vapor quality

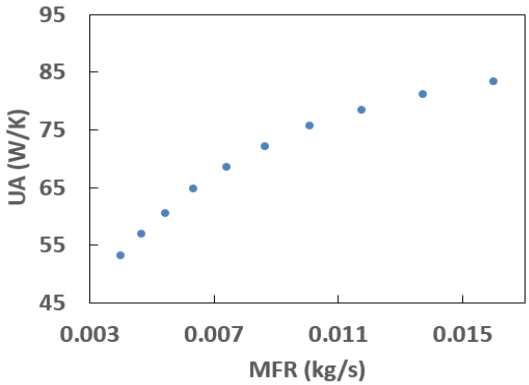

(f) UA versus ref. MFR

Figure 51: Evaporator UA sensitivity study results

Table 13: Evaporator heat exchanger sensitivity analysis

Parameter	Set Point	Variation Range	UA Variation Range	UA Deviation from the Set Point
Air Inlet Temperature	43ºC	37.15 ~ 68.8 ºC	50.4 ~ 80.9 W/K	-33.3 ~ 7.2%
Inlet RH	90%	1 ~ 100%	72.1 ~ 81.8 W/K	-4.5 ~ 8.3%
AFR	0.04 m^3/s	0.016 ~ 0.064 m^3/s	47.7 ~ 91.0 W/K	-36.8 ~ 20.5%
Evaporating Temperature	32 ºC	12.8 ~ 37.63 ºC	65.8 ~ 79.8 W/K	-12.9 ~ 5.7%
Inlet Refrigerant Vapor Quality	0.3	0.12 ~ 0.48	71.5 ~ 77.8 W/K	-5.2 ~ 3.1%
MFR	0.01 kg/s	0.004 ~ 0.016 kg/s	53.1 ~ 83.4 W/K	-29.6 ~ 10.5%

Since there are two distinct periods in the VCC: the peak moisture removal period when the inlet air is humid and the low moisture removal period when the inlet air is relatively dry, both cases were considered in simulation. Taking the air inlet temperature and the MFR as an example, and by using the parametric analysis feature of CoilDesigner, the air inlet temperature was varied from 40 to 70 ºC, MFR from 0.007 to 0.012 kg/s, to cover the variation range observed in the experimental test. Whereas, the following parameters were fixed: the inlet RH was set to be 90%, AFR 0.0378m^3/s,

evaporating temperature 33 ºC, and vapor quality 0.3. The results are presented in Figure 52.

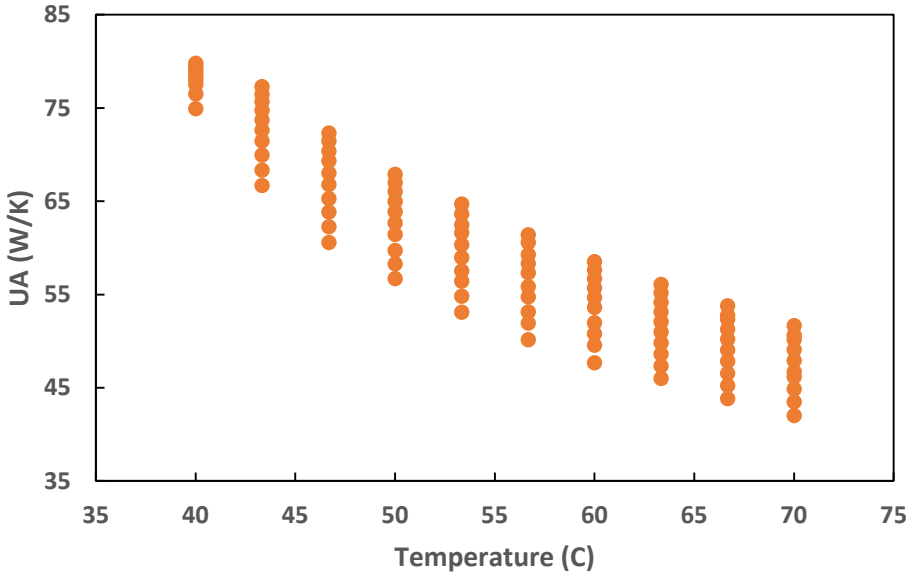

(a) UA versus air inlet temperature

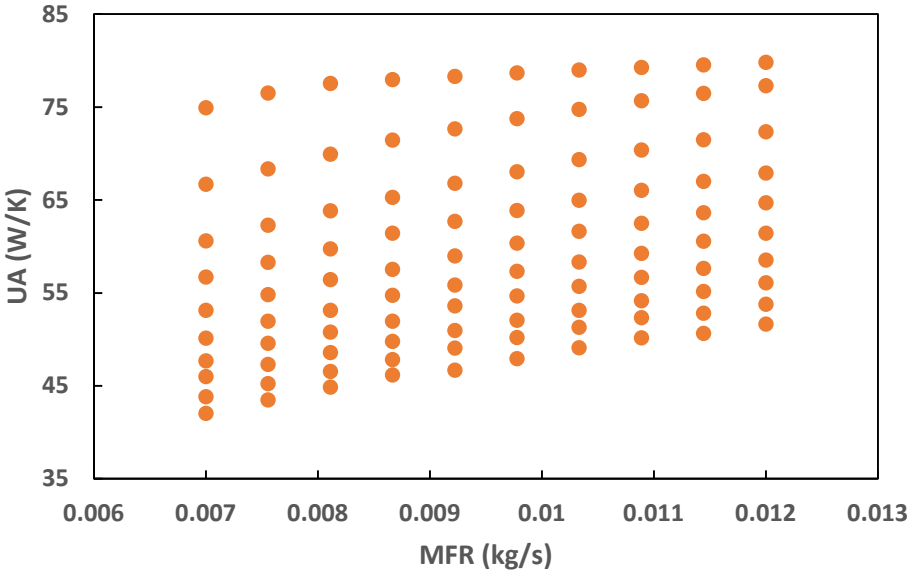

(b) UA versus refrigerant mass flow rate

Figure 52: Evaporator UA during peak dehumidification period

Then, for the low dehumidification period, the inlet RH was changed to 20%, while the other parameters remained as before. The results are shown in Figure 53.

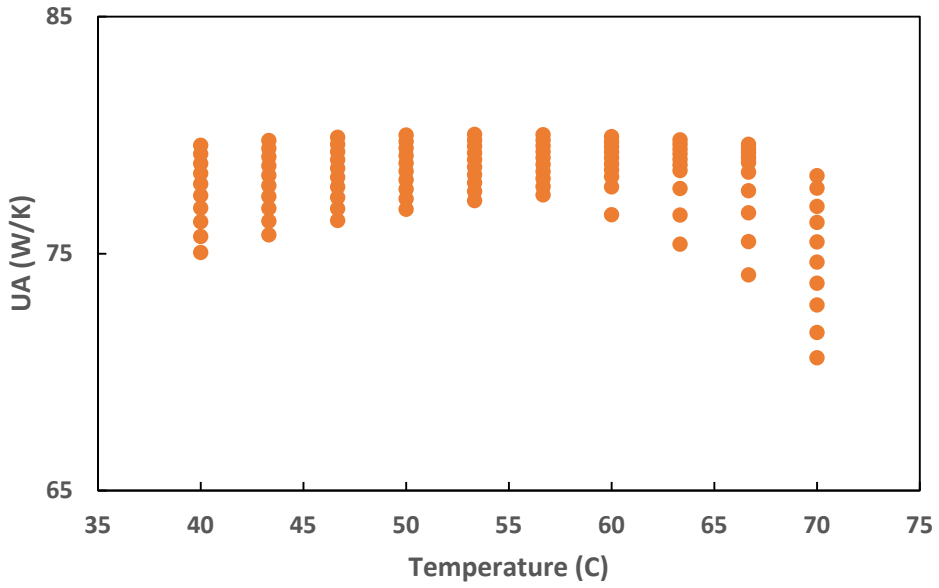

(a) UA versus air inlet temperature

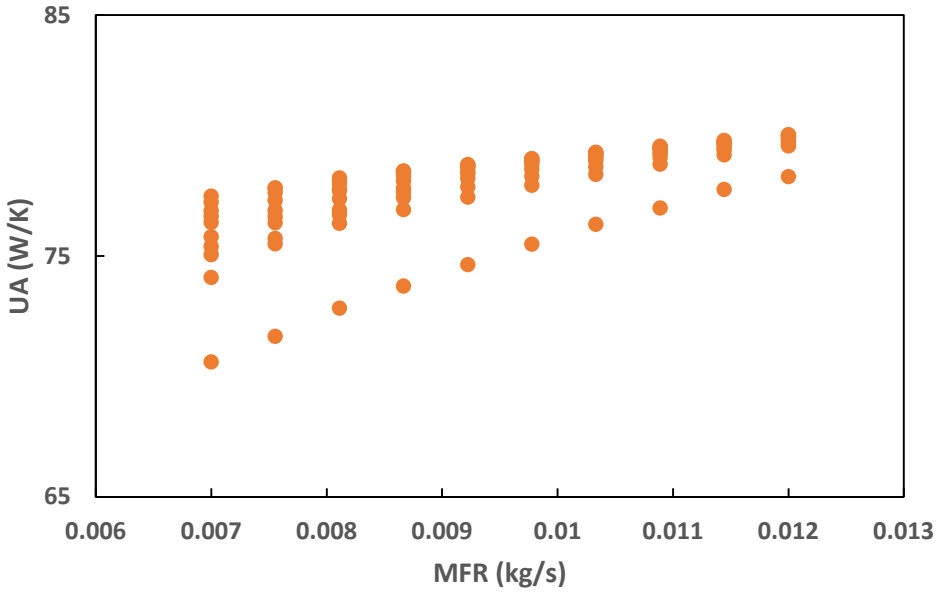

(b) UA versus refrigerant mass flow rate

Figure 53: Evaporator UA during low dehumidification period

It was found from the comparison between these two humid cases that during peak dehumidification period (RH: 90%), the UA value decreases with the increase of the inlet air temperature (Figure 52). However, it stays at a higher level and doesn't change much (Figure 53) during low dehumidification period (RH: 20%). Therefore, it is necessary to consider the inlet air temperature and RH at the same time. Then, the HR was varied from 0 to 0.28 kgw/kga, which was corresponding to RH variation from 1% to 100%, and the remaining parameters were set to be the same as the previous two studies for the evaporator. The results are presented in Figure 54. It was shown in Figure 54 that for the evaporator of the investigated LG hybrid HPCD, the UA has a slightly decreasing trend around 78 W/K with an inlet air HR from 0 to 0.05 kgw/kga due to the limitation of heat transfer during a very low HR level where there shows no superheat degree, and then the UA decreases with the increase of the HR. The reason could be explained that, as the HR of the air is increased, the latent heat load increases and at the same time the sensible heat load decreases, therefore, there is less two-phase region and more single-phase region for the refrigerant in the evaporator, which reduces the refrigerant-side heat transfer coefficient, so that the UA decreases. And the UA value has a trend to increase with the increase of refrigerant MFR since the Reynolds number of the refrigerant-side is increased. However, it is strongly affected by the HR. Therefore, a 3-D diagram was presented to depict the UA-HR-MFR relationship for clearer observation as shown in Figure 55.

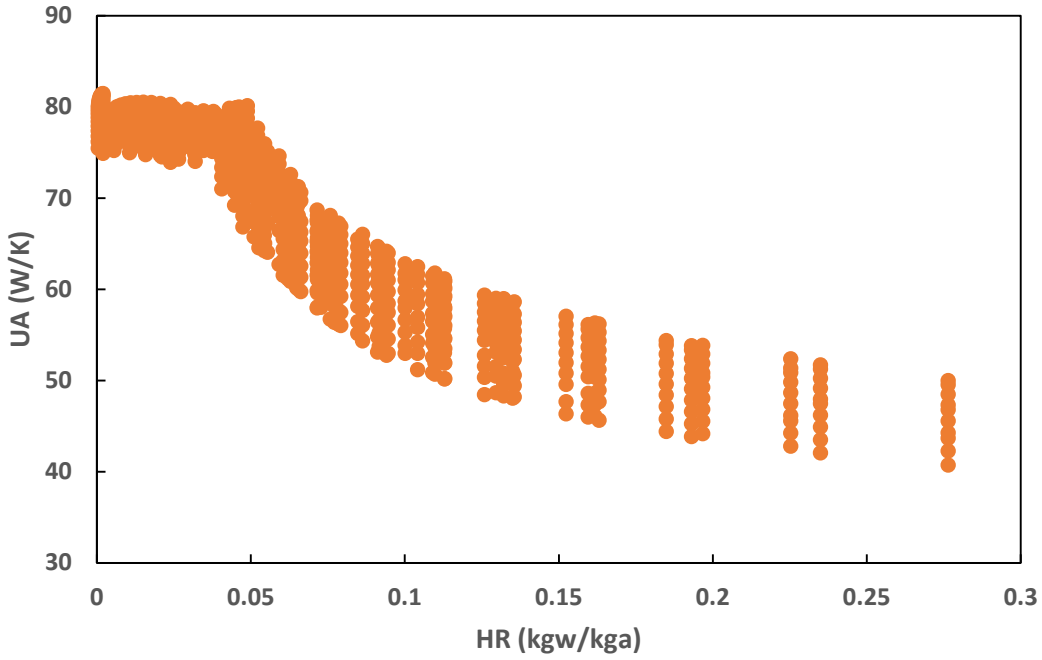

(a) UA versus inlet humidity ratio

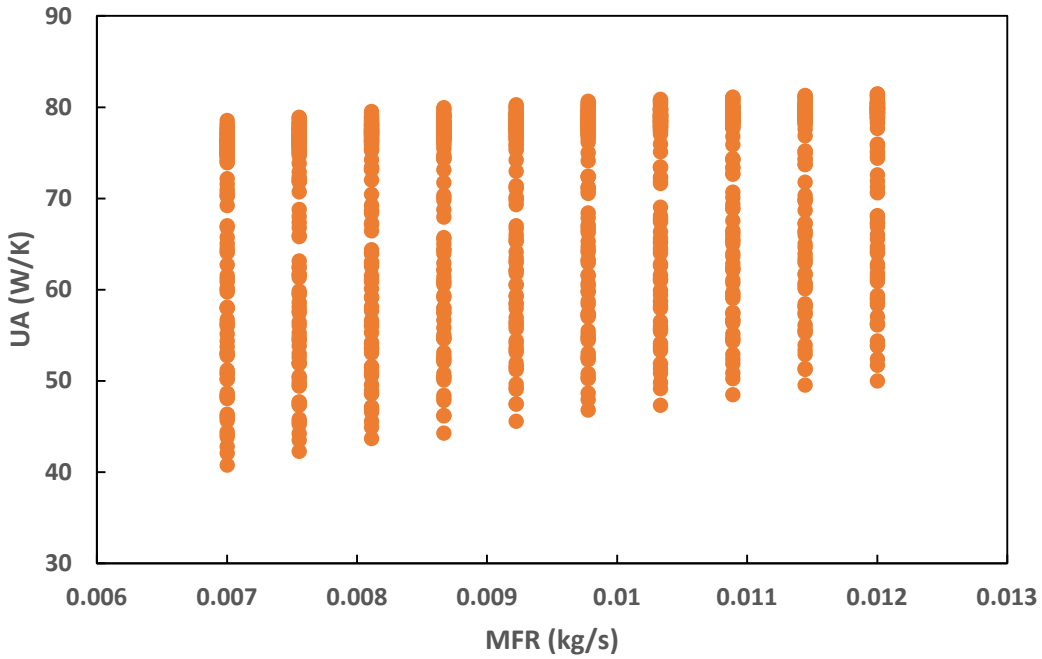

(b) UA versus refrigerant mass flow rate

Figure 54: Evaporator UA

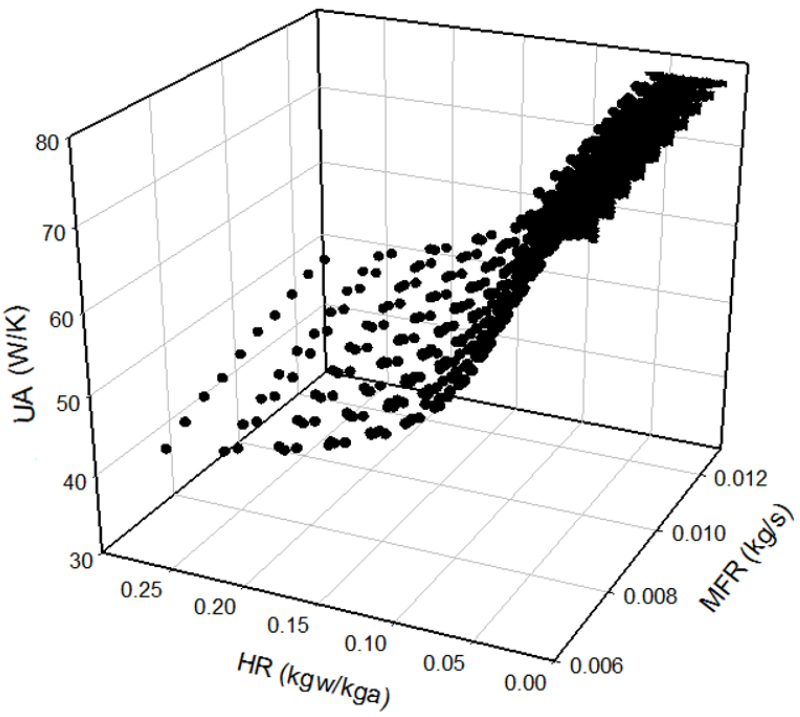

Figure 55: Evaporator UA versus inlet humidity ratio and refrigerant mass flow rate

From the 3-D diagram, it could be seen that with a small HR and large MFR, the UA value is higher.

Similarly, for the condenser, a parametric study was conducted with the input parameters and their set point shown in the first two columns in Table 14. For each case study, one of these parameters' set point value was varied by up to ± 60% with a physical meaning besides the RH value (the range set from 1 to 100%), while keeping the other variables fixed at the set point. The input variation range was derived as shown in column three, and the UA variation range was shown in column four accordingly. The UA value was calculated to be 140.7 W/K at the set point, and then its deviation from the set point was determined in column five.

Table 14: Condenser heat exchanger sensitivity analysis

Parameter	Set Point	Variation Range	UA Variation Range	UA deviation From the Set Point
Air Inlet Temperature	35ºC	14.0 ~ 41.2 ºC	120.9 ~ 141.9 W/K	-14.0 ~ 0.9%
Inlet RH	99%	1 ~ 100%	140.9 ~ 142.6 W/K	0.2 ~ 1.4%
AFR	0.04 m^3/s	0.016 ~ 0.064 m^3/s	85.0 ~ 150.5 W/K	-39.6 ~ 7.0%
Condensing Temperature	72 ºC	39.2 ~ 115.2 ºC	74.9 ~ 154.5 W/K	-46.8 ~ 9.9%
Delta T	10K	4 ~ 16K	139.2 ~ 143.5 W/K	-1.0 ~ 2.0%
MFR	0.01 kg/s	0.004 ~ 0.016 kg/s	90.7 ~ 142.7 W/K	-35.5 ~ 1.5%

Figure 56 depicts the results. It shows that the condensing temperature, the AFR and the MFR have the largest impact on the UA, in which, similarly with the evaporator discussion, the condensing temperature and MFR were chosen as an example to be discussed further.

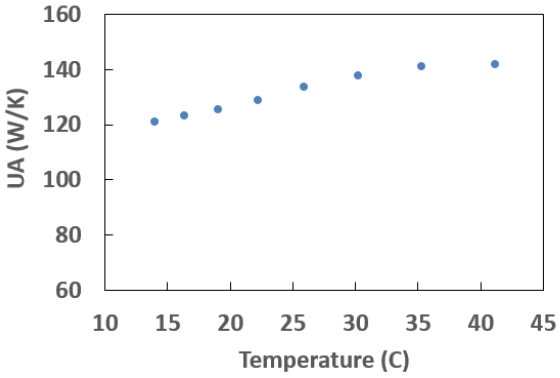

(a) UA versus air inlet temperature

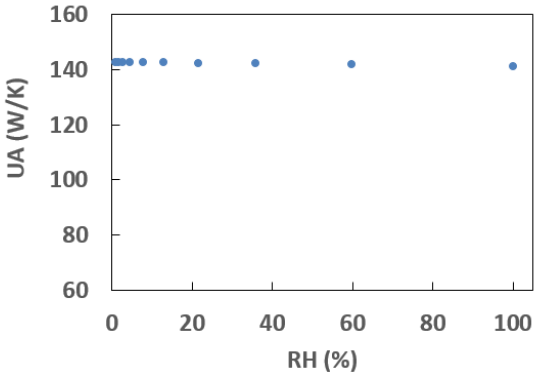

(b) UA versus air inlet RH

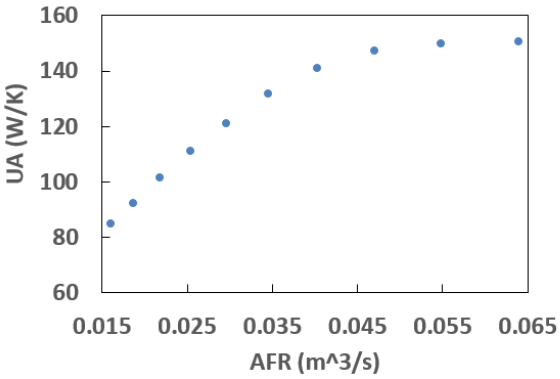

(c) UA versus AFR

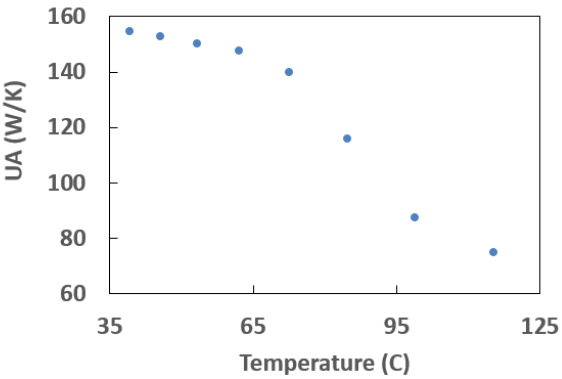

(d) UA versus condensing temperature

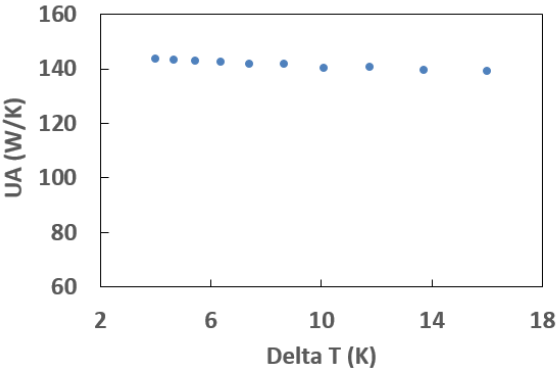

(e) UA versus delta T

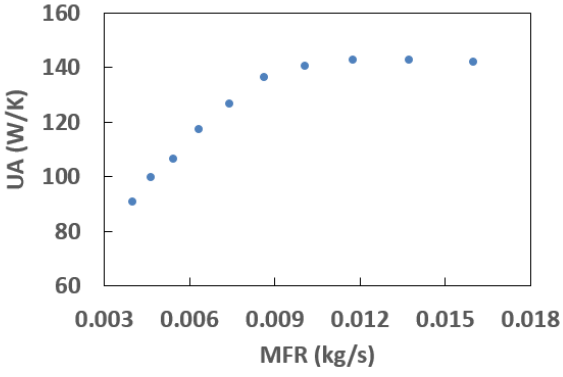

(f) UA versus ref. MFR

Figure 56: Condenser UA sensitivity study results

A further parametric study was performed concentrating on the condensing temperature and MFR. The condensing temperature was changed from 40 to 80 ºC, and MFR from 0.007 to 0.012 kg/s, and the air inlet temperature was fixed at 35 ºC, inlet RH at 98%, AFR at 0.0378 m^3/s, and delta saturation temperature for at 10K. The correlations between the UA and two input parameters are shown in Figure 57 and a 3-D relationship diagram is shown in Figure 58.

The UA also shows an increase with the increase of MFR as discussed before for the evaporator part, and the higher the condensation temperature, the smaller the UA as shown in Figure 58 which is due to a less two-phase region for the refrigerant of the conderser.

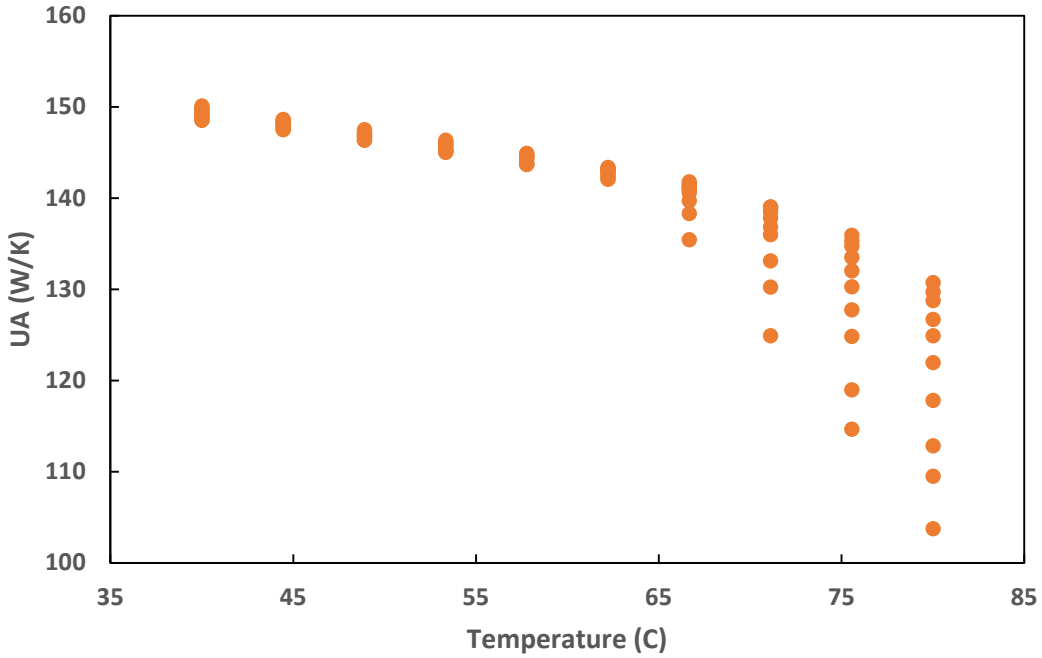

(a) UA versus condensing temperature

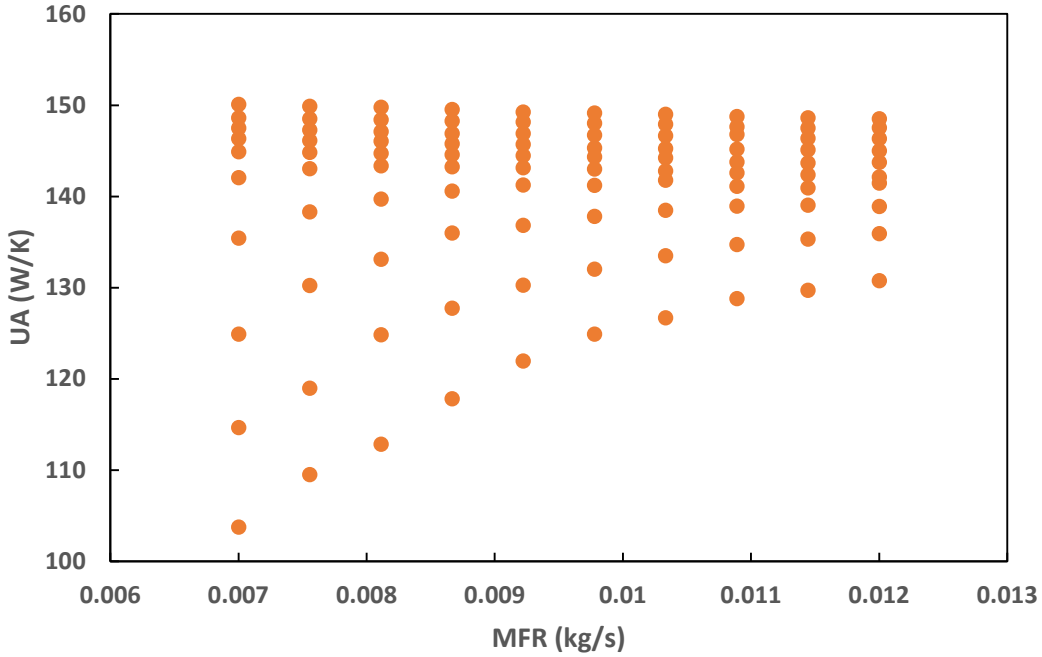

(b) UA versus refrigerant mass flow rate

Figure 57: Condenser UA

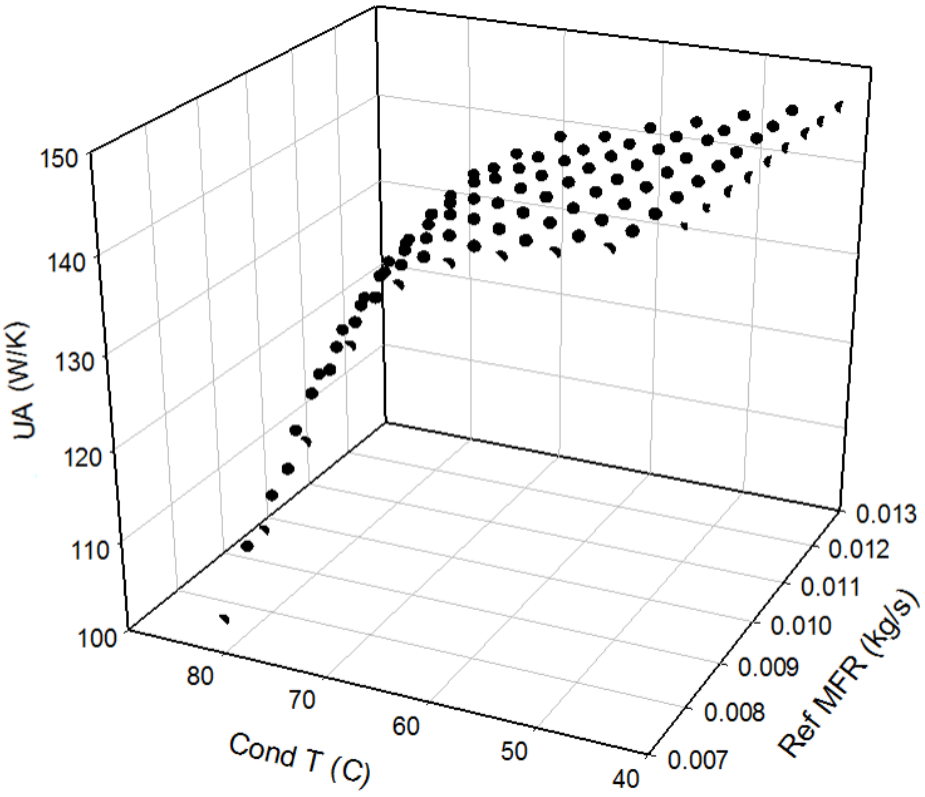

Figure 58: Condenser UA versus condensing temperature and refrigerant mass flow rate

Finally, the UAs simulated from the experimental data are shown in Figure 59 and Figure 60. The MFR was at a relatively steady state and did not affect the UA. The evaporator inlet HR increased for the first 60 minutes, and then decreased after as shown in Figure 25. This trend matches with the change of UA value shown in Figure 59. The condensation temperature went up before 80 minutes, and then went down as shown in Figure 31. It shows a good fit with the UA variation shown in Figure 60. Moreover, the condenser has a larger UA value than that of the evaporator which means that the heat is easier to be conducted over the heat exchanger.

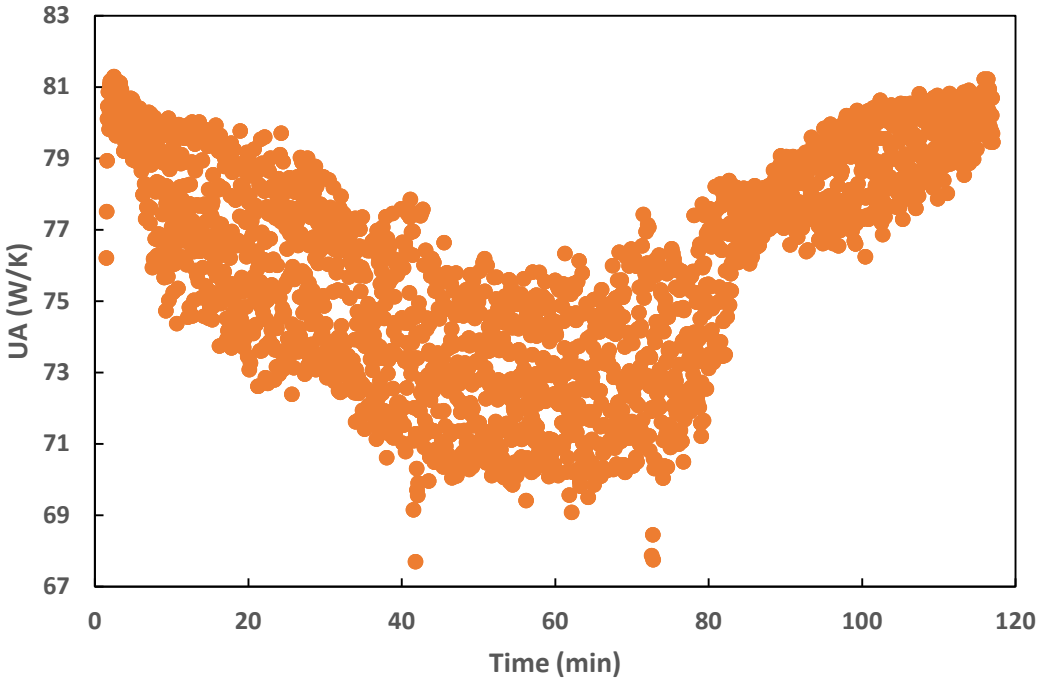

Figure 59: Evaporator UA in Eco Mode test 1

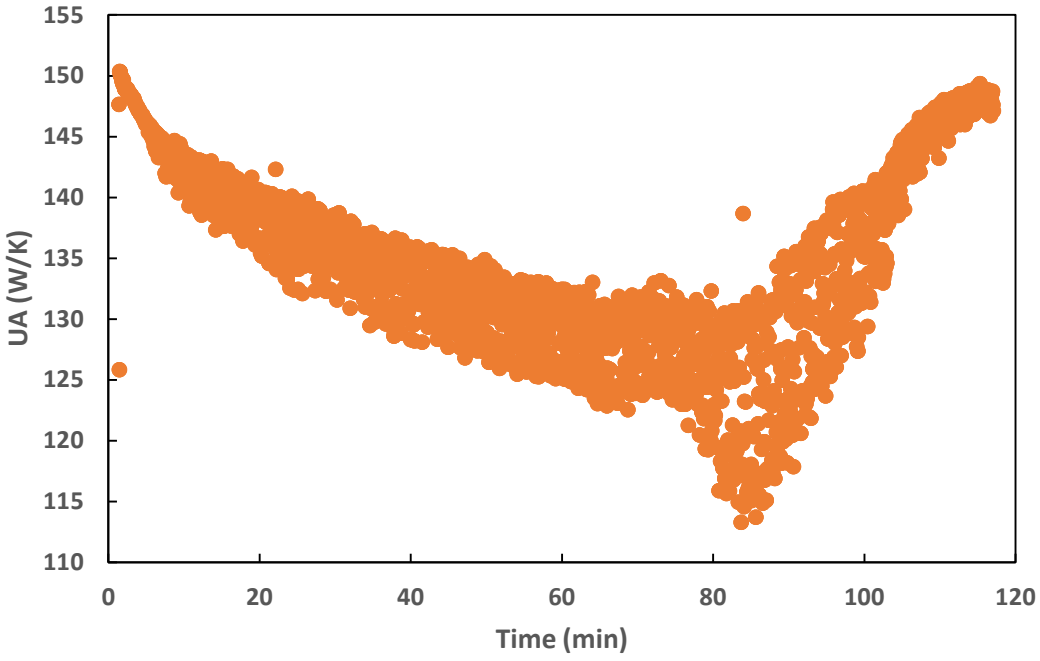

Figure 60: Condenser UA in Eco Mode test 1

Moreover, the analysis shows that a higher MFR increases the heat transfer performance. Since a higher MFR also requires a higher compressor input, its optimization is needed for maximizing the system's COP. The UA correlations can also be derived with respect to each influencing parameter to be used in a HPCD model for its improvement in future work.

4.2 Clothes Drying Process

The clothes drying process in the drum is discussed in this chapter.

4.2.1 Psychrometric Process

For the air loop, the process is at a relatively constant pressure so that the CD's psychrometric process at 10 minutes is shown in a psychrometric chart at constant pressure (Figure 61) as an example.

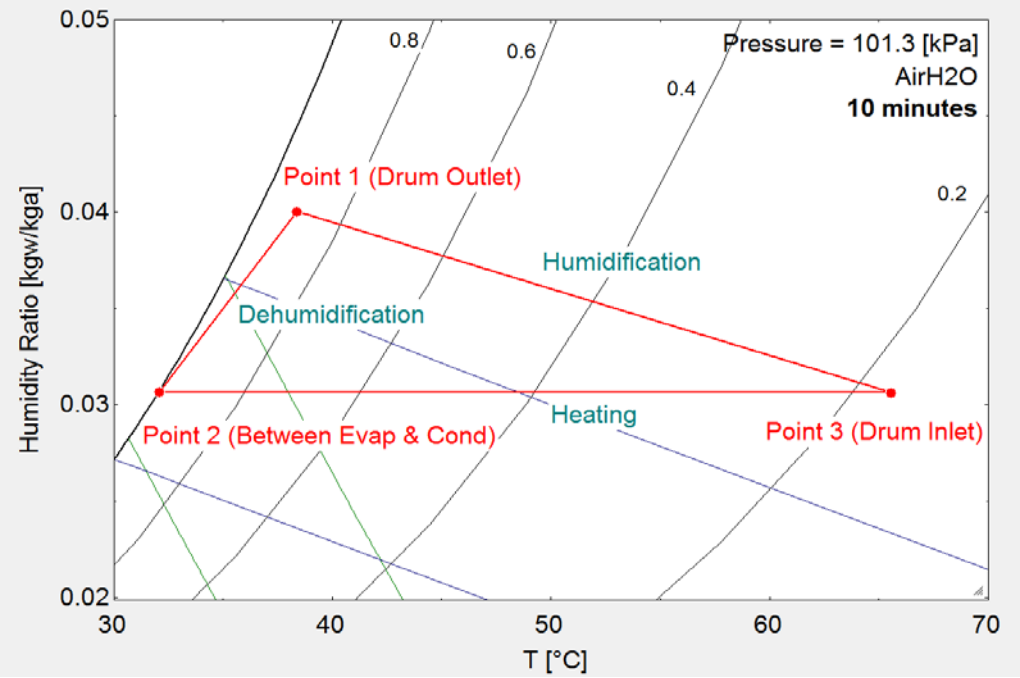

Figure 61: Psychrometric process at 10 minutes

From point 1 (drum outlet) to point 2 (evaporator outlet), the humid air from the drum passes through the evaporator where the cooling and dehumidification take place. After point 2, the relatively dry air passes through the condenser where it is sensibly heated up at a constant HR level. After the condenser, air at point 3 (drum inlet) is then supplied into the drum, where it is humidified by picking up the moisture from the clothes. The driving force in the drum is the difference of partial vapor pressure between the relatively humid-and-cool air near the wet clothes and the relatively dry-and-hot air supplied to the drum. Therefore, the increase of the drum inlet temperature helps the evaporation of water content in clothes [36]. The water contained in the clothes evaporates so that the drum air HR is increased. The enthalpy of vaporization from the moisture is used for the sensible cooling of the air, which explains the temperature drop at the drum outlet from the inlet. This drying process was assumed to be an isenthalpic process as proposed by Braun 2002 [36] and Lena 2010 [37]. However, the calculation for drum inlet and outlet enthalpies shown in Figure 62 indicates an average of 8.5 kJ/kg enthalpy loss through the drum, which is 5.2% of the average air inlet enthalpy. This part of the enthalpy loss could be related with energy loss to the surrounding air [38]. The energy balance in drum can be built by Equation 16.

$$\left(C_{P,clothes}M_{clothes} + C_{P,water}M_{water} + C_{P,drum}M_{drum}\right)\frac{\partial T_{drum}}{\partial t} = \dot{m}_{air}(h_{in} - h_{out}) - \dot{m}_{waterremoval}h_{latent} - Q_{loss} \quad \text{Equation 16}$$

where, $C_{P,clothes}$, $C_{P,water}$, and $C_{P,drum}$ are the specific heat of the dry clothes, water and drum metal, respectively;

$M_{clothes}$, M_{water}, and M_{drum} represent the mas of the bone dry clothes, water in clothes, and the drum, respectively;

T_{drum} is the temperature of the drum and the clothes;

$\frac{\partial T_{drum}}{\partial t}$ is the temperature change rate;

$\dot{m}_{air}$ is the mass flow rate of the dry air;

h_{in}, h_{out} are the drum inlet and outlet enthalpy;

$\dot{m}_{waterremoval}$ is the water removed;

h_{latent} is the vaporization enthalpy at drum outlet;

Q_{loss} is the energy loss from the drum to the surroundings.

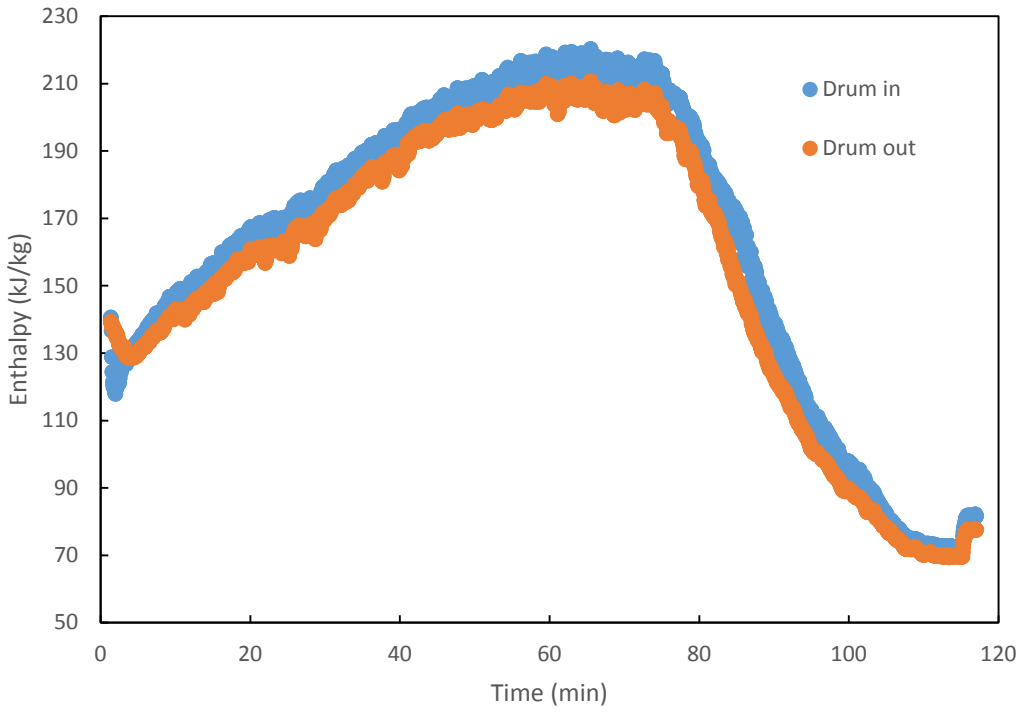

Figure 62: Drum inlet and outlet enthalpies

The above heat transfer equation in the drum is based on the assumption that the clothes, water contained and the drum metal are at the same temperature level [39]. However, Sivakumar (1997 [38]) assumed that the temperature of the clothes was identical to the dry-bulb air temperature leaving the drum. In the experimental test, no thermocouple was installed to measure the temperature of the clothing so that it was not able to validate these assumptions.

After the humidification in the drum, the air leaves the drum at a cooler and more humid condition than inlet. The process is recirculated until the end of the test. For the vented CDs, the air at point 1 is directly discharged to the ambient. Figure 63 shows the psychrometric processes for 8 different time points across the drying process for LG hybrid HPCD. The drum outlet RH remained above 80% for the first half period, and then decreased until the inlet and outlet HRs reached to the same level.

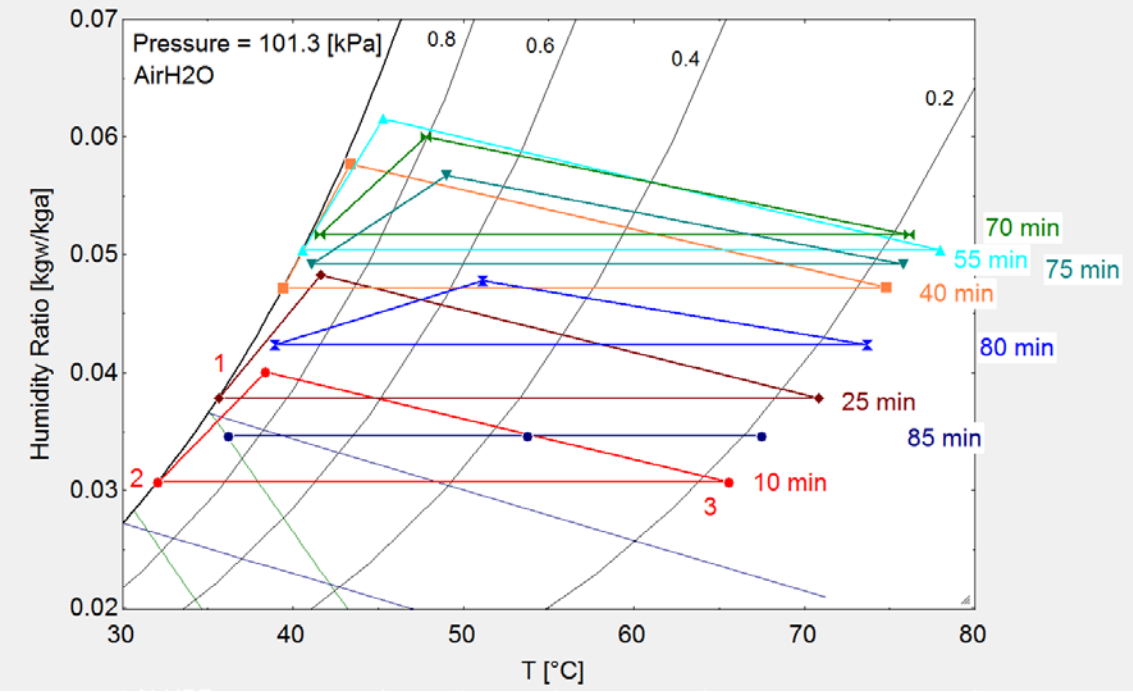

Figure 63: Progress of psychrometric process

4.2.2 Leakage

For the CDs, there is a high possibility of air leakage from the internal air flow to the surroundings because the tumbling drum is a moving part, while the cabinet is stationary. The air leakage could be an energy loss source for a closed system no matter where it is located. Particularly, for the HPCDs, the leakage of humid air affects the evaporator performance and therefore, influences the condenser in a negative way. If the hot and dry air is leaked out, a thermal loss from the drum would affect the water removal rate directly. However, the locations and the amount of the leakage are very difficult to determine. In general, the locations with high static pressure and relative motion are most likely to be a leaking location like a fan outlet.

Braun (2002) indicated that about 20% of the total air of a conventional CD leaks from the drum seals, especially near the drum outlet [36], and Lena (2011) conducted a simulation study for CD leakages. By assuming the leakage occurred between the heater and the drum with a gap up to 1 mm, an air leakage of 30% to 55% with different AFR and power supplies, and 32% of the water vapor leakage were estimated. The energy loss resulted from air leakage was determined to be 6.6 to 11.8%, in which the heat loss took about 6.7% [40]. Since the enthalpy loss calculation through the drum in Chapter 4.2.1 was similar to Lena's simulation result, the air and water vapor leakage percentage could also be similar. The water vapor leakage could be 25.7% according to the deviation between the actual water removed and the water removed through evaporator simulation in Chapter 4.1.2., while the air leakage could be even higher to be about from 24% to 45%.

Figure 64 depicts the possible air leakages locations for LG hybrid HPCD. Because the condenser was located right next to the evaporator, no leakage was assumed in between. The makeup air that is the reverse air leakage was supposed to be at the fan inlet, where is the lowest static pressure of the air path.

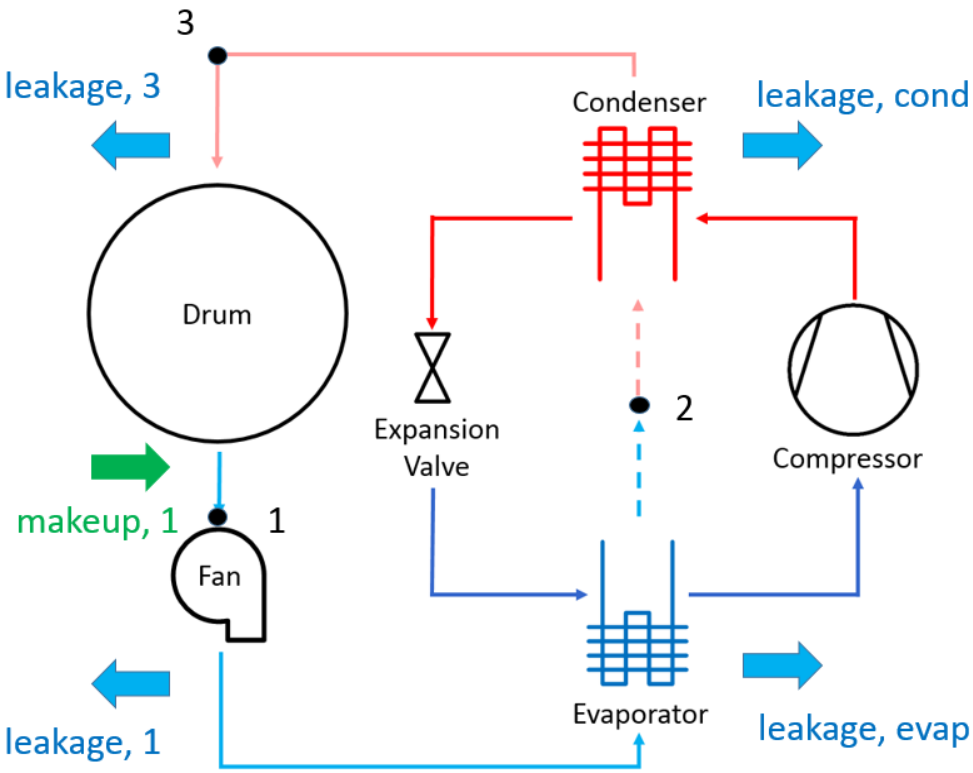

Figure 64: Air leakage locations

The mass balance of the air loop including the air leakages is listed in following equations.

For dry air mass balances:

Drum (3-1):

$$\dot{m}_{a,1} = \dot{m}_{a,3} - \dot{m}_{a,leak,3} + \dot{m}_{a,makeup,1}$$ Equation 17

Evaporator (1-2):

$$\dot{m}_{a,2} = \dot{m}_{a,1} - \dot{m}_{a,leak,1} - \dot{m}_{a,leak,evap}$$ Equation 18

Condenser (2-3):

$$\dot{m}_{a,3} = \dot{m}_{a,2} - \dot{m}_{a,leak,cond}$$ Equation 19

For water vapor mass balances:

Drum (3-1):

$$\dot{m}_{v,1} = \dot{m}_{v,3} - \dot{m}_{v,leak,3} + \dot{m}_{waterremoval} + \dot{m}_{v,makeup,1}$$ Equation 20

$$\dot{m}_{v,1} = \omega_1 * \dot{m}_{a,1}$$ Equation 21

$$\dot{m}_{v,3} = \omega_3 * \dot{m}_{a,3}$$ Equation 22

where $\dot{m}_{waterremoval}$ is the water removal rate in the drum.

Evaporator (1-2):

$$\dot{m}_{v,2} = \dot{m}_{v,1} - \dot{m}_{v,leak,1} - \dot{m}_{condensate} - \dot{m}_{v,leak,evap}$$ Equation 23

$$\dot{m}_{v,2} = \omega_2 * \dot{m}_{a,2}$$ Equation 24

where $\dot{m}_{condensate}$ is the water condensation rate through the evaporator.

Condenser (2-3):

$$\dot{m}_{v,3} = \dot{m}_{v,2} - \dot{m}_{v,leak,cond}$$ Equation 25

A better insulation of the CD will promote its temperature level and increase the overall efficiency.

4.2.3 Mass Transfer Rate

The mass balance regulates the mass transfer inside the drum as listed in 4.2.2. However, the mass transfer between the moisture contained in the drying load and its nearby air, which determines the water removal rate in the drum, is difficult to decide

because the water evaporation rate varies among different kinds of fabrics, and the HR difference between the surface of the load and the air is relatively higher than the HR variation in the air between the inlet and outlet of the drum. There are only few studies conducted for this mass transfer issue.

Deans (2001) [39] proposed a following mass transfer equation for clothes drying process:

$$\dot{m}_a(\omega_{out} - \omega_{in}) = kA\left(a\omega_{surface} - \frac{\omega_{in}+\omega_{out}}{2}\right) \quad \text{Equation 26}$$

where,

k is the mass transfer coefficient between the clothes surface and the air (kg/m²·s);

A is the effective clothes surface area (m²);

a is the activity coefficient in desorption-isotherm;

$\dot{m}_a$ is the dry air mass flow rate (kg/s);

ω_{in}, ω_{out}, and $\omega_{surface}$ are the HRs of the drum inlet, outlet and the saturated air at clothes surface.

This equation describes the average mass transfer rate between the load and the air that the change of the HR along the drum resulted from after the evaporation of the clothes' surface water [39].

And the activity coefficient is calculated from the relationship introduced by Lambert (1991) [41],

$$a = 1 - \frac{\beta M_c + \delta}{1 + \delta^{\gamma M_c}} \quad \text{Equation 27}$$

where β, δ and γ are constants for different fabrics, and M_c is the moisture content per kg of dry textile (which is dimensionless).

The mathematical approximation describes the sorption-isotherm, which represents the correlation between the moisture content and the surface equilibrium humidity level of a fabric according to experiments for each fabric, and the curve varies among different fabric compositions. The increase in the moisture content usually promotes the water activity (a), but not necessarily in a linear manner. Although the process performs in an opposite direction (drying not wetting), and is also affected by temperature, the approximated curve can be utilized to describe the mass transfer inside drum [42].

The desorption-isotherm curves are presented in Figure 65, which is originally taken from Krischer (1963) [43]. The relationship covers a range of water content from 0 to 1 ($kg_{water\ vapor}/kg_{dry\ air}$). Several fabrics such as wool, cotton and nylon were introduced, and cotton was utilized in the experimental tests with $\beta = 18$, $\delta = 2$ and $\gamma = 30$.

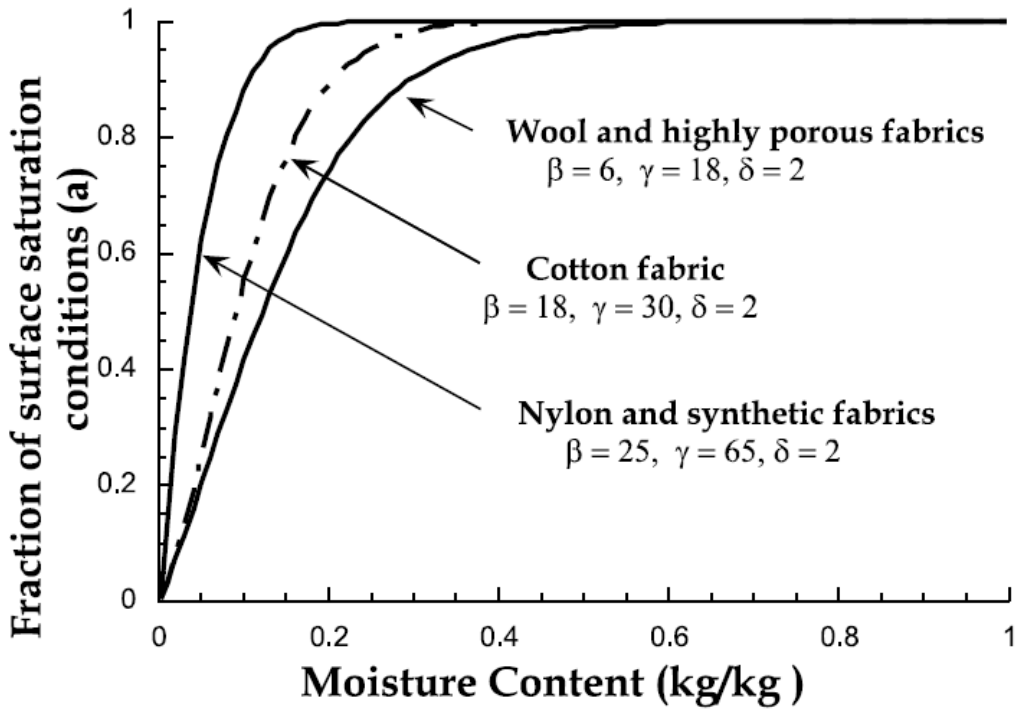

Figure 65: Desorption isotherms for fabrics

The mass transfer coefficient (k) which described the mass transfer between the cloth surface and the air could be determined using the mass transfer equation and the effective area of the clothes (A) by assuming the surface HR of the clothes to be 1 during dehumidification, and the desorption-isotherm curve for cotton fabric in Figure 65 was utilized to determine the activity coefficient (a). Then the average k was calculated to be 0.237 g/m²·s from 20 to 60 minutes. Since the same test clothes was used for all the tests in this study, clothes' surface area (A) was constant. Therefore, kA could be evaluated instead of k alone, and was estimated to be 0.401 g/s.

5 Conclusions

Four effective tests were conducted with two different operating modes for a state-of-the-art hybrid HPCD from LG. Experimental data were collected for system performance measurement, and the energy savings of HPCDs were also analyzed. The conclusions are summarized as follows:

- The testing of CDs followed DOE test standard (2005). EF defined as the BDW divided by the energy consumption was utilized to evaluate the HPCD's energy efficiency performance. The total energy consumption was evaluated to be 267 kWh/year for Eco Mode. There could be 633 kWh/year (or 70%) energy consumption reduction by using a HPCD instead of a typical electric CD in the U.S. About 35.9 billion kWh/year nationwide energy savings is projected by replacing the conventional CDs with HPCDs. Therefore, the energy saving potential of introducing the HPCD to the U.S. is significant.
- The HPCD's system performance was evaluated by investigating the HR, temperature, pressure, refrigerant MFR and air flow rate in Eco Mode. The comparison between Eco Mode and Speed Mode was also investigated through HR, temperature and power consumption. Speed Mode dries the clothes 20% faster because of the effect of the electric heater while consumes 96% more energy with 53% smaller EF than the Eco Mode.
- The performance of the heat exchangers was evaluated with the simulation in CoilDesigner. The heating capacity was about 1.48 kW for Eco Mode. The latent capacity dominated the cooling capacity with an average of 0.92 kW out

of 1.18 kW (78%), and it decreased at the end of the dehumidification process while the sensible heat increased. The dehumidification rate was 0.372 g/s.

- The evaporator UA was mainly affected by the AFR, inlet HR and refrigerant MFR while the condenser UA was mainly affected by the condensation temperature, AFR and the refrigerant MFR for the hybrid HPCD tested.
- There was an enthalpy loss of 8.5 kJ/kg (5%) through the drum, which would be related with energy loss to the surrounding environment. Moreover, there was a high possibility of air leakage ranging from 24% to 45% and the water vapor leakage was estimated to be 26%. The mass transfer coefficient k between the clothes and the air was calculated with the desorption-isotherm curve to be 0.237 $g/m^2 \cdot s$. The information collected in chapter 4 can be utilized for CD modeling or further analysis for future research.

6 Future Work

In this study, a number of tests were conducted with LG hybrid HPCD, and the test results were analyzed. After reviewing the results, there are some ideas that could potentially offer improvements for HPCDs. One important direction is to improve the refrigerant-side.

6.1 Improvement of Refrigerant-side

6.1.1 Vapor Injection Technique

The two-stage vapor injection technique has been studied by some researchers because of its remarkable performance improvements as compared to a conventional single-stage cycle. There is no two-stage HPCDs emerged in the market yet. However, UMDDryer Team [44] presented a prototype utilizing vapor injection technology which improved the cooling capacity, heating capacity and heating COP by 24, 19 and 20%, respectively.

The refrigerant flow path used in a vapor injection cycle (VIC) circulates in a similar way to in a general VCC. The main difference is that the single phase refrigerant coming out from the condenser is partially expanded to an intermediate pressure and then flows to the flash tank where it is separated into two parts: the vapor refrigerant is injected into the compressor from its intermediate-pressure port, and the liquid refrigerant undergoes the lower-stage expansion process and passes through the evaporator before being supplied to the compressor [45]. The air flow stream remains the same. Figure 66 shows the schematic diagram of a VIC.

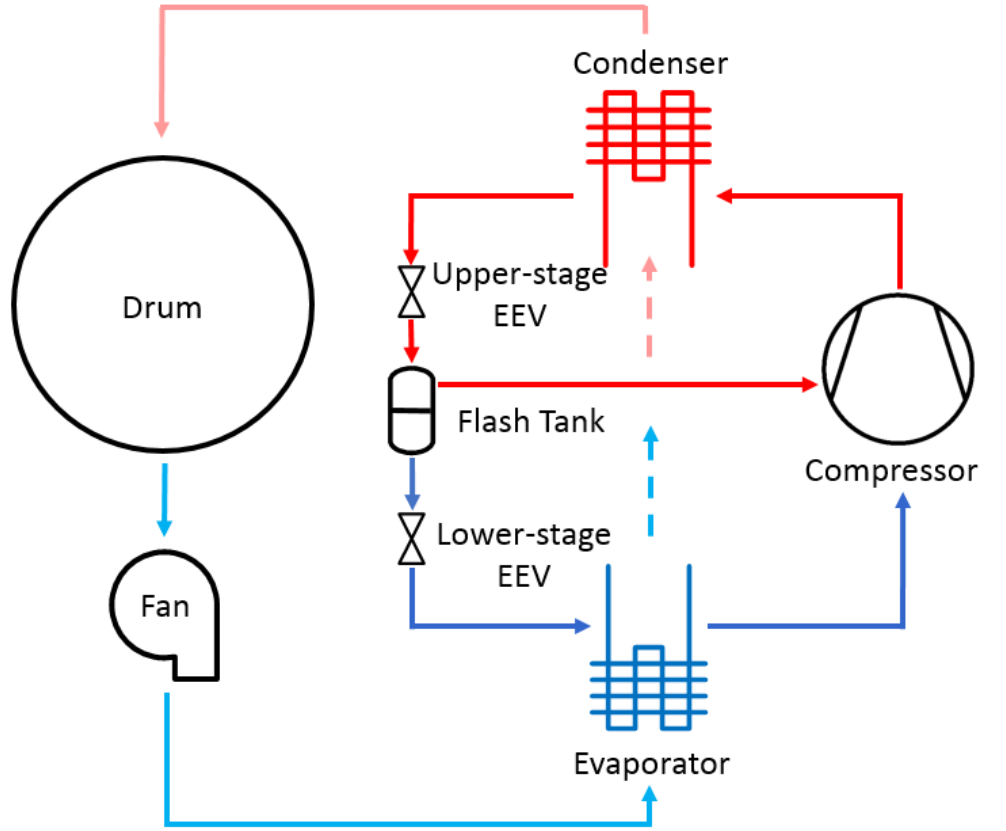

Figure 66: Schematic diagram of vapor injection cycle

In a VIC, the two-phase separation in the flash tank leads to a lower enthalpy at the inlet of the evaporator as compared to that of the basic VCC, which results in a larger enthalpy difference across the evaporator, and increases the cooling capacity [44]. Since the saturated vapor injected into the compressor is at a lower temperature level than that of the vapor in the compressor, the discharge temperature is reduced, which results in a higher isentropic efficiency. This compression process of a two-stage cycle approaches an isentropic process [46]. The improved compression efficiency causes a higher mass flow rate, which results in a better volumetric efficiency. Also, the enhanced compression

efficiency reduces the compressor power consumption, which leads to a higher system COP.

6.1.2 Suction Line Heat Exchangers

Suction line heat exchangers (SLHX) is another approach to improve the refrigerant cycle thermal efficiency. It has been already widely used in refrigerators, but has not been commercialized in HPCD so far. However, a patent for a hybrid HPCD with SLHX was issued to General Electric Company in 2012 [47].

As shown in Figure 67, the SLHX is installed at the end of the condenser and evaporator. The refrigerant flows out of the condenser enters into the SLHX at state point 3 for further cooling. Then, passes through the expansion device to lower the pressure and controls the refrigerant MFR. Whereas the vapor refrigerant from the evaporator absorbs heat from the relatively hot liquid refrigerant from the condenser between state point 3 and 4 so that its temperature is increased before entering the compressor, and the superheating degree at state point 1 is also increased. At the same time, the temperature of the liquid refrigerant coming out of the condenser also decreases by this heat exchange. In this way, the heating capacity of the condenser and the evaporator's cooling capacity are both enhanced because the inlet refrigerant enthalpy of the evaporator is reduced by cooling the liquid before entering the EEV [47] [48].

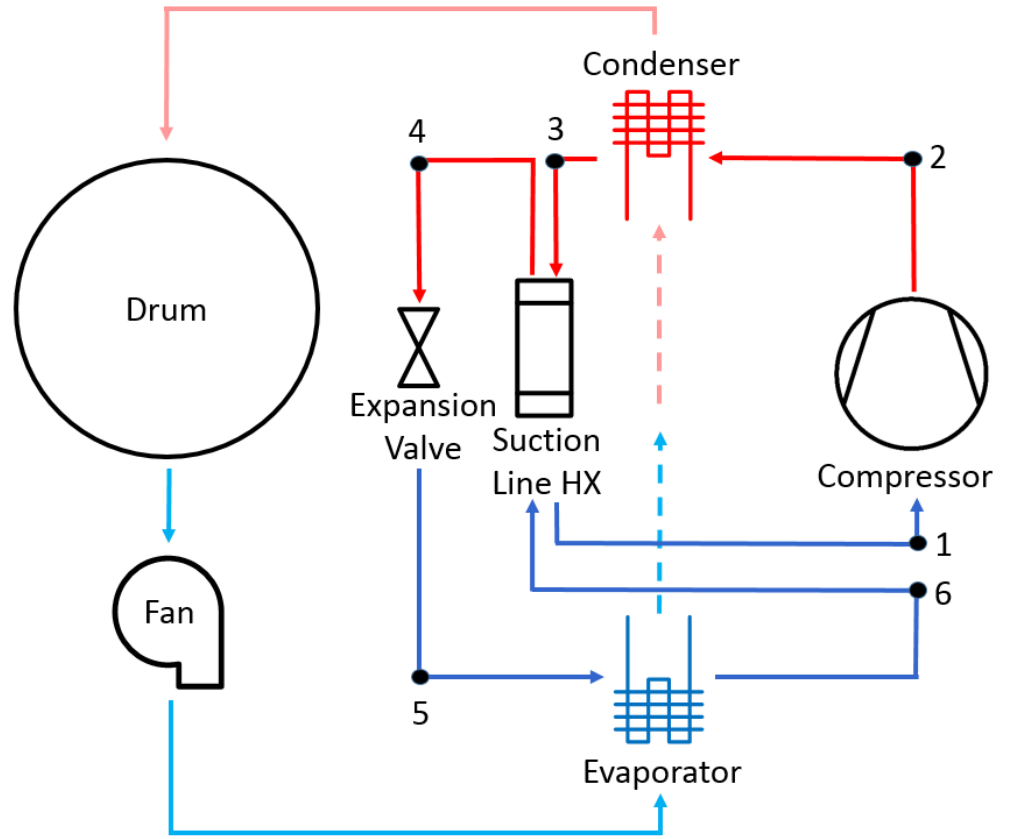

Figure 67: Schematic diagram of heat pump clothes dryer with a suction line heat exchanger

6.1.3 Heat Exchanger Optimization

The investigation of the microchannel heat exchangers (MCHX) have garnered more attention in recent years because there are many attractive benefits for utilizing MCHXs in various industrial applications. A MCHX can be significantly smaller than a tube-and-fin heat exchanger, which will make contribution to reducing the overall volume and weight of the system so that the capital cost as well as the installation cost can be lower. In addition, there will be less refrigerant charges in a MCHX. Moreover,

the MCHX's higher surface area and smaller wall thickness result in a higher heat transfer coefficient, and with a smaller dimension, a larger heat flux heat transfer can be achieved. Therefore, a higher efficiency is obtained, which will enhance the overall energy savings [49]. However, the smaller size of the hydraulic diameter would increase the wall friction, and cause a higher pressure drop [50] which is a drawback of replacing a general tube-and-fin heat exchanger with a MCHX. However, this can be avoided by utilizing multiple parallel channels. Figure 68 shows the schematic diagram of a HPCD with MCHXs.

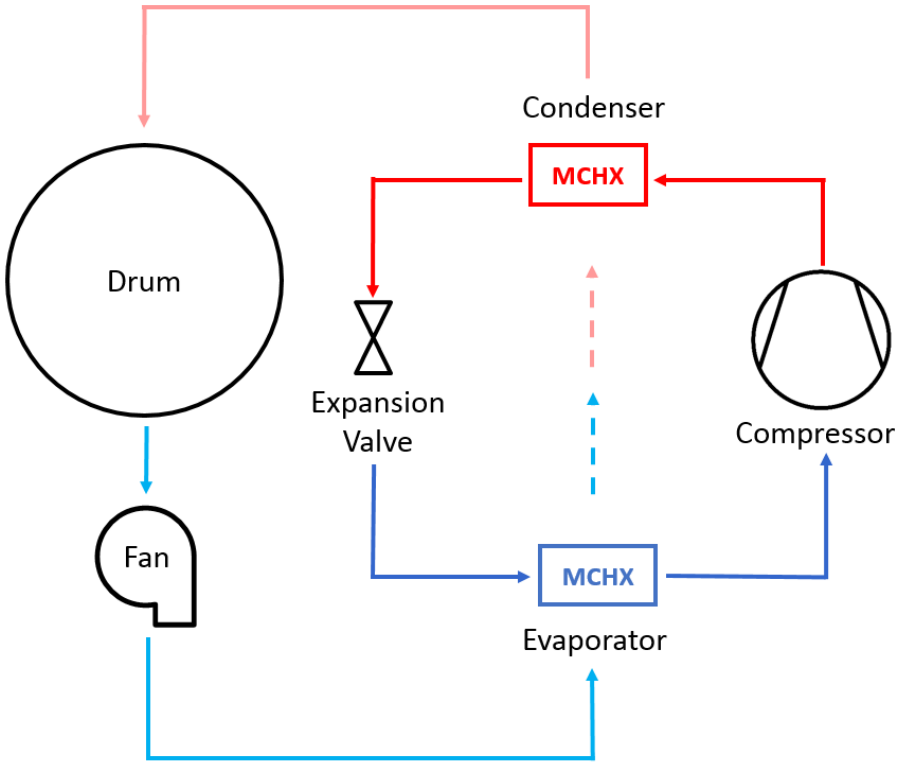

Figure 68: Schematic diagram of heat pump clothes dryer with microchannel heat exchangers

6.1.4 Others

In addition to the improvements in refrigerant-side, there are many other challenging prospects for improving system performance as described next.

6.1.4.1 Lint Control

Although for most of the CD models a lint trap is installed at the drum outlet duct to collect the lint produced from the drying load, some portion of the lint travels beyond the trap. Particularly, for ventless HPCDs, the lint's migration into the region of the heat exchangers may lead to the lint clogging so that it affects the air flow rate and effective heat transfer between the refrigerant and air loop. It has become one of the forefront concerns of the CD manufacturers since the increased temperature caused by the lint accumulation may cause fire hazard and safety issues. Several methods can be considered.

- Install air flow sensors to detect the obstruction in the air path for cycle termination and offer warning to the users;
- Develop a better lint filter;
- Design the heat exchangers especially the evaporator to be in a way to prevent the spread of the lint [51].

6.1.4.2 Air Loop

For most of the conventional CDs in the U.S., the vented duct is utilized to dump out the humid air. However, there is an opportunity or recovering waste energy from the vented air. More study can be conducted to compare a fully closed air loop versus a combination of open and closed air loop to recover some of the energy.

6.1.4.3 Heat and Drainage Recovery

For the residential vented CDs, a heat recovery system can be set up to collect and store the waste heat for the use of other heating purposes like increasing the room temperature in cold days or heating up the water rather than venting the exhaust air out of the house directly. Similarly, a drainage water reuse system can be built.

6.1.4.4 Control Strategy

Although more newly produced CDs are adopting the automatic termination feature, the accuracy of the sensors vary among different models, which seriously affect the effectiveness of the cycle termination, so that a regulatory standard for sensor accuracy is needed. The moisture and/or temperature sensors are typically installed at the exhaust duct for most of the CDs in the U.S. Placing the sensors along the tumble vanes around the drum which can move with the drum can lead to more direct detection of the humidity ratio in the drum and provide better end-of-cycle monitoring [25].

Moreover, since each laundry has a different weight and material, a load control system can be introduced to improve the drying performance and save energy [6].

6.1.4.5 Drum Design

It is needed to improve the distribution of the tumble vane inside the drum to improve the separation of the clothes and dry them more evenly so that drying time can be reduced. Moreover, since a portion of heat is wasted by conduction through the drum metal, a better insulation can be added to the drum to reduce the heat loss.

References

[1] "Monthly Energy Review," U.S. Energy Information Administration, Washiongton, DC, 2015/02.

[2] "International Energy Outlook 2014," U.S. Energy Information Administration, Washington, DC, 2014/09.

[3] "Emissions of Greenhouse Gases in the United States 2009," U.S. Energy Information Administration, Washington, DC, 2011/03.

[4] "How is electricity used in United States homes?," U.S. Energy Information Administration, 4 June 2014. [Online]. Available: http://www.eia.gov/tools/faqs/faq.cfm?id=96&t=3.

[5] "Residential Energy Consumption Survey (RECS)," U.S. Energy Information Administration, 2009. [Online]. Available: http://www.eia.gov/consumption/residential/.

[6] "ENERGY STAR Market & Industry Scoping Report Residential Clothes Dryers," ENERGY STAR, November 2011.

[7] S. Meyers, V. Franco, A. Lekov, L. Thompson and A. Sturges, "Do Heat Pump Clothes Dryers Make Sense for the U.S. Market?," in *2010 ACEEE Summer Study of Energy Efficiency in Buildings*, Pacific Grove, CA, August 2010.

[8] "Electronic Code of Federal Regulations, Appendix D to Subpart B of Part 430—Uniform Test Method for Measuring the Energy Consumption of Clothes Dryers," U.S. Department of Energy, February 10, 2014.

[9] "2014 Emerging Technology Award: Advanced Clothes Dryers," ENERGY STAR, [Online]. Available: http://www.energystar.gov/about/awards/energy-star-emerging-technology-award/2014-emerging-technology-award-advanced-clothes-dryers.

[10] Association of Home Appliance Manufacturers.

[11] "Rules and Regulations," U.S. Government, Thursday, January 6, 2011.

[12] C. Badger, R. Foster, C. Wold and C. Granda, "Super Efficient Dryer Initiative," in *Energy Star Partner Meeting*, 2012.

[13] E. Bush, D. Damino and B. Josephy, "Heat Pump Tumble Driers," in *Energy Efficiency in Domestic Appliances and Lighting EEDAL*, Coimbra, 2013.

[14] "Federal Register Part Two," Energy Efficiency and Renewable Energy Office (EERE), Wednesday, August 14, 2013.

[15] "Energy Conservation Program: Test Procedures for Residential Clothes Dryers; Final Rule," Energy Efficiency and Renewable Energy Office (EERE), 14 August 2013. [Online]. Available: http://www.regulations.gov/#!documentDetail;D=EERE-2011-BT-TP-0054-0024.

[16] K. Gluesenkamp, "Residential Clothes Dryer Performance Under Timed and Automatic Cycle Termination Test Procedures," Energy and Transportation Science Division, October 2014.

[17] "Rules and Regulations," Federal Register, Thursday, January 6, 2011.

[18] L. Stawreberg, "Energy Efficiency Improvements of Tumble Dryers - Technical Development, Laundry Habits and Energy Labelling," Karlstad Sweden, 2011.

[19] T. M. I. Mahlia, C. G. Hor, H. H. Masjuki, M. Husnawan, M. Varman and S. Mekhilef, "Clothes drying from room air conditioning waste heat: thermodynamics investigation," *The Arabian Journal for Science and Engineering*, vol. 35, no. 1B, April 2010.

[20] "Clothes Dryers for Consumers," ENERGY STAR, 2014. [Online]. Available: https://www.energystar.gov/products/certified-products/detail/clothes_dryers.

[21] "Clothes Dryers Key Product Criteria," Environmental Protection Agency, 2014. [Online]. Available: https://www.energystar.gov/index.cfm?c=clothesdry.pr_crit_clothes_dryers.

[22] "10 CFR 430.32 - Energy and water conservation standards and their effective dates," Legal Information Institute, [Online]. Available: https://www.law.cornell.edu/cfr/text/10/430.32.

[23] "Residential Clothes Dryers," Energy Efficiency & Renewable Energy, [Online]. Available:

http://www1.eere.energy.gov/buildings/appliance_standards/product.aspx/productid/36.

[24] D. Denkenberger, S. Mau, C. Calwell and E. Wanless, "Residential Clothes Dryers: A Closer Look at Energy Efficiency Test Procedures and Savings Opportunities," Natural Resources Defense Council, November 9, 2011.

[25] D. Denkenberger, C. Calwell, N. Beck, B. Trimboli and D. Driscoll, "Analysis of Potential Energy Savings from Heat Pump Clothes Dryers in North America," March 2013.

[26] *XProps Version 2.0,* 2010.

[27] "Engineering Equation Solver (EES)," F-Chart Software, LLC, Madison, WI, 2010.

[28] H. Jiang, V. Aute and R. Radermacher, "CoilDesigner: a general-purpose simulation and design tool for air-to-refrigerant heat exchangers," *International Journal of Refrigeration,* pp. 601-610, 2006.

[29] "Electronic Code of Federal Regulations, Appendix D2 to Subpart B of Part 430—Uniform Test Method for Measuring the Energy Consumption of Clothes Dryers," U.S. Department of Energy, 16 April 2015. [Online]. Available: http://www.ecfr.gov/cgi-bin/retrieveECFR?SID=b48736ddbf29fcfe9285bb7ea3e524e1&r=SUBPART&n=10y3.0.1.4.18.2#ap10.3.430_127.d.

[30] "Rotary Compressor for Air Conditioning," LG Electronics Inc..

[31] "ASHRAE Handbook," 2001.

[32] "Laminar and Turbulent flows in pipes," [Online]. Available: https://www.academia.edu/3157721/Laminar_and_Turbulent_Flows_in_Pipes.

[33] R. J. Moffat, "Describing the Uncertainties in Experimental Results," *Experimental Thermal and Fluid Science,* vol. 1, pp. 3-17, 1988.

[34] F. P. Incropera, T. L. Bergman, A. S. Lavine and D. P. DeWitt, Fundamentals of Heat and Mass Transfer, Hoboken, NJ: John Wiley, 2007.

[35] L. H. Tang, M. Zeng and Q. Wang, "Experimental and numerical investigation on air-side performance of fin-and-tube heat exchangers with various fin patterns," *Experimental Thermal and Fluid Science,* vol. 33, pp. 818-827, 2009.

[36] J. E. Brauna, P. K. Bansalb and E. A. Grolla, "Energy efficiency analysis of air cycle heat pump dryers," *International Journal of Refrigeration,* vol. 25, pp. 954-965, 2002.

[37] L. Stawreberg and L. Nilsson, "Modelling of Specific Moisture Extraction Rate and Leakage Ratio in a Condensing Tumble Dryer," *Applied Thermal Engineering,* vol. 30, pp. 2173-2179, 2010.

[38] S. Gopalnarayanan and R. Radermacher, "Heat Pump Assisted Dryer Using Refrigerant Mixtures - Batch Mode Drying," *ASHRAE Transactions: Symposia,* pp. 888-895, 1997.

[39] J. Deans, "The modelling of a domestic tumbler dryer," *Applied Thermal Engineering,* vol. 21, pp. 977-990, 2001.

[40] L. Stawreberg, "Energy Efficiency Improvements of Tumble Dryers," Karlstad, 2011.

[41] A. J. D. Lambert, F. P. M. Spruit and J. Claus, "Modelling as a Tool for Evaluating the Effects of Energy-Saving Measures. Case Study: A Tumbler Drier," *Applied Energy*, vol. 38, pp. 33-47, 1991.

[42] J. Deans and D. Tranxaun, "A computer simulation of a tumbler dryer," *Transport Phenomena in Heat and Mass Transfer*, vol. 2, 1992.

[43] O. Krischer and K. Kroll, "Die wissenschaftlichen Grundlagen der Trocknungstechnik," p. 56, 1963.

[44] UMDDryer Team, "Max Tech Appliance Design Competition Final Report," Max Tech and Beyond Appliance Design Competition for Ultra-Low-Energy-Use Appliances and Equipment, 2013.

[45] Y. Hwang, X. Xu, R. Radermacher and H. Pham, "Control Strategy of Vapor Injection Cycle," in *International Refrigeration and Air Conditioning Conference*, West Lafayette, IN, 2010.

[46] C. W. Roh and M. S. Kim, "Effect of Vapor-Injection Technique on the Performance of a Cascade Heat Pump," *International Journal of Refrigeration*, p. 4, 2013.

[47] W. W. Wang, "Heat exchanger for a heat pump laundry dryer". United States Patent US 20120060387 A1, 15 March 2012.

[48] J. H. Jeong, S. G. Park, D. Sarker and K. S. Chang, "Numerical simulation of the effects of a suction line heat exchanger on vapor compression refrigeration cycle performance," *Journal of Mechanical Science and Technology*, vol. 26, no. 4, pp. 1213-1226, 2012.

[49] K. O. Jatuporn, K. Sakamatapan and S. Wongwises, "Flow boiling pressure drop of R134a in the counter flow multiport minichannel heat exchangers," *Experimental Thermal and Fluid Science*, vol. 36, pp. 107-117, 2012.

[50] M. Feidt, T. Popescu, M. Marinescu, H. Pop and G. Popescu, "Microchannel Heat Exchangers - Present and Perspectives," *UPB Scientific Bulletin, Series D: Mechanical Engineering*, vol. 74, no. 3, pp. 55-70, 2012.

[51] P. Pescatore and P. Carbone, "High Efficiency, High Performance Clothes Dryer," TIAX, Cambridge, MA, April 20, 2005.

[52] A. M. Bassily, "Modeling and optimization of heating and drying processes in a clothes dryer," Ames, 2000.

[53] F. P. Incropera and D. P. Dewitt, Fundamentals of Heat and Mass Transfer, 6 ed., Hoboken: Wiley, 2007, pp. 490-515.